YEAR 2.
DEVELOPMENT OF A BIOSENSOR FOR DETECTING ODORS AT LANDFILLS
Final Report

January 2023

Author
Daniel E. Meeroff, Ph.D.

Florida Atlantic University, Department of Civil, Environmental & Geomatics Engineering

And

Co-Author
Sharmily Rahman, MSCV

Florida Atlantic University, Department of Civil, Environmental & Geomatics Engineering

Hinkley Center for Solid and Hazardous Waste Management
University of Florida
P. O. Box 116016
Gainesville, FL 32611
www.hinkleycenter.org

PROJECT TITLE: YEAR 2. DEVELOPMENT OF A BIOSENSOR FOR DETECTING ODORS AT LANDFILLS

PRINCIPAL INVESTIGATOR(S):

Daniel E. Meeroff, Ph.D., Interim Dean of Undergraduate Studies, Florida Atlantic University, Phone: (561) 297-2658, E-Mail: dmeeroff@fau.edu

PROJECT WEBSITE: http://labees.civil.fau.edu/leachate.html

PROJECT DURATION: 2022 - 2023

ABSTRACT:

Nuisance odors from landfills have more impact than just being an annoyance to nearby residents. With an ever-increasing population, a larger number of communities are located in closer proximity to landfills than ever before. This has brought along with it, more regular conflicts with landfill authorities surrounding the issue of odors, resulting in complaints, lawsuits, fines, and even re-siting operations. The absence of an objective method of quantifying nuisance odors makes the task of creating regulations and setting standards even more complicated. The current research focuses on a method to objectively quantify landfill odors. The human odorant binding protein 2A (hOBPIIa) can be produced using published recombinant gene technology and can be used as a biosensor to quantify odorants through spectrofluorometric measurements. The current work is a continuation of the previous work by Rahman (2020) accomplished in the Year 1 study. In the Year 2 study, the spent biosensor after it reacts with an odorant is shown to be regenerated by applying additional fluorophore following Le Châtelier's principle, so that the same batch of protein can be used to run multiple experiments with odorants. An important part of the work miniaturized the earlier version of the experimental setup and incorporates a much more efficient flow-through system. This setup is capable of collecting real-time readings, increasing the overall accuracy and shortening the duration of each set of the experiment. The current work also explores the response of the biosensor with an expanded group of pure odorants, including hydrogen sulfide, ammonia, toluene, formaldehyde, tert-butyl mercaptan, and methyl mercaptan as well as their mixtures, thus expanding the list of odorants tested under this principle. The results show that the protein shows a concentration-dependent response differing on the hydrophobicity of the target compound.

Key words:
Landfill odors, biosensor, human odorant binding protein, odor detection, spectrofluorometry

PROJECT METRICS:

List graduate or postdoctoral researchers **funded** by **THIS** Hinkley Center project.

Last name, first name	Rank	Department	Professor	Institution
Rahman, Sharmily	Ph.D.	CEGE	Meeroff	FAU

1. List research publications resulting from THIS Hinkley Center project. Has your project been mentioned in any research and/or solid waste publication/newsletters/magazines/blogs, etc.?

- A peer-reviewed manuscript "Development of a biosensor for objectively quantifying nuisance odors" was submitted in an Elsevier Journal which is currently under review.
- A two-part article was published online on Waste360 (November 11, 2021):
  - https://www.waste360.com/landfill-operations/odor-management-landfills-part-1-current-state-art
  - https://www.waste360.com/landfill-operations/odor-management-landfills-part-2-novel-biosensor-measuring-odors-landfills

- Rahman, S., Meeroff, D.E. (2020). Development of a Biosensor for Objectively Quantifying Odorants. Odor and Air Pollutants Conference Proceeding 2020 (pp 427-463).
- Rahman, S. (2020). *Development of a biosensor for objectively quantifying odorants.* (Master's Thesis, Florida Atlantic University). (Order No. 27962421). Available from Dissertations & Theses @ Florida Atlantic University - FCLA; ProQuest Dissertations & Theses A&I; ProQuest Dissertations & Theses Global. (2414449391).
- Rahman, S. (2022). *Development of a biosensor for objectively quantifying nuisance odors near landfills.* (Doctoral dissertation, Florida Atlantic University).

2. List research presentations resulting from (or about) THIS Hinkley Center project. Include speaker presentations, TAG presentations, student posters, etc.

- Dr. Meeroff was invited to speak at EREF Orlando on October 20, 2021, "Detection of Nuisance Odors using Odor Binding Protein Sensor: EREF Funded Project Update"
- Dr. Meeroff was invited to speak at WasteExpo 2022 on May 9-11 in Las Vegas, NV, "Innovative Solutions and Technologies for Keeping Odors at Bay"
- Rahman, S. "Year 2. Development of a Biosensor for Detecting Odors at Landfill" at TAG meeting, March 2022 and November 2022.
  - Video Link and Minutes: TAG 1 (video)
  - Video Link and Minutes: TAG 2 (video)

3. List who has referenced or cited your publications from this project. Has another author attributed your work in any publications?

None so far

4. How have the research results from THIS Hinkley Center project been leveraged to secure additional research funding? What additional sources of funding are you seeking or have you sought? Please list all grant applications and grants and/or funding opportunities associated with this project. Indicate if additional funding was granted.

The FAU Technology fee competitive grant was applied for in Spring 2021 and was awarded and received in February 2022. The grant funded purchase of a flow-through spectrofluorometer $23,000.

5. What new collaborations were initiated based on THIS Hinkley Center project? Did any other faculty members/researchers/stakeholders inquire about this project? Are you working with any faculty from your institution or other institutions?

Other faculty include Dr. D. Binninger (FAU-Biology) and Dr. M. Jahandar Lashaki (FAU-CEGE)

6. How have the results from THIS Hinkley Center funded project been used (not will be used) by the FDEP or other stakeholders? (1 paragraph maximum). Freely describe how the findings and implications from your project have been used to advance and improve solid waste management practices

None so far

ACKNOWLEDGEMENTS

The researchers would like to acknowledge the William W. "Bill" Hinkley Center for Solid and Hazardous Waste Management for funding this project. The researchers would also like to thank the Technical Advisory Group members and all the stakeholders for their invaluable advice, feedback, and support of this work. In addition, the contributions of Dr. Masoud Lashaki, Dr. Fred Bloetscher, Dr. David Binninger, and Dr. Bishow Shaha for supervision of the doctoral dissertation are acknowledged.

Full Name: Sharmily Rahman
Email: rahmans2018@fau.edu
Degree: Ph.D.
Department: FAU CEGE

Bio: Sharmily led the FAU team that finished first place in the 2019 SWANA Student Design Competition for Evaluating Recycling Rate Metrics to Achieve 80% Recycling Goal for Phoenix, AZ. She is the recipient of the FAU Graduate Student Leadership Prize and the FAU Presidential Fellowship to pursue her doctoral degree.

TAG members:
Owrang Kashef (CDM)
Craig Ash (WM)
Ravi Kadambala (CDM)
Jeff Roccapriore (WM)
André McBarnette (Stantec)
Dan Schauer (Geosyntec)
Damaris Lugo (Broward County)
Amanda Krupa (SWA)
Amede Dimonnay (Broward County)
Jarod Gregory (Trinity Consultants)
Hanting Wang (Greeley and Hanson)
Catherine Vanyo (Brown and Caldwell)
Sally Gordon (King County, WA)
Bishow Shaha (Geosyntec)

TABLE OF CONTENTS

LIST OF FIGURES

LIST OF TABLES

LIST OF ACRONYMS AND ABBREVIATIONS

1-AMA	1-Aminoanthracine
ASTM	American Society of Testing and Materials
bOBP	Bovine Odorant-Binding Proteins
FIDOL	Frequency (F), intensity (I), duration (D), offensiveness (O), and location (L)
GC/MS	Gas Chromatography/Mass Spectrometry
HAP	Hazardous Air Pollutant
hOBP	Human Odorant-Binding Proteins
LFG	Landfill Gas
MSW	Municipal Solid Waste
OBP	Odorant-Binding Protein
OD	Optical Density
OR	Olfactory Receptors
PID	Photo-Ionization Detector
pOBP	Porcine Odorant-Binding Proteins
ppb	Parts per billion
ppm	Parts per million
ppt	Parts per trillion
SDS-PAGE	Sodium Dodecyl Sulfate Polyacrylamide Gel Electrophoresis
SLPM	Standard Liters per Minute
VOC	Volatile Organic Compound

1 INTRODUCTION

1.1 Background

Anaerobic decomposition of readily biodegradable components of solid waste produces potentially toxic, noxious, and health threatening compounds that generate odors at municipal solid waste (MSW) facilities (Palmiotto et al. 2014). Ritzkowski et al. (2006) found that such emissions can last up to 30-100 years even after the landfill is technically closed, which is an unavoidable situation because of the nature of the waste materials buried into landfills. Nuisance odor complaints arising from landfills have become more acute as an increasing population is encroaching closer to existing solid waste management facilities, even though these facilities were initially intended to be located some distance away from centers of human activity. Such issues, along with the already existing uncertainties associated with odor measurement, have made dealing with nuisance odors a significant challenge to solve for solid waste management facilities, eventually leading to lawsuits, regulatory actions, and permitting difficulties.

While determining the source of odor can be a complicated task, detecting and characterizing complex odors is not any easier, particularly since the technology used for these purposes has not developed to the level of a reliable surveillance method. Theoretically, odors emitted from landfills should be measured by identifying, sampling, and quantifying the concentrations of all constituent odorants from all sources, but it is the most challenging part to accomplish since there are numerous sources of odors as well as a wide variety of odor-causing compounds in landfills (Paxeus 2000; Bruno et al. 2007; Kjeldsen 2010). Currently, measurement techniques and regulatory tools vary, ranging from the relatively simple use of odor detection panels to perceive the presence/absence of odorants to the more complex use of electronic nose technology and atmospheric dispersion models to predict odor impacts on neighboring receptors (Laor et al. 2014). However, state-of-the-art odor measurement techniques all suffer from severe limitations including that they are subjective, largely inaccurate, irreproducible, odorant-specific, overly complex, and/or expensive (Liu et al. 2013; Sankaran et al. 2021; Laor et al. 2014). This uncertainty calls for a need to develop an analytical odor measurement technique that can objectively and cost-effectively quantify odors so that regulatory agencies can establish reasonable and objective odor standards with certainty and avoid conflict with the surrounding community.

1.2 Major Odorants and Possible Sources of Odor at Landfills

Landfill odors are generated from various substances including sulfur compounds such as hydrogen sulfide, dimethyl sulfide, methanethiol, and propanethiol; nitrogen compounds such as ammonia and amines; and hydrocarbons such as benzene, phenols, terpenes, styrene, toluene, xylene, acetone, methanol, n-butanone, n-butyl aldehyde, volatile fatty acids, etc. (Parker et al. 2002; Fang et al. 2012). Some of these are known to have very high odor intensity even at extremely low concentration levels that are difficult to detect by conventional technologies. Generally speaking, sulfur compounds, including hydrogen sulfide, methyl mercaptan, and dimethyl sulfide, are found to be the primary sources of malodor in landfill settings (Parker et al. 2002; Fang et al. 2012). Tansel and Inanloo (2019) mentioned that hydrogen sulfide, exerting a strong rotten egg smell upon its release into

the environment, is the main compound that originates a strong odor in landfills even though landfill emissions typically contain less than 15 ppb hydrogen sulfide (ATSDR 2016). This is because humans are extremely sensitive to hydrogen sulfide odors and can smell its odor at concentrations as low as 0.5 ppb (ATSDR 2016). The biodegradation of gypsum drywall, a primary component of construction and demolition (C&D) debris, is one major cause of hydrogen sulfide generation in landfill operations (Yang et al. 2016). Besides the sulfur compounds, amines, and nitrogenous heterocyclic compounds also generate offensive odors in landfills. Most of the odorous compounds in landfills belong to a non-ionic hydrophobic organic group having a molecular weight of less than 300 (Schiffman et al. 2004), even though reactive inorganic gases such as ammonia and hydrogen sulfide that contribute to strong odor do not belong to any specific functional group.

Depending on waste composition and time of decomposition in landfills, one odorant may dominate over another and can generate its characteristic smell, or many different odorants can contribute characteristic odors at the same time. The individual aromas of different odorants are perceived simultaneously as an individual unpleasant smell. Sometimes odorants mask other odors, and sometimes odorants are additive or synergistic. **Table 1** describes the common odor categories of typical landfill odors.

Table 1: Landfill odor categories and descriptors (Decottignies et al. 2009; Curren 2012)

Odor Character Category	Common Descriptors
Non-descriptive	Trash
Sulfur/Cabbage/Garlic	Rotten egg, natural gas, skunk
Rancid	Sour, dirty diaper, sweet-sour
Fecal/Sewery	Feces, manure, sewage
Fragrant/Fruity	Perfume
Solvent/Hydrocarbon	Chemical
Burnt	Burnt rubber, exhaust, burnt trash
Putrid/Dead Animal	Dead animal
Earthy/Musty/Grassy	Musty, decaying vegetation
Sweet	Sweet trash
Fishy/Ammonia	Ammonia

There are a number of sources in landfills from where odors are generated, such as household garbage or municipal solid waste (MSW), wastewater treatment biosolids disposed in landfills, landfill gas (LFG), various landfill activities, and vehicle operations. MSW in landfills often generates rancid, sulfur, and fragrant odors with rancid odors being dominant near on-site locations and sulfur odors being dominant in off-site locations (Curren et al. 2016). Curren et al. (2016) also reported that the emission of rancid and sour odors in landfills is due to the presence of acetaldehyde (sweet, fruity), acetic acid (vinegar), butyric acid (rancid), etc. The MSW near off-site locations that emits a sulfur odor mostly originates from methanethiol rather than hydrogen sulfide (Curren et al. 2016).

Biosolids disposal in landfills also contributes to generating nuisance odors that may vary between landfills depending on the type of biosolids and how they were processed (Maulini-Duran et al. 2013). For example, air-dried biosolids and anaerobic wastewater residuals generate sulfur odors, whereas alkaline biosolids contribute to volatile emissions in landfills (Sivret et al. 2014; Fisher et al. 2019). In addition, the amino acids and carbohydrates in the biosolids are decomposed by microorganisms, which may also release various odorous compounds including amines, mercaptans, sulfur compounds, fatty acids, etc. (Fisher et al. 2018).

Landfill gas (LFG) is another source of odor emissions in landfills that are generated due to the anaerobic decomposition of waste (Ritzkowski et al. 2006). Both organic and inorganic sulfur compounds in LFG, including hydrogen sulfide, sulfur dioxide, methyl mercaptan, etc. contribute to odor emissions in landfills (Tansel and Inanloo 2019). Hydrogen sulfide contributes to 90% of the mass concentration of all sulfur gases in LFG (Jin 2015; Kim et al. 2005b; Scheutz et al. 2009; Xia et al. 2015). Similar to biosolids, the characteristics of LFG emissions also vary between landfills depending on the type of waste, pH, alkalinity, waste age, moisture content, etc. (Yazdani 2015). The main components found in LFG are summarized in **Table 2**.

Table 2: Components of LFG and their concentrations (Takuwa et al. 2009)

Compound	Typical concentration
Methane (CH_4)	30%–60%
Carbon dioxide (CO_2)	20%–50%
Nitrogen (N_2)	<10%
Oxygen (O_2)	<2%
Water (H_2O)	Saturated
Trace compounds	$< 4.0\times10^{-3}$ mol/mol

According to **Table 2**, LFG consists mostly of methane and carbon dioxide, both of which are odorless. Only the trace compounds that make up a very low percentage of LFG, including volatile organic compounds (VOCs) and hazardous air pollutants (HAPs) are responsible for causing odors in landfills. (El-Fadel et al. 1997; Davoli et al. 2003; Fang et al. 2012). The most commonly found odorous components in LFG and their probable release mechanisms are summarized in **Table 3**.

Table 3: Odorous Compounds in LFG along with their sources and possible release mechanism (Parker et al. 2002)

Trace component	Probable source	Probable release mechanism
Hydrogen	Organics acids Metals	Anaerobic microbial respiration Corrosion
Hydrogen sulfide	Sulfate wastes	Anaerobic microbial respiration
Vinyl chloride	Chlorinated solvents	Anaerobic microbial respiration

Trace component	Probable source	Probable release mechanism
Simple alkanes & alkenes	Organic wastes	Anaerobic microbial respiration
Organic acids	Organic wastes	Anaerobic microbial respiration
Mercaptans	Organic material	Anaerobic microbial metabolism
Alcohols & ketones	Organic wastes Solvents	Anaerobic microbial respiration Microbial metabolism Evaporation & gas stripping Aerosols
Aldehydes	Organic wastes	Microbial metabolism
Limonene	Plant material	Anaerobic microbial respiration
Ammonia	Organic wastes	Anaerobic microbial respiration
Amines	Organic wastes	Microbial metabolism Aerosols
Esters	Organic acids & alcohols	Chemical reaction or microbial action Aerosols
Chlorinated hydrocarbons	Solvents & paints in waste	Evaporation, gas stripping
Simple aromatic hydrocarbons	Solvents & paints in waste	Evaporation, gas stripping
Chloro and chlorofluorohydrocarbons	Foams & propellants in waste	Out-gassing
Mercury	Inorganic waste	Microbial methylation Evaporation Dust

Other than the odor generated from the waste disposed in landfills, various solid waste operational activities such as constructing LFG collectors by drilling through the waste mass and excavating trenches can cause fugitive emissions in the landfill air through the borehole (McKendry et al. 2002). In addition, external sources such as spreading and compaction vehicles, as well as trucks operating in and around landfill sites, also emit VOCs (e.g., toluene), which are found to generate nuisance odors (Chiriac et al. 2007).

1.3 Odor Characteristics

Human perception of odors is highly subjective and varies widely from person to person. Therefore, dimensioning procedures are available for characterizing odors that may help identify the source of the odor and possibly mitigate the issue. In several countries, five interactive components, commonly known as FIDOL or FIDOR, are widely used to

facilitate odor investigation in an area through characterization of the odor annoyance, determining its impact, and its adverse effect on humans (Bokowa et al. 2021; Nicell 2009). FIDOL/FIDOR stands for frequency (F), intensity (I), duration (D), offensiveness (O), and location (L) or receptor (R) (Bokowa et al. 2021). Among the various classifications of odor characteristics, the four most common parameters used to characterize odor are detectability, intensity, quality, and hedonic tone (van Harreveld et al. 2022). Descriptions of these four standard dimensions are provided in the following subsections.

1.3.1 Detectability

Detectability refers to the minimum concentration of an odorant that a person can perceive (CalRecycle 2019). It is related to the odor detection threshold (ODT), which is the minimum concentration of an odorant detected by the olfactory system of 50% of the human test population (Yuwono and Lammers 2004). ODT largely varies among individuals (Pearce et al. 2006) depending on several factors, including a person's sensitivity to odor, perception of odor, environmental fate and transport mode at that specific time, etc. Most importantly, the same odor that is unpleasant to one person might not be unpleasant at all to another person. Also, in some cases, repeated exposure to an odorant might artificially increase the threshold value of that compound because of nose blindness (Sela & Sobel 2010). Although there is no clear relationship between the odor threshold value and the molecular weight of the odorants, while conducting research with 223 odorous substances having a molecular weight between 12-170, Nagata and Takeuchi (2003) found that the odor threshold value tends to decrease as the molecular weight of the odorants increases (**Figure 1**-left) in the range to 20-160. This tendency becomes more apparent when comparing a homologous series of odorous substances (e.g., alcohol, aldehyde, mercaptan, ketone, and hydrocarbon), as represented in **Figure 1** (right).

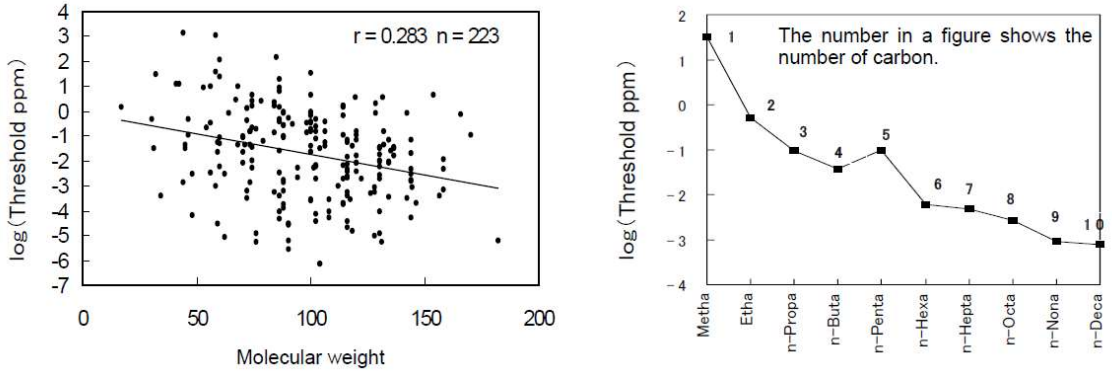

Figure 1: General trend of decreasing odor threshold against increasing molecular weight (left), and general trend of decreasing odor threshold with increasing number of carbon atoms in aliphatic alcohols (right) (Nagata and Takeuchi 2003)

The odor threshold values for possible trace components found in landfill gas are presented in **Table 4** as reported by Ruth (1986). Since odor threshold is a subjective term, the reported threshold values for odorous compounds are generally an estimate (ATSDR 2016).

Table 4: Odor descriptions of various gases found in landfills along with their detection limits for humans (Ruth 1986)

Compounds	Odor (Description)	Detection Limits	
		$\mu g/m^3$	$\times 10^{-9}$ mol/mol
Sulfur compounds			
Sulphur dioxide	irritating	1175	449.3
Carbon disulfide	disagreeable, sweet	24	7.7
Dimethyl trisulfide	rotten cabbage	6.2	1.2
Dimethyl sulfide	rotten cabbage	2.5	1.0
Hydrogen sulfide	rotten eggs	0.7	0.5
Benzyl mercaptan	unpleasant	1.6	0.3
Thiophenol	putrid garlic	1.2	0.3
Allyl mercaptan	garlic coffee	0.2	0.1
Propyl mercaptan	unpleasant	0.2	0.1
Dimethyl disulfide	rotten cabbage	0.1	0.026
Methyl mercaptan	rotten cabbage	0.04	0.02
Amyl mercaptan	putrid	0.1	0.02
Ethyl mercaptan	rotten cabbage	0.032	0.01
Carbon oxysulfide	pungent	NA	NA
Nitrogen Compounds			
Dimethylamine	fishy, amine	84.6	46.0
Ammonia	pungent, sharp	26.6	38.3
Aminomethane	fishy, pungent	25.2	19.5
Trimethylamine	fishy, pungent	0.1	0.046
Skatole	feces, chocolate	0.00004	0.00001
Volatile Fatty Acids			
Acetic	vinegar	2500	1019.1
Propionic	rancid, pungent	84	27.8
Formic	biting	45	24.0
Valeric	unpleasant	2.6	0.6
Butyric	rancid	1.0	0.3
Ketones/Aldehydes			
Methanol	alcohol	13000	9953.1
2-Pentanone	sweet	28000	7967.5
Acetone	sweet, minty	1100	463.9
Ethanol	alcohol	342	342
Butanone	sweet, minty	737	250.4
Phenol	medicinal	178	46
Acetaldehyde	green sweet	0.2	0.1

The lower the threshold value of an odorant, the higher its importance in odor perception (Parker et al. 2002). This is because odorants having low odor threshold values can be

perceived by human noses even when they are present in very small amounts. As an example, adding only three drops of ethyl mercaptan to an Olympic-sized swimming pool creates a smell strong enough to be detected by the human nose (Sela & Sobel 2010), indicating that ethyl mercaptan has a very low odor threshold value. Parker et al. (2002) provided an odor ranking plan based on the threshold value of odorants, as shown in **Table 5**. According to this plan, odorants with higher threshold values are represented by lower ranks, while higher ranks represent those with lower threshold values.

Table 5: Odor ranking plan based on detection concentration for humans (Parker et al. 2002)

Odor Ranking	**1**	**2**	**3**	**4**	**5**
Detection Concentration Range ($\mu g/m^3$)	>1000	100-1000	10 - 100	10 – 1	<1

Parker et al. (2002) also provided an odor importance ranking for the 12 most commonly found odorants in landfills based on their odor ranking value along with a physical property ranking (1 if mobility is lower than benzene and 2 if mobility is higher than benzene) as presented in **Table 6.** Among the 12 most common odorants, hydrogen sulfide and methanethiol (methyl mercaptan) were given the highest odor importance value. The organo-sulfur compounds listed are the most commonly detected odorants in landfills due to their association with older waste, where the corresponding emissions contain relatively low amounts of other compounds, including carboxylic acids, aldehydes, and esters.

Table 6: Ranking of odor importance in landfills based on physical and odor rankings (Parker et al. 2002)

Chemical Name		**Chemical Group**	**Physical Ranking**	**Odor Ranking**	**Odor Importance**
1	Hydrogen sulfide	Organo Sulfur Compounds	2	5	10
2	Methanthiol	Organo Sulfur Compounds	2	5	10
3	Carbon disulfide	Organo Sulfur Compounds	2	3	6
4	Propanethiol	Organo Sulfur Compounds	1	5	5
5	Butyric acid	Carboxylic acids	1	5	5
6	Dimethyl disulfide	Organo Sulfur Compounds	1	5	5

Chemical Name		Chemical Group	Physical Ranking	Odor Ranking	Odor Importance
7	Ethanal	Aldehyde	1	5	5
8	Ethanethiol	Organo Sulfur Compounds	1	5	5
9	Butanethiol	Organo Sulfur Compounds	1	4	4
10	Pentene	Alkenes	2	2	4
11	Dimethyl sulfide	Organo Sulfur Compounds	1	4	4
12	Ethyl butyrate	Ester	1	4	4

1.3.2 Odor Intensity

Odor intensity is the strength of an odor at a concentration level that has already exceeded its threshold value, i.e., the detection limit (Pearce et al. 2006). Typically, unpleasant odorants that have a lower threshold value, e.g., hydrogen sulfide, can be perceived with a higher odor intensity even at a very low concentration level (Belgiorno et al. 2013). To express the perceived intensity of odor, a 6-point scale is often used, with 0 being no perceived odor and 5 being a very strong odor (Kulig 2004), as shown in **Table 7**.

Table 7: Scale of odor intensity (Kulig 2004)

Scale of Odor Intensity	Discernible Odor Intensity	Examples
0	No odor	Carbon dioxide, methane
1	Odor almost imperceptible	Butene
2	Very weak odor	Propane
3	Weak odor	Methanol
4	Strong odor	Hydrogen sulfide
5	Very strong odor	Ammonia

In general, as the concentration of an odorant increases, the intensity of the odor also increases. However, the relationship between odor concentration and odor intensity is not linear. Several mathematical functions have been established to correlate the interdependency between odor concentration and odor intensity. The relationship between these two follows an exponential function according to Steven's law (**Figure 2**-left), whereas according to the Weber-Fechner equation, the relationship between them is logarithmic (**Figure 2**-right) (Belgiorno et al. 2013; Curren et al. 2013; Stuetz and Frechen 2001).

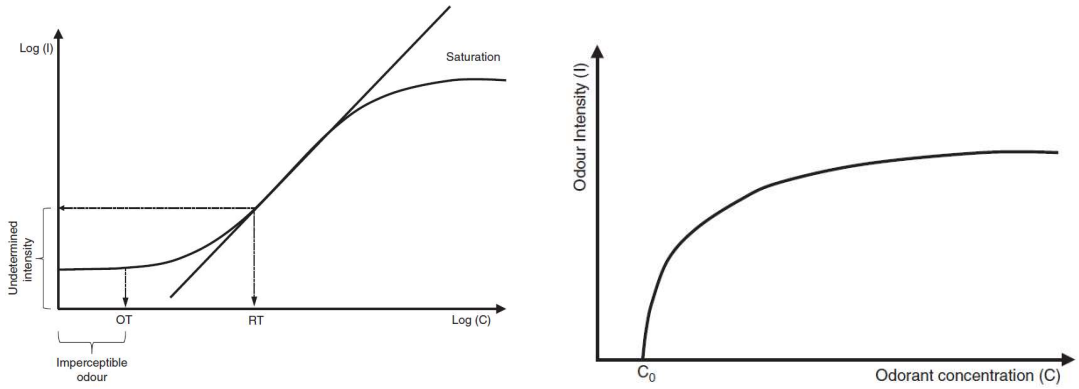

Figure 2: Relationship between odor concentration and intensity according to Steven's Law (left) and the Weber-Fechner model of change in odorant concentration vs odor intensity (right) (Belgiorno et al. 2013)

1.3.3 Odor Quality

Odor quality describes how an odorous substance smells like i.e., whether it is pungent, rancid, fruity, etc. (Yuwono and Lammers 2004). Based on psychological testing, seven primary classes of olfactory stimulants generate specific responses in separate olfactory cells according to their smell, as shown in **Table 8** (WEF 1978). The odor classes include a specific model compound and its odor sensitivity limit.

Table 8: Concentrations of Primary Odor Classes to Generate an Equal Odor Intensity (WEF 1978)

Odor Class	Model Compounds	Concentration to Generate Equal Odor Intensity (ppm)
Putrid	Dimethyl disulfide	0.1
Musky	Pentadecanlacton	1
Minty	Menthone	6
Camphoraceous	1,8-Cineole	10
Floral	Phenyl ethyl methyl ethyl carbinol	300
Ethereal	Ethylene dichlor	800
Pungent	Formic acid	50,000

An odor wheel is another useful tool that categorizes more detailed odor qualities of the substances commonly found in solid waste management facilities. The chemical names of the odorants are placed along the rims of the wheels to identify compounds potentially responsible for generating the specific odor categories, as shown in **Figure 3**.

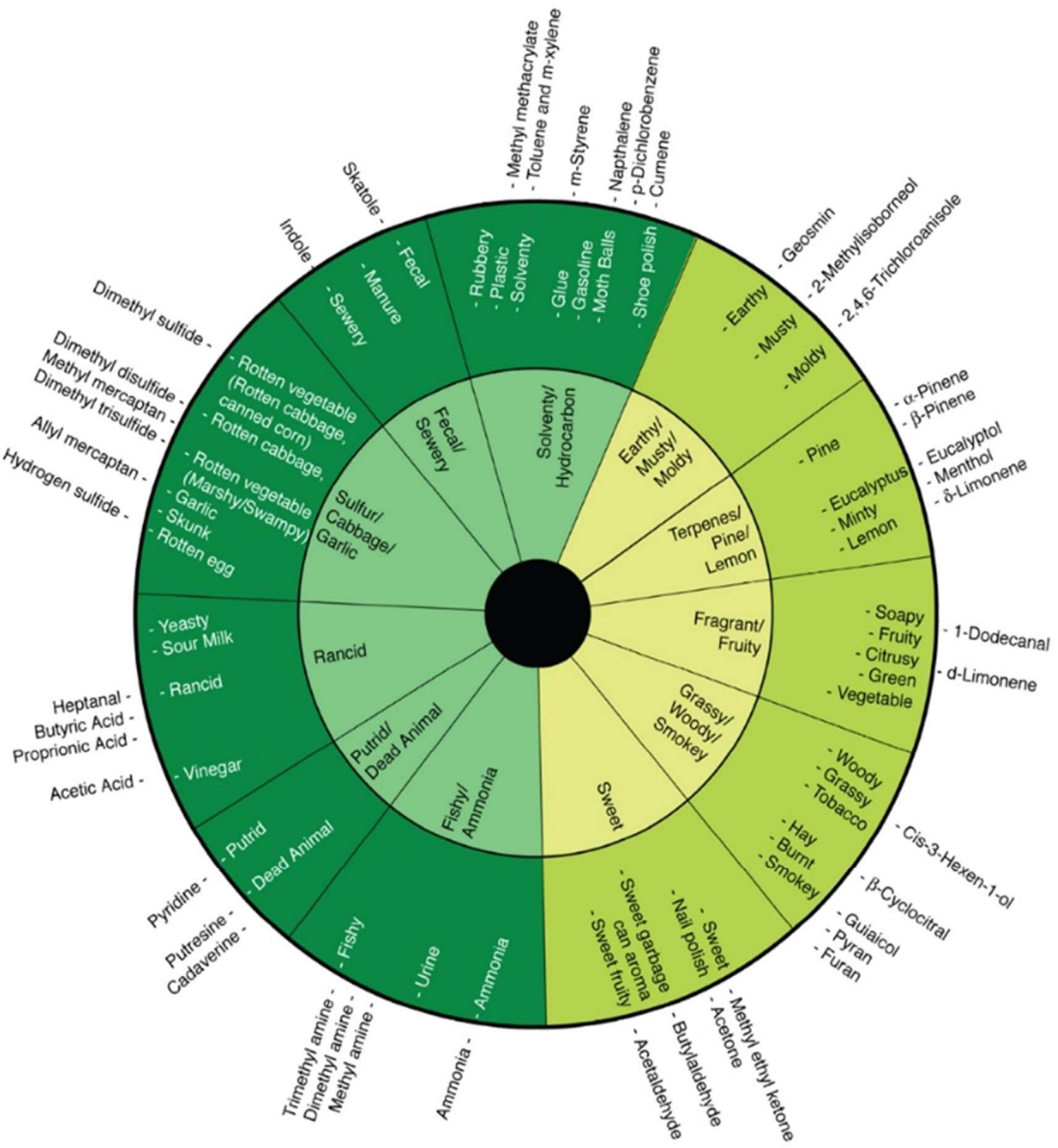

Figure 3: Example of an odor wheel describing odorant qualities from solid waste management operations (Suffet et al. 2009)

The American Society for Testing and Materials (ASTM) established 146 descriptors for describing odors (Zarzo 2021). The odor descriptions for the most commonly found odorants in landfills are presented in **Table *9***.

Table 9: Description of odor associated with various landfill gas components (ATSDR 2016)

Component	Odor description
Hydrogen Sulfide	Strong rotten egg
Ammonia	Pungent acidic or suffocating
Benzene	Paint thinner-like
Dicholoethylene	Sweet, ether-like, slightly acrid
Dichloromethane	Sweet, chloroform-like
Ethylbenzene	Aromatic, benzene-like
Toluene	Aromatic, benzene-like
Trichloroethylene	Sweet, chloroform-like
Tetrachloroethylene	Sweet, ether-like/chloroform-like
Vinyl chloride	Faintly sweet

1.3.4 Hedonic Tone

Hedonic tone measures the relative pleasantness of an odor as the human nose perceives it. Hedonic tone is a very subjective term since what may seem to be a pleasant smell to one person might not be agreeable at all to another person (CalRecycle 2019). Thus, it all depends on personal sensitivity and perception of odor that normally vary according to an individual's age, gender, living environment, etc. (Pearce et al. 2006). A 9-point scale (**Table 10**) is used to describe hedonic tone ranging from -4 to +4, with -4 being an extremely unpleasant odor, 0 being neutral and +4 being an extremely pleasant odor (Li et al. 2019). When the intensity of an unpleasant odor increases, the value for hedonic tone goes further down in the negative direction for that compound (Sucker et al. 2008).

Table 10: Verbal descriptions associated with each point of the hedonic scale of odors (Li et al. 2019)

Hedonic Tone	Verbal Description	Examples
+4	Extremely pleasant	Vanilla
+3	Moderate pleasant	Apple
+2	Pleasant	Hay
+1	Slightly pleasant	Mushroom
0	Neutral	Carbon dioxide
-1	Slightly unpleasant	Butyric acid
-2	Unpleasant	Iso-valeric acid
-3	Moderate unpleasant	Mercaptans
-4	Extremely unpleasant	Hydrogen sulfide

1.4 Health Hazards

Prolonged exposure to odor-causing compounds potentially poses a threat to human health, particularly to nearby residents and those with pre-existing conditions such as individuals who are elderly, children, or immuno-compromised (De Feo et al. 2013). The most common symptoms of odor exposure include eye, nose, and throat irritation, certain types of congenital anomalies, olfaction disorder, headache, nausea, cough, palpitations, shortness of breath, stress, drowsiness, and alterations in mood (Elliott et al. 2009, NYSDOH 2011, NIH 2011, ATSDR 2017, CDC 2019). Palmiotto et al. (2014) reported

that, among other odorants, hazardous air pollutants (HAPs) and non-methane volatile organic compounds (NMVOCs) emitted from LFG are primarily responsible for adversely affecting the health of individuals living near landfills. Exposure to VOC emissions is found to increase the risk of lung and colorectal cancer (Saalberg & Wolff 2016; Di Lena et al. 2016). Nuisance vectors (such as flies, mosquitos, ticks, etc.) and their associated diseases also adversely affect people living near landfills (Howard 2001). A study by Sakawi et al. (2011) on 190 respondents living within a 2 km radius of a landfill in Malaysia found that malodor from landfills had adversely impacted 80.5% of the respondents' health, whereas 83.7% of respondents reported inability to maintain their quality of life due to the malodor. Nearly 60% of the respondents moved out to escape the perceived health threat associated with the landfill odors (**Figure 4**).

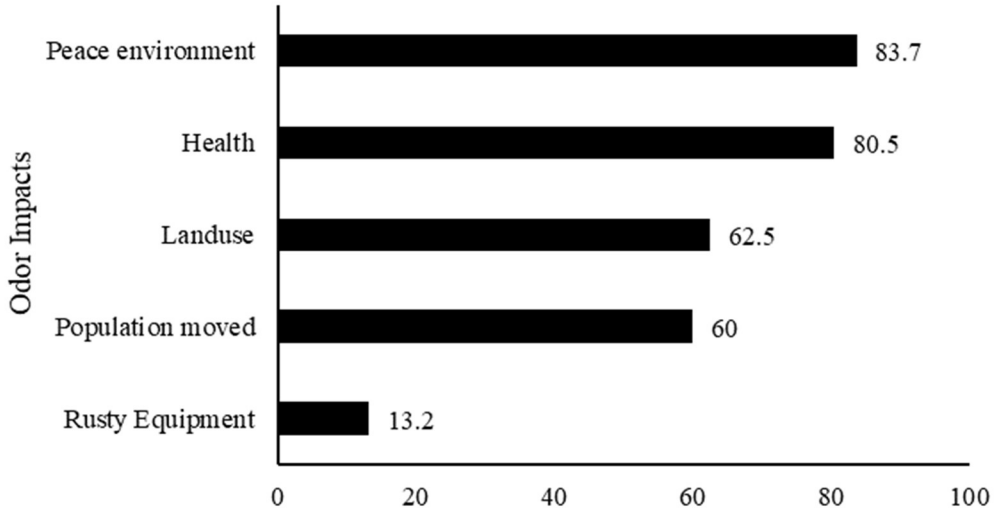

Figure 4: Percentage of respondents impacted by landfill odors in Malaysia in each category (Sakawi et al. 2011)

Hydrogen sulfide, one of the most odorous gases encountered in landfills, is associated with various human health effects at various exposure levels (ATSDR 2001). While evaluating the relationships between hydrogen sulfide odor and health outcomes, a study conducted by Heaney et al. (2011) on 23 individuals living within 0.75 miles of a regional landfill in Orange County, NC, found that odor largely contributes to altering the daily activities, moods, and health conditions of those residents. **Table 11** shows the relationship between twice-daily odor reports, mood states, irritants, and physical symptoms, organized by decreasing binary odor odds ratio.

Table 11: Different mood states along with the number of recorded instances and odds ratio of such cases, together with 95% CI (Heaney et al. 2011)

Outcome	No. of records	Binary odor OR[a] (95% CI)
Mood states		
Angry, grouchy, ill-tempered	336	3.9 (1.8, 8.5)
Gloomy, blue, unhappy	358	3.1 (1.6, 6.1)
Nervous or anxious	420	2.5 (1.3, 5.0)
Stressed	558	2.1 (1.2, 3.8)
Weary, bushed, exhausted	469	1.8 (0.8, 4.0)
Active, energetic, peppy	415	0.6 (0.2, 1.5)
Confused, poor concentration	262	0.3 (0.03, 2.1)
Mucous membrane irritation		
Burning eyes	368	5.3 (2.5, 11.6)
Burning nose	386	5.0 (2.5, 10.2)
Burning throat	309	3.3 (1.5, 7.1)
Upper respiratory		
Runny nose	555	2.6 (1.4, 4.9)
Cough	334	2.0 (1.0, 3.9)
Difficulty breathing	310	1.9 (0.9, 4.2)
Sore throat	359	1.9 (0.8, 4.2)
Gastrointestinal		
Dizzy or lightheaded	176	4.1 (1.3, 12.5)
Headache	387	3.3 (1.5, 7.4)
General ill feeling	310	2.7 (1.1, 6.6)
Nausea or vomiting	127	2.7
Diarrhea	164	2.6 (0.2, 29.5)
Loss of appetite	181	0.7
Skin		
Skin irritation	187	4.7 (1.1, 21.0)
Skin boils	166	4.6 (0.6, 37.8)
Ringing in ears	176	2.9 (0.6, 14.2)
Itchy skin	295	1.9 (0.6, 5.6)
Skin rash	210	1.2 (0.2, 6.3)

[a] Conditional fixed effects logistic regression models adjusted for time of day (morning/evening) of diary record. OR= odds ratio; CI= confidence interval.

1.5 Nuisance Odor Complaints

The presence of a landfill near residential properties can lead to a sharp increase in odor complaints that eventually deteriorate the relationship between the landfill authorities and the surrounding population (Vidovic 2018). This situation may lead nearby residents to file recurring complaints of nuisance odors (ATSDR 2016), which may even result in major investments due to re-siting, litigation, enforcement, and mitigation costs (Jedra 2022). As an example, in March 2019, the residents living near the Grand Central Sanitary Landfill

in Pen Argyl, PA, filed two lawsuits in two consecutive months due to offensive odors originating from the facility in which 90 complainants requested at least $4.5 million of reimbursement by the landfill authority (Salamone 2019). In a separate case, residents of Slate Belt, PA, asked for $100,000 in reimbursement against the landfill authority for creating a public nuisance arguing that the odors resulted in more than $5 million in damages. Similar odor-complaint related scenarios have become more common across the United States for decades. The issue of odor complaints is more acute in urban areas compared to rural areas due to increasing population growth and sprawling development around urban solid waste management facilities (Ying et al. 2012). As reported in several studies (Li et al. 2018, Seok & Missios 2007, Hite et al. 2001), housing prices are also adversely affected by the presence of nearby landfills. While conducting a study in Dryden, NY, Baker (1982) found that the property values reduced by 21% within a range of 0.25 miles from the landfill, while the reduction was only 0.55% at 2 miles from the landfill. Another study by Nelson et al. (1992) in Minnesota reported that housing prices decreased by 6.2% for each mile closer to the landfill. The deterioration of property values in nearby residential areas is more acute in places that are surrounded by a high-volume landfill (accepting over 500 tons of waste per day) rather than a low-volume one (Ready 2010). Ready (2010) found that high-volume landfills cause property values to decrease up to 12.9%, while low-volume landfills lower property values by 2.5%. While conducting studies on the socio-economic status of the population living nearby landfills, it was found that landfill sites are disproportionately present in areas that are heavily populated with people of color where the property values are already low (Martuzzi et al. 2010; Norton et al. 2007). This situation typically makes those populations more vulnerable to the effects of landfill odors compared to their more affluent counterparts.

1.6 Odor Measurement Techniques

Odor characterization and quantification are crucial components for odor measurements. However, the task of objectively quantifying odor emissions has turned out to be a major challenge. Without proper objective quantification, it is not possible to set legal boundaries for odor emission limits. State-of-the-art odor measurement techniques today are carried out by sensorial or analytical methods. Sensorial techniques use the human nose to carry out the sensory evaluation of the properties of an odor (Lewkowska et al. 2015). These techniques include dynamic olfactometry and field olfactometry. Analytical methods of odor measurement include the usage of complex instruments such as electronic nose technology, gas chromatography/mass spectrometry (GC/MS), atmospheric dispersion modeling, etc. The following subsections address the advantages and limitations of the current state-of-the-art odor measurement techniques.

1.6.1 Dynamic Olfactometry

Dynamic olfactometry is the most common quantitative measurement of odor. It uses a group of trained human panelists to detect the presence of odorants in the ambient air (as shown in **Figure 5**). The reason behind using human olfaction for odor quantification is that human noses are often more responsive in recognizing a smell than the most common chemical detectors available (Delahunty et al. 2006). Since the human perception of smell is largely a subjective issue, multiple panelists are selected according to their sensitivity to *n*-butanol in the range of 2.0×10^{-8} to 8.0×10^{-8} mol/mol and within a specified standard

deviation (Laor et al. 2014). In dynamic olfactometry, a sample of odorous air is collected at the source in Tedlar bags (refer to **Figure 5**) or other cylinders (Brattoli et al. 2011). The sample is then diluted with odorless fresh air, which is directed towards the panelists' noses through a device called an olfactometer. The concentration of the odorant gas in the air is slowly increased (i.e., the dilution of the odorant is slowly decreased) until all members of the panel can perceive the smell of the odorant, which is considered as the threshold of the odorous emissions (St. Croix Sensory 2005; Baltrėnas et al. 2012). The concentration of the odorant is then determined by applying sophisticated statistical methods (Laor et al. 2014). During this process, the panel may also be asked to rate the odor based on its intensity, quality, and irritation intensity, etc. (Schiffman et al. 2015).

Figure 5: Tedlar bags used to collect sample air in dynamic olfactometry (left) and trained panelists sniff odorous samples in the laboratory collected in the bag (right) (Mennenbeck 2014)

The most obvious limitation associated with dynamic olfactometry lies in its innate subjectivity, which may introduce inaccuracy and lack of reproducibility (Belgiorno et al. 2013). The result may vary substantially if a different panel is selected. Dynamic olfactometry is also costly and results are difficult to reproduce (Yuwono & Lammers 2004). It is also unsafe to practice when the odorants contain poisonous gases as it would threaten the panelists' health. Although it is possible to determine odor concentration with this method, it is not possible to determine the level of the nuisance the odorant creates for the nearby residents. The method is also unable to identify the effective contribution of individual components present in an odorant mixture (Brattoli et al, 2011). Moreover, it cannot identify the individual constituent of the odorants separately in the case a mixture of odor is present. Thus, in a landfill, where several odorants may be perceived simultaneously that create an unpleasant odor, dynamic olfactometry cannot be used to identify the individual constituent odorants that make up the mixture in such a case.

1.6.2 Field Olfactometry

Field olfactometry is accomplished using a device known as a field olfactometer such as a Nasal Ranger®, Barneby box, or mask scentometer (as shown in **Figure 6**) (Newby & McGinley 2004; Sheffield et al. 2004; Henry et al. 2011b; Laor et al. 2014). With this device, the field assessors adjust the ratio of odorous (non-filtered) and non-odorous (filtered) air. The Dilution to Threshold (D/T) ratio refers to the number of dilutions at which an odorant can be detected under field conditions (Laor et al. 2014). The higher the D/T value, the stronger the field odor is perceived by the field assessor. The advantage of field olfactometry over dynamic olfactometry is that the readings can be obtained in the field with scentometers instead of having to take the sample back to a lab, which introduces another potential error (Brattoli et al. 2011).

Figure 6: Barneby box (left) and nasal ranger (right) used in field olfactometry (McGinley & McGinley 2004; Laor et al. 2014)

Similar to dynamic olfactometry, field olfactometers can cause odor fatigue in the field due to the difficulty of not exposing the device to the odorous environment before the actual readings are taken (Henry et al. 2011b; Bokowa 2010b). The readings obtained can be three times lower than that of lab olfactometry, which might be caused by insufficient air purification through the cartridges of the instrument or due to the assessors' sensitivity not completely recovered between the dilutions (Bokowa 2010b). Also, the readings in the field can tend to vary widely with shifts in the odor plume intensity and wind speed/direction (Brattoli et al. 2011). Moreover, the presence of background odors, synergistic effects, masking agents, etc. are all limiting factors that complicate the quantification process in field olfactory (Henry et al. 2011; Bokowa 2010).

1.6.3 Electronic Nose (Artificial Olfactometry)

The electronic nose (E-nose) is an instrument that allows real-time odor monitoring by means of an array of electrochemical sensors coupled to a data acquisition system and pattern recognition software that was developed to mimic the human olfactory system (Brattoli et al. 2011; Yuwono & Lammers 2004). The multiple sensor arrays of the E-nose consist of a number of chemical, electrical, optical, mechanical, and/or piezoelectric sensors along with a transducer (as shown in **Figure 7**) that act together to mimic the olfactory receptor network inside the human nose. (Brattoli et al. 2011; Yuwono & Lammers 2004). When an odorant is passed through the instrument, the sensors detect it through a chemical change as they interact with the compound. The chemical change is

then converted to an electronic signal by means of a transducer (Brattoli et al. 2011). This electronic impulse is then captured by the data acquisition system, similar to the function of human olfactory nerves. The signal is then processed by the pattern recognition software, which acts as a "brain" of the device. Each distinctive odor stimulus generates specific signals known as fingerprints (or smell prints) in the E-nose, which are recorded to create a library of databases that help detect an unknown odorant and measure its concentration (Yuwono & Lammers 2004).

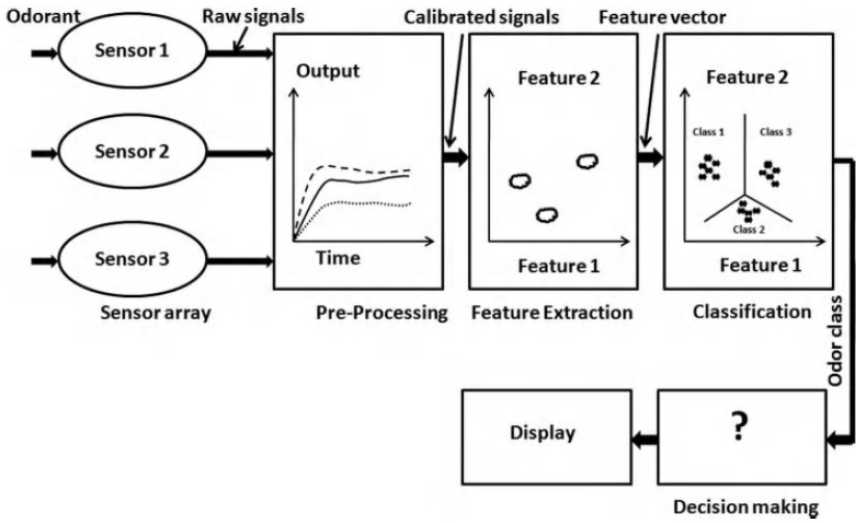

Figure 7: Block diagram showing the various components of an e-nose system (Belgiorno et al. 2013)

Even though the E-nose technology can detect simple and complex odors by replacing the human nose so humans do not have to be present, the calibration of the device is still conducted by laboratory olfactometry measurements, which is again associated with human subjectivity (Delgado-Rodríguez et al. 2012). That is why a possible correlation between the results acquired by electronic nose and by dynamic olfactometry has been reported by Capelli et al. (2008) during an odor emissions monitoring study in ambient air from a solid waste facility in Italy. The other limiting factor of the E-nose technology is that it can only detect odorants having concentrations in the range of 10^{-9} mol/mol, which is much higher than what the human nose can detect, and thus discrimination and quantification of odors existing in low concentrations is not possible with E-nose (Pearce et al. 2006).

1.6.4 Gas Chromatography/Mass Spectrometry (GC/MS)

Gas chromatography (GC) is a separation technique that becomes more powerful when it is paired with a mass spectrometry (MS) detection technique. GC/MS allows the identification and quantification of odorants even when the constituents of an odorant mixture are present in very small concentrations. The principle of this technique is based on separating the odorant compounds from the odor mixture according to their affinity with the stationary phase in a gas chromatographic column. As the compounds present in the sample progress through the separation column, they emerge and are then identified by their characteristic mass to charge ratio and quantified using the mass spectrometer

detector, as shown in **Figure 8** (Conti et al. 2020; Yuwono & Lammers 2004). In the detector, the separated compounds are bombarded with ions to break them up into their characteristic building blocks identified by the mass to charge ratio. The results obtained are in the form of a mass spectrum, which is then compared to a reference library to identify and quantify the specific compound.

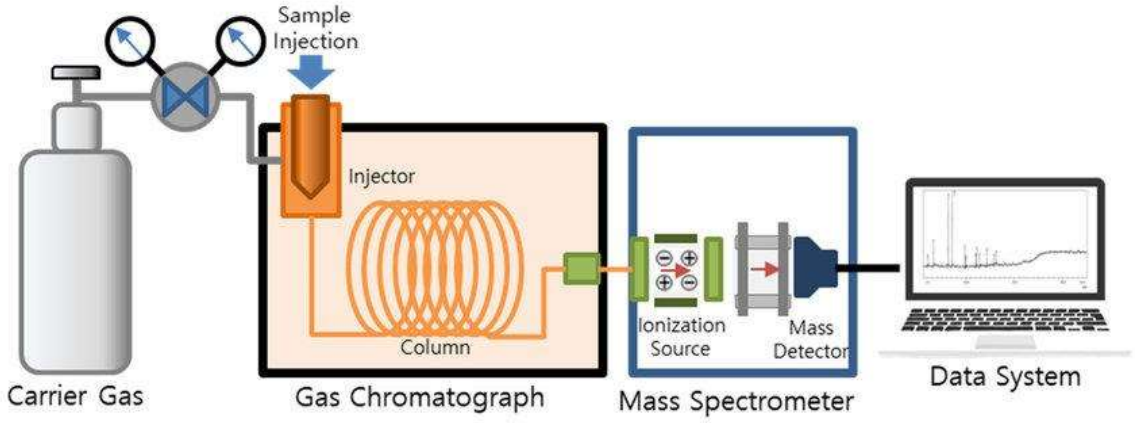

Figure 8: Diagram showing the pathway of the odorants through the Gas Chromatography/Mass Spectrometry (GC/MS) (Kim and Choi 2020)

The major disadvantage associated with GC/MS is that even if it can measure the concentration of the constituent odorants present in a mixture of odor, it cannot give information about the actual intensity of the odor or synergistic effects (Davoli, 2004; Zarra et al., 2007b; Belgiorno et al. 2013). Many times, the intensity of the odor mixture does not match the concentration of its constituent compounds. Also, there is no direct correlation between odor intensity and the concentration of the constituent odorants. Besides, the technique only works when all components present in the sample can be successfully separated in a gas chromatography column and are already referenced in published libraries of known odorants. Moreover, GC/MS is quite an expensive instrument that requires highly skilled personnel to be able to perform the analysis (Polyakova et al. 2016; Brattoli et al. 2011).

1.6.5 Atmospheric Dispersion Modeling

An atmospheric dispersion model is an analytical method used to predict odor impact at a certain distance and height downwind from the emission source. As an input, the dispersion model requires source odor concentrations, which are typically determined using subjective measurements such as human assessment techniques or E-nose measurements. Thus, the results obtained from the dispersion model largely depend on the accuracy of the source concentration measurement acquired by a subjective measurement technique that also unrealistically assumes the meteorological factors to be constant, including temperature, humidity, pressure, wind speed, direction, etc. (Laor et al. 2014). Also, dispersion models can not accurately predict the number of dilutions required to reach the threshold concentration at a specific distance from the source. Thus, odor annoyance cannot be accurately predicted unless the relationship between odor concentration and perceived intensity and offensiveness is quantified with certainty (Laor et. al, 2014). The

other shortcoming of atmospheric dispersion modeling is that such models are odorant specific and non-quantitative (calibrated using a subjective method).

1.6.6 Limitations of the State-of-the-Art Odor Measurement Techniques

Although a number of odor detection techniques are available to detect and measure the concentration of individual odor-causing compounds at very low detection limits with rapid response times, most of them have their own shortcomings as well (Liu et al 2013; Sankaran et al. 2021). No one single technique is able to perform all forms of analysis, and most of them only work for specific isolated odorants (Delgado-Rodríguez et al. 2012; Laor et al. 2014). As an example, Carlson et al. (2006) developed a chemical sensor using molecular imprinting technology that can detect fluorene at a very low concentration level (10 parts per trillion) but was unable to detect its chemical analogues such as naphthalene, fluoranthene, or anthracene. Also, all the conventional techniques discussed in the previous sections are associated with some degree of human subjectivity in the analysis (Lebrero et al. 2011). Moreover, most methods are overly complex as well as expensive even though they do not always effectively characterize odor strength or intensity and thus are essentially non-quantitative. **Figure 9** summarizes the pros and cons of the most current state-of-the-art odor measurement techniques.

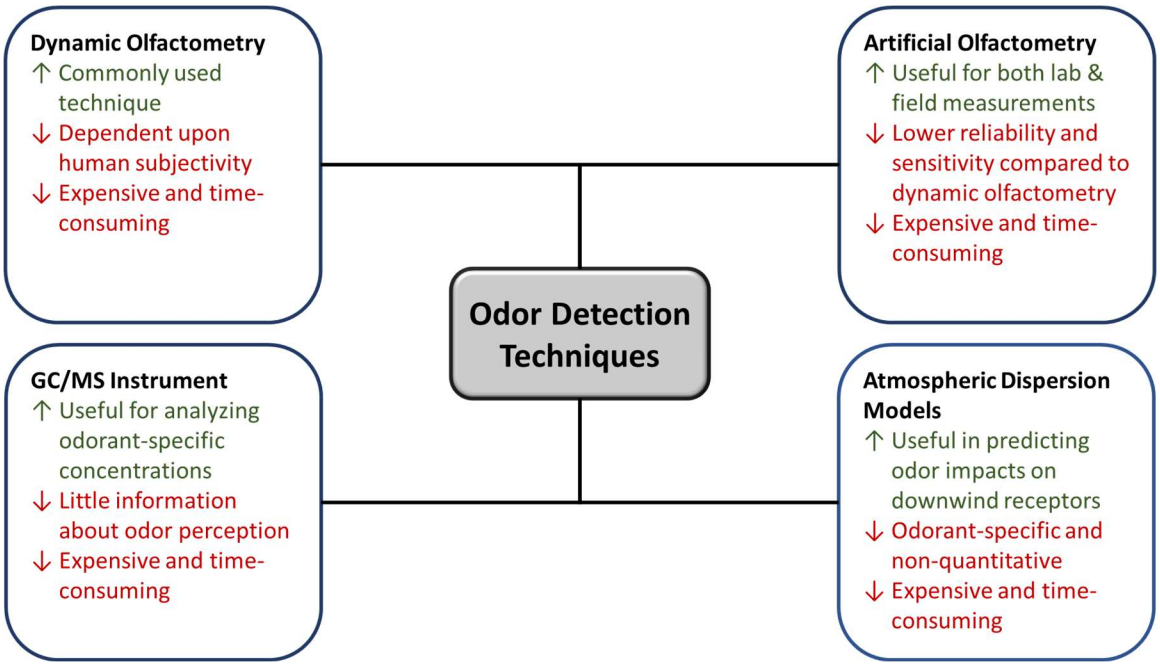

Figure 9: Pros and cons of the state-of-the-art odor detection techniques (Meeroff and Rahman 2021)

Even though great strides have been made in the past few years in the field of odor science, research is still needed to develop an objective odor measurement technique that can overcome the uncertainties associated with the conventional techniques with regard to odor quantification and also do so at a reasonably low cost. Such initiatives will allow regulatory agencies to establish verifiable odor standards and odor limits for industrial facilities based

on objective regulatory frameworks. Before proposing a solution to this issue, it is necessary to understand how the sense of smell actually works in the human body, which will be discussed in detail in the following sections. The widely accepted chemical theory of the human sense of smell explains the mechanism of chemical binding to specific protein receptors based on which technology for objective quantification of odors can be developed without subjective interpretation.

1.7 Human Olfaction Science

Humans can detect up to 10,000 odors and are able to distinguish between odorants whose difference in concentration varies by as little as ±7% (Bushdid et al. 2014; Sela & Sobel 2010). Even the slightest change in the molecular structure of the odorants can be perceived by humans. For example, odorants having an equal number of carbon atoms but from different functional groups or belonging to the same functional groups but having a difference in chain length of only one carbon can be distinguished by the human sense of smell (Sela & Sobel 2010). However, the mechanism behind the human perception of smell is still not fully understood, even though scientists believe olfactory receptors play a vital role in the response to different odors (Bothmer 2006). The complete process of the human olfaction mechanism is summarized in **Figure 10**.

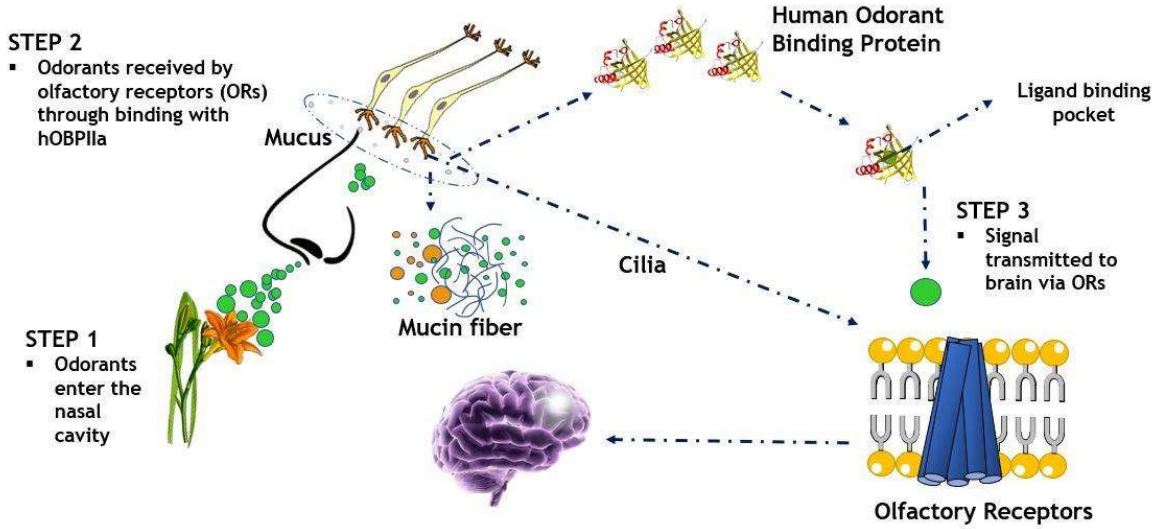

Figure 10: Illustration of the mechanism of the sense of smell involving the action of odorant binding proteins (OBPs)

Briefly, after inhalation, odorant molecules first enter into the nasal cavity and pass through a series of small bones known as turbinates (Trotier et al. 2007). Deep inside the nasal cavity, a nasal mucus surrounds the olfactory membrane (less than 1 square inch in size) at the surface of the nasal epithelium (Tegoni et al. 2000). In this mucus, there are mucin fibers that regulate which molecules get to enter further and which do not, using several filtering mechanisms. In the olfactory membrane, there are small hair-like cells known as cilia that connect the olfactory neurons or olfactory receptors (ORs). The human nasal cavity contains 10-20 million olfactory neurons (Van Riel et al. 2015) that interact with odorant molecules and convey the sensation of smell through the olfactory bulb in the form of electric signals to the brain (ASTDR 2016). However, before reaching the neurons, the

odorant molecule must pass the barrier of hydrophilic mucus. Since odorants are typically hydrophobic, they need a vehicle to be conveyed through the mucus to reach the neurons (Tegoni et al. 2000). Along with other biological compounds and enzymes, nasal mucus contains human odorant binding proteins (hOBPs) that bind with these odorant molecules and facilitate their transport towards the cilia before they reach the olfactory receptors (Heydel et al. 2013, Schiefner et al. 2015). The odorant binding proteins have a large hydrophobic ligand-binding pocket inside their molecules where they trap the odorants. As soon as the receptors detect the odorants, a signal is sent to the brain to build an olfactory image (Heydel et al. 2013). This is how humans perceive the sense of smell.

1.8 Odorant Binding Protein (OBP)

Odorant binding proteins (OBPs) are part of the lipocalin superfamily and are secreted in high concentrations (10 mM) in the nasal epithelium (Heydel et al. 2013). They have the ability to form reversible bonds with volatile chemicals such as airborne odorants with micromolar affinities and are known to have dissociation constants in the micromolar range (Briand et al. 2002). Additionally, OBPs have been found to convey inhaled odorants toward the olfactory neurons quite well and play a role in selecting or deactivating odorant molecules (Brind et al. 2002). It is crucial to distinguish between OBPs and other proteins since most of the proteins that are part of the lipocalin superfamily can also bind with hydrophobic molecules.

Vertebrate and insect OBPs are quite dissimilar in their structural pattern. However, their role in olfaction has been shown to be similar (Wei et al. 2008). In general, there is less than 20% similarity among the amino-acid sequence between the members of the lipocalin superfamily (Tegoni et al. 2000). Vertebrate OBP has a generic structural pattern where 8 stranded antiparallel β-barrels are bound on both sides with an α-helix (Briand et al. 2002). A central apolar cavity, “calix”, is present inside the barrel within which odorant binding takes place in the ligand-binding site. Since OBPs with varying amino acid sequences show broad binding activity in the same animal species, they can bind with odorants of different chemical structures. OBPs have been observed to be monomers, dimers, or heterodimers and have molecular weights in the range of 18~20 kDa (Heydel et al. 2013; Briand et al. 2002). These subtypes are mostly acidic (pH 4~5); however, a few exhibit basic or neutral states (Heydel et al. 2013).

1.8.1 Odorant Interactions with the OBPs

OBP was theorized to be an odorant carrier when Pelosi et al. (2014) discovered that bovine OBP (bOBP) can bind with pyrazine (2-isobutyl-3-methoxypyrazine), a bell-pepper odorant having a low detection threshold. Later on, binding affinity was observed in the case of bOBP and porcine OBPs (pOBPs) for medium-sized hydrophobic odorants (Tegoni et al. 2000). The dimer bOBP was considered the prototypic OBP. In this case, the naturally occurring endogenous ligands within the inter-dimer open cavity are substituted by two odor molecules (Spinelliet al. 1998; Paolini et al. 1999). The monomeric pOBPs are different from bOBP in that the pOBPs do not hold any natural ligand within their β-barrel cavities; additionally, they are reported to have one binding site for each monomer (Paolini et al. 1999). While the cysteine residue commonly observed in most OBPs exists as a

disulfide bridge for pOBPs, it is completely missing in bOBP (Paolini et al. 1999). The 3-dimensional structure of bOBP (left) and pOBP (right) is shown in **Figure 11**.

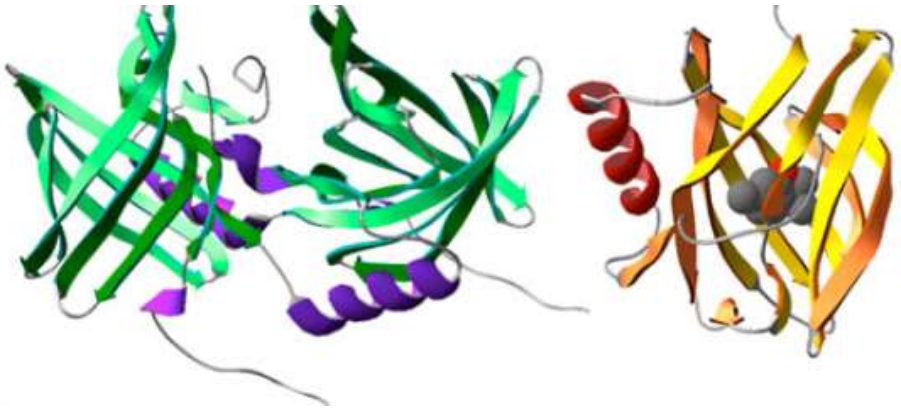

Figure 11: Tertiary structure of bovine OBP (bOBP), (left) and porcine OBP (pOBP), (right) modeled using DeepView software (Pelosi et al. 2014)

Researchers have demonstrated that heterocyclic derivatives have the highest affinity towards OBPs, while fatty acids with short-chain, spherically-shaped terpenoids (such as camphor and its analogues) have less affinity (Tegoni et al. 2000). Thiazoles, pyrazine, terpenoids, menthol, thymol, aliphatic alcohols, and aldehydes have dissociation constants in the range of 0.1-1.0 μM with OBPs which makes for good affinity (Tegoni et al. 2000). Through relative fluorescence intensity in displacement assays with rat OBPs, it has been established that each type of OBP binds with a specific class of odorants. For instance, rOBP-1 tends to bind with heterocyclic compounds (e.g., pyrazine and its derivatives), rOBP-2 has an affinity for long-chain aliphatic aldehydes as well as carboxylic acids and rOBP-3 usually interacts with odorants having a ring structure (Briand et al. 2002).

1.8.2 Human Odorant Binding Protein-2A (hOBPIIa)

Two possible odor binding protein genes, which are 95% identical, have recently been discovered in humans, hOBPIIa and hOBPIIb (Briand et al. 2002; Tegoni et al. 2000). The hOBPIIa gene has been found in the nasal mucosa, lung, lachrymal, and salivary glands, whereas hOBPIIb gene has been found mainly in the genital sphere organs (e.g. prostate and mammary glands) (Tegoni et al. 2000; Lacazette et al. 2000). The amino acid sequence of hOBPIIa and rat OBP-2 is 45.5% identical, whereas hOBPIIb is 43% identical to that of human tear lipocalin-1 (Heydel et al. 2013). The monomeric hOBPIIa contains a central eight-stranded antiparallel β-barrel (strands A–H) with a C-terminal α-helix, as well as a traditional lipocalin fold similar to all other OBPs as shown in **Figure 12** (Schiefner et al. 2015). Furthermore, another short β-barrel (strand I) at the downstream of the α-helix, which is slightly antiparallel to strand A, and a disulfide bridge which is located between cys59 and cys151 have been detected in hOBPIIa. Inside the β-barrel, the entire cavity holds a positive charge, specifically at the entrance of the loop region, which is most commonly observed for all amino acid side chains pointing toward the cavity (Schiefner et al. 2015). OBPs are generally acidic in nature; however, the measured isoelectric point of a recombinant hOBPIIa manufactured by Briand et al. (2002) while characterizing its odorant binding activity was found to be 7.8 (neutral).

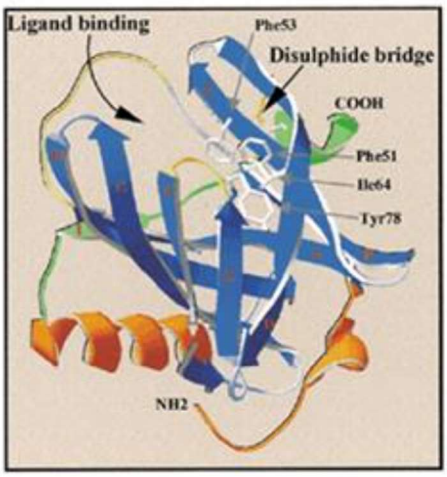

Figure 12: Tertiary structure of hOBPIIa. β barrels, α-helices and disulfide bridge are indicated in blue, green, and yellow respectively (Lacazette et al. 2000)

1.8.3 Odorant Affinity to hOBPIIa

hOBPIIa is capable of binding a wide variety of hydrophobic odorants having different structures and sizes with affinities in the micromolar range due to the presence of its remarkably large ligand-binding cavity inside the β-barrel. However, comparatively low affinity has also been observed for some very strong odorants such as 2-isobutyl-3-methoxy pyrazine and eugenol (K_{diss} > 10 μM) (Schiefner et al. 2015; Briand et al. 2002; Heydel et al. 2013). Due to having very strong affinity for aldehydes (e.g., undecanal: K_{diss} ~ 0.3 μM, lilial, the odor of the lily of the valley: K_{diss} ~ 0.5 μM, and vanillin: K_{diss} ~ 1 μM) and large chain fatty acids (K_{diss} ~ 0.3 μM), a more restricted binding specificity has been observed for hOBPIIa compared to porcine OBP and rOBP-1 or rOBP-3 (Heydel et al. 2013; Briand et al. 2002). Moreover, the affinity for aldehydes is even stronger with respect to acids due to the presence of a lysine residue (Heydel et al. 2013) located at the edge of the pocket that binds strongly with aldehydes by forming a preferential hydrogen bond (shown in **Figure 13**). As the molecular size of the bound odorant increases, the affinity of hOBPIIa for aldehyde compounds (either aliphatic or aromatic) also increases (Tcatchoff et al. 2006). When the odorants are transferred to olfactory receptors (ORs) from the cavity, water enters the cavity, recovering the chemical integrity of lysine and aldehydes (Charlier et al. 2009).

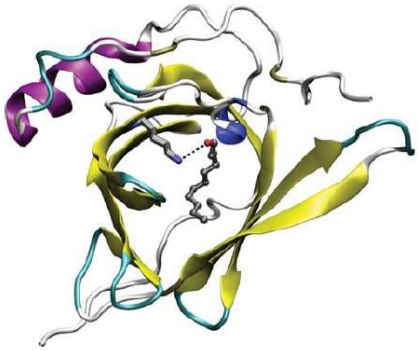

Figure 13: Tertiary structure of hOBPIIa bonded with the aldehyde, undecanal (carbon atoms are indicated in grey, oxygen is in red, and nitrogen is in blue), in the middle of the ligand binding pocket (Heydel et al. 2013)

Castro et al. (2021) conducted a study where 60 different odorant compounds (30 pleasant and 30 unpleasant) were tested via molecular docking experiments to determine their influence on the binding energy to hOBP. One of the critical findings of the study was that hOBP would preferentially bind with the pleasant odorants rather than the unpleasant ones, or it may have a tendency to bind with the pleasant odorants displacing the unpleasant ones as the pleasant molecules show higher binding energy ($\Delta G_{binding}$). The binding site and the binding strength are also different for the pleasant and unpleasant odorants. For example, the docking experiment showed the majority of the pleasant odorants bind at the same location which occurs at the top of the β-barrel of hOBP, as shown in **Figure 14** (left); whereas the location of the binding sites varies among the unpleasant odorants. Many bind outside the barrel but at different locations, as shown in **Figure 14** (right).

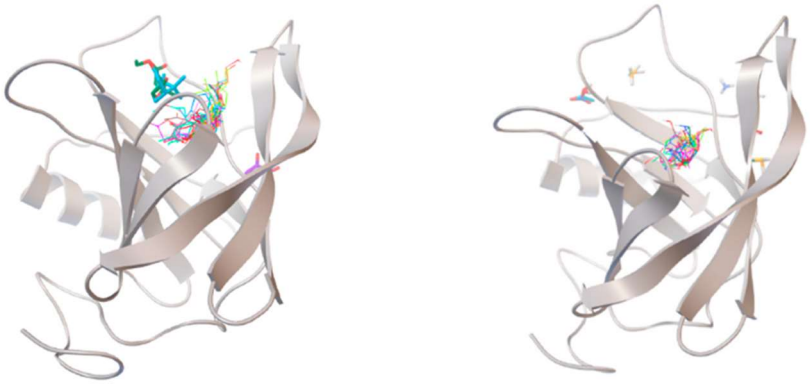

Figure 14: The binding sites of hOBP to pleasant odorants at the top of the β-barrel (left) and the binding sites of hOBP to unpleasant odorants at different locations outside the barrel (right). The odorants in the most populated binding site are represented in diverse color lines, while odorants in other locations are shown in colored sticks (Castro et al. 2021)

The study also found that the molecular weight (MW), the octanol-water partition coefficient (log K_{ow}, that defines the hydrophobicity level), and the vapor pressure (Vp–volatility) are the physicochemical properties that directly impact binding efficiency and correlate with the binding energy ($\Delta G_{binding}$). Also, these properties play a comparatively greater role on the binding energy ($\Delta G_{binding}$) of unpleasant odorants versus pleasant ones. **Table 12** presents various physicochemical properties along with the binding energies ($\Delta G_{binding}$, in descending order) for several unpleasant odorants, some of which are commonly found in landfills. The most volatile unpleasant odorants (higher Vp) in this list are found to have lower binding energy with the protein ($\Delta G_{binding}$ values between -0.6 to -2.8 kcal/mol). Molecules that are hydrophilic (negative log K_{ow} values), especially those that are small, also show lower binding energy, suggesting that these molecules might not even need to bind with the protein to gain access to the olfactory receptors; rather they directly diffuse themselves in the mucus. Toluene, which has the highest log K_{ow} value (2.73) in this table (as it is a pure hydrophobic compound), shows the highest binding energy (-5.7 kcal/mol) indicating that the bond is the strongest among others. Also, hydrocarbons with longer chains show a particularly strong bond with the protein (Castro et al. 2021).

Table 12: Description of unpleasant odorant molecules according to physicochemical and structural characteristics (Castro et al. 2021)

Name and Odor Description	Formula	Molecular weight (MW) (g/mol)	log K_{ow}	Vp	$\Delta G_{binding}$ (kcal/mol)
Hydrogen sulfide (rotten eggs)	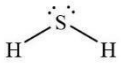	34.08	-1.38	13,376	-0.6
Phosphine (rotten fish/garlic)	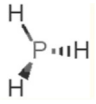	33.99	-0.27	29,300	-0.6
Methyl mercaptan (rotten cabbage)	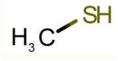	48.11	0.78	1510	-1.1
Ammonia (pungent/sharp)	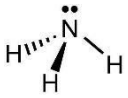	17.03	-2.66	7500	-1.4
Dimethylphosphine (metallic/fish/garlic)	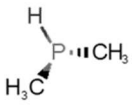	62.05	1.67	760	-1.6

Name and Odor Description	Formula	Molecular weight (MW) (g/mol)	log K_{ow}	Vp	$\Delta G_{binding}$ (kcal/mol)
Chlorine (pungent/irritating)		70.90	0.85	5830	-1.9
Nitrogen dioxide (pungent/acrid)	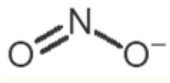	46.006	0.06	720	-2.8
Chloroform (ether-like/pungent)	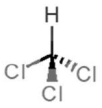	119.37	1.97	197	-2.9
Acetic acid (vinegar-like/pungent)	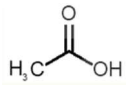	60.05	-0.17	15.730	-3.0
Nitric acid (acrid/suffocating)	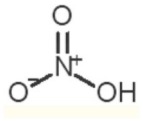	63.013	-0.21	63.1	-3.1
Butyl mercaptan (skunk)		90.18	2.28	45.5	-3.3
Benzyl mercaptan (unpleasant, strong)	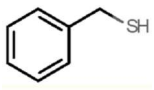	124.20	2.5	0.470	-5.2
Toluene (paint-thinner/pungent)	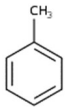	92.14	2.73	28.4	-5.7

1.8.4 OBP-Fluorophore Interaction

A fluorophore is used to understand the interaction of different ligands such as odorant molecules with proteins and to study the properties and structures of the protein itself (Mikhailopulo et al. 2008; Abdurachim et al. 2006; Sreejith et al. 2009; Kazakov et al. 2009). Adding an extrinsic fluorophore, for example, TNS (6,P-toluidinylnaphthalene-2-sulfonate) and fluorescein to a protein can work as effective probes for this purpose, as they do not modify the protein structure or its properties in any way (Kmiecik & Albani 2010). Small-molecule fluorescent turn-on probes are used to detect and monitor enzyme activities such as glycosidases, proteases, lactamases, and kinases (Kobayashi et al. 2009, Sakabe et al. 2012, Xing et al. 2005, Shults & Imperiali 2003). In such a case, the fluorescents react with the enzyme and convert from a non-fluorescent product to a fluorescent one. There are other fluorophores, such as environmentally sensitive fluorophores, that show weak fluorescence in polar environments but strong fluorescence in hydrophobic environments (as shown in **Figure 15**) upon binding with the protein, as reported by Zhuang et al. (2013).

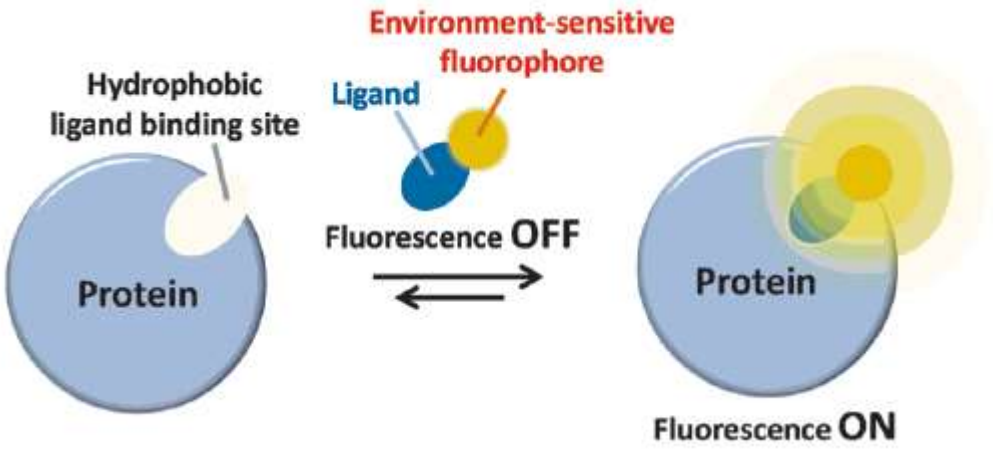

Figure 15: Mechanism of fluorescent turn-on probe where the ligand attaches to the specific hydrophobic ligand binding site of the protein and the surrounding hydrophobic environment allows the environment-sensitive fluorophore to emit strong fluorescence (Zhuang et al. 2013)

The interactions of hOBPIIa with a number of extrinsic fluorophore probes, including DAUDA (11-(5-(dimethylaminonaphthalenyl-1-sulfonyl) amino) undecanoic acid), NPN (N-phenyl-1-naphthylamine), DACA (dansyl-DL-α-(aminocaprylic acid) and ASA ((+)-12-(9-anthroyloxy)stearic acid) have been investigated (Mei et al. 1997; Lechner et al. 2001). DAUDA shows a weak emission intensity with a peak at 490 nm, while DACA, ASA, and NPN have their emission peaks at 475 nm, 425 nm, and 400 nm, respectively (Briand et al. 2002). Studying the spectral properties of probe fluorescence emissions confirmed that the binding site of the recombinant hOBPIIa lies in the hydrophobic ligand-binding pocket within the β-barrel.

1-aminoanthracene (1-AMA) is a fluorophore that is widely used to study the interaction between certain proteins and their ligands, including those belonging to the lipocalin

superfamily (Ramoni et al. 2002; Wei et al.2008). Since 1-AMA is a hydrophobic ligand, it shows a strong fluorescence signal upon binding to a hydrophobic site in a protein. Upon binding with the OBPs, 1-AMA forms a complex that shows a sharp spike in emission intensity upon ultraviolet light excitation, whereas 1-AMA alone in solution does not show such an emission peak when excited by ultraviolet radiation (Silva et al. 2014; Paolini et al. 1999; Briand et al. 2003). Research has also been conducted to observe the interaction of the OBP-fluorophore complex with different alcohols such as ethanol, methanol, and dimethyl sulfoxide while using the alcohols as solvents (Briand et al. 2000). It was observed that the alcohols tended to displace the 1-AMA from the OBP-fluorophore complex in general; however, methanol has a relatively low displacement rate (as shown in **Figure 16**) and thus can be potentially used as a solvent while spectrofluorometrically studying the interactions of OBP-fluorophore complex with other molecules.

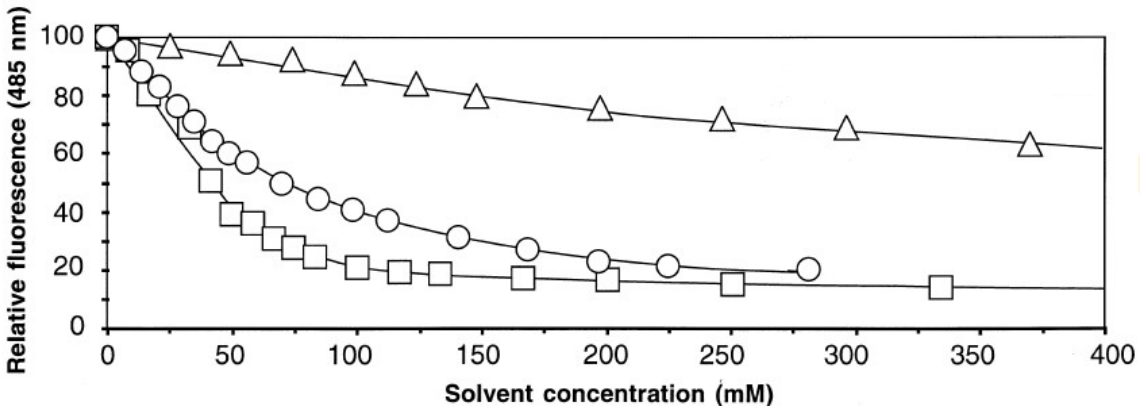

Figure 16: Fluorescence curve of 1-AMA at 485 nm with increasing solvent concentration. 1-AMA is displaced the least by methanol, leading to relatively high fluorescence emission even though the solvent concentration is increased (Triangle: methanol, Circle: ethanol, Square: dimethyl sulfoxide) (Briand et al. 2000)

1.9 Biosensor Development Using OBP

Recently, OBPs have been increasingly used as biosensors for various purposes. There are certain characteristics that make OBPs ideal candidates for use as sensors (Ko et al. 2010). OBPs are thermally stable, which is ideal for environmental monitoring. Also, the presence of an increased concentration of organic solvents has no effect on OBPs in general (Wei et al. 2008). Furthermore, OBPs can easily accommodate site-directed mutagenesis that helps them bind in a certain way with specific compounds (Wei et al. 2008). For example, re-engineered pOBP has been used to monitor polycyclic aromatic hydrocarbons in the environment as they have a good affinity for these compounds and can modify their specificity by changing amino acid residues (Wei et al. 2008). Moreover, OBPs can be readily synthesized from recombinant DNA in bacteria, making commercial availability possible at a relatively low cost.

An effective biosensor needs to be sensitive enough so that it can detect different compounds (Kim et al. 2008; Song et al. 2008; Mirmohseni et al. 2008), and efforts have been made in this regard by researchers to improve the sensitivity of systems relying on biosensors (Choi et al. 2004; Kang et al. 2006; Lee et al. 2009; Kim et al. 2009; Yoon et

al. 2009). As such, OBPs can also be used to boost the sensitivity of olfactory receptor-based biosensors (Ko & Park 2008), which has already been described for a *Drosophila* OBP (Xu 2005). OBPs have also been used for detecting important ligands in complex environments, as described in a work by Lu et al. (2014) where honeybee OBPs were designed to detect ligands found in floral odors and pheromones. Ramoni et al. (2007) investigated the use of advanced nano-biosensors derived from bOBP that can detect the presence of hazardous compounds in airports and other public places. The usage of the protein scaffold of the lipocalin OBP to detect explosives has also been investigated by the same author. Capo et al. (2018) used pOBP as a biosensor to detect BTEX pollutants (e.g. benzene, toluene, ethyl-benzene, and xylene isomers). OBP-based sensors can potentially be used as a screening device to monitor VOCs emitted by organisms as part of a non-invasive medical procedure, as reported by Cave et al. (2019).

Although there is a growing body of research into applying OBPs as a biosensor, none of these usages address the problem of measuring odorant concentration using OBP, especially hOBPIIa. As described in **section 1.6**, most of the currently available odorant measuring techniques depend on subjective methods. The ability to objectivity quantify odorants is crucial to developing enforceable regulations around odor limits, and hOBPIIa can potentially be used as a biosensor in developing such methodologies.

1.10 Odor Detection Using OBP

Silva et al. (2013) first explored the idea of using pOBP to control odor where a cationized cotton surface coated with pOBP was used to mask the smell of cigarettes by delaying the release of citronellol, a fragrance often used in perfumes. In that study, the concentration of the odorant molecule (citronellol) that caused the fluorescence (1-AMA) to decay to half-maximal intensity was measured spectrofluorometrically. This opened the door to the possibility that OBPs can be used effectively to trap unpleasant odors from fabrics and can be more efficient than cyclodextrins in this regard (Silva et al. 2014). Furthermore, increasing the temperature was found to increase the affinity of OBP towards a particular fragrance. This has practical implications, such as for textiles, where treating clothes with OBP can be a way to make perfumes last longer than usual as the temperature rises from ambient to human body temperature. An artificial olfactory sensing device using the OBP of anthropophilic mosquito (*Anopheles gambiae*, Ag) functionalized on a free-standing silicon nanowire array (AgOBP-SiNW) has been developed by Gao et al. (2020) that recognized various human-derived VOCs at a very low detection level (down to parts per billion) by electric readouts, which opens new possibilities of using OBP for developing a human body odor sensor array.

The usage of OBPs in new and exciting ways has led to the idea that it could be used as an effective biosensor in objectively quantifying odorants in real air samples using spectrofluorometry (Rahman 2020). As mentioned earlier, the large ligand-binding cavity inside the β-barrel of hOBPIIa allows it to bind with a diverse array of hydrophobic odorants (Briand et al. 2002). Also, since the protein is non-specific, it binds with a large number of volatile odorants of varying concentrations (Pelosi 2001). Thus, by adding a biomolecular fluorescent marker with the protein, for example, 1-AMA, the odorant-protein binding can be quantified (as shown in **Figure 17**) using a fluorescence

spectrofluorometer (Rahman 2020), much like the monoclonal antibody analytical method that was developed for enumeration of specific microorganisms (Straub and Chandler 2003). Since the human nervous system processes odor intensity based on the number of bound receptor sites, and the biosensor protein-fluorescent response is concentration-dependent, this new technology will allow for authentic quantification of odors without subjective interpretation.

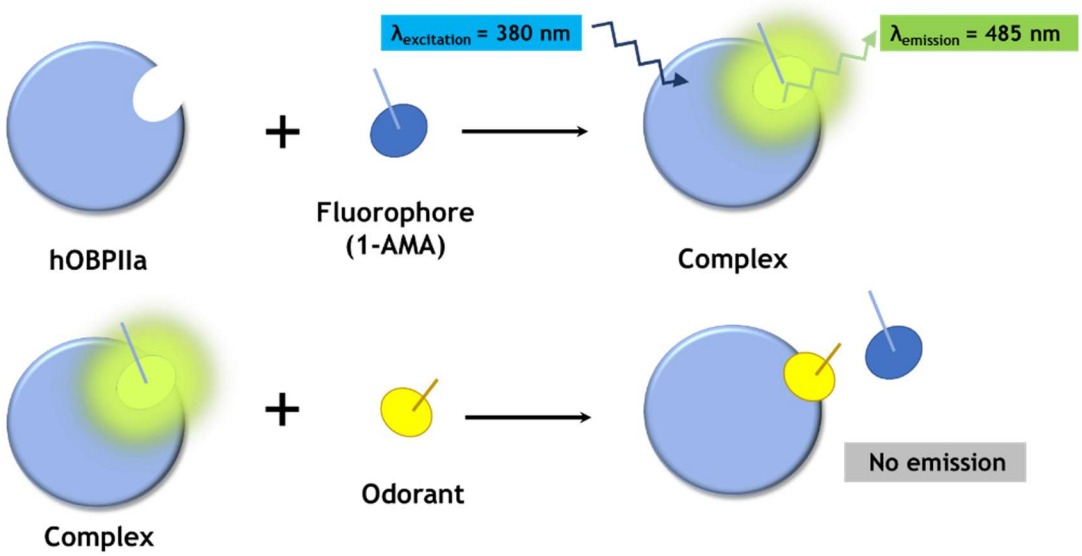

Figure 17: Mechanism of quantifying odorants with hOPBIIa by means of spectrofluorometric analysis. First the protein combined with fluorophore (1-AMA) forms a biosensor complex which emits light at 485 nm wavelength upon exciting at 380 nm in a spectrofluorometer. As the odorant molecules are exposed to this complex, the protein molecules release the fluorophores and instead bind with the odorants, resulting in a decrease in fluorescence intensity which can be used to determine how much odorant has actually combined with the protein (i.e., concentration of the odorants) (Rahman 2020)

Another important aspect of the application of odor binding protein as a biosensor is the reversibility of the reaction, which opens up the possibility of regenerating the spent biosensor (**Figure 18**). Although OBPs have been used in detecting various classes of odorants, the protein has only been used in a one-time approach with no attempts made to induce the release of the odorant such that the protein can recombine with the fluorophore to reset the initial biosensor molecule. If the reaction is reversible in this way, then the cost for commercial uses of such biosensors can be dramatically reduced.

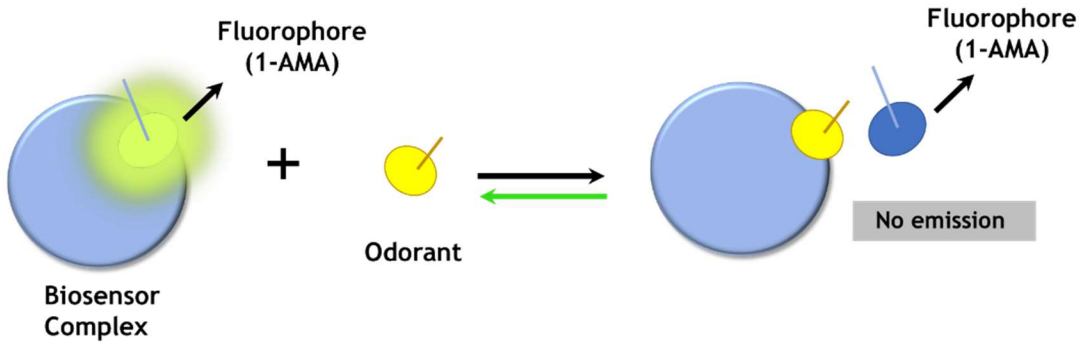

Figure 18: In case of a reversible reaction, the protein-fluorophore bond can be recreated to increase the fluorescence intensity to its initial level, allowing the reuse of the sensor for another odorant-protein binding assay

The preliminary study already conducted by Rahman (2020) showed that combining hOBPIIa with 1-AMA at a 1:1 ratio (1µM hOBPIIa: 1µM 1-AMA) in a Potassium Phosphate-KOH buffer solution forms a biosensor complex that shows a sharp emission peak at 485 nm upon exciting at 380 nm (yellow line in **Figure 19**). The optimum concentration ratio of hOBPIIa to 1-AMA was verified by Roblyer (2017) to be 1:1. Fluorescence analysis conducted on all the individual components of the biosensor complex (i.e., Potassium Phosphate-KOH buffer, 1 µM 1-AMA in buffer, 1 µM hOBPIIa in buffer) showed that there was no peak near 485 nm for any of the component curves (**Figure 20**), affirming that the protein-fluorophore complex (hOBPIIa:1-AMA) accounts for the high emission intensity at that wavelength.

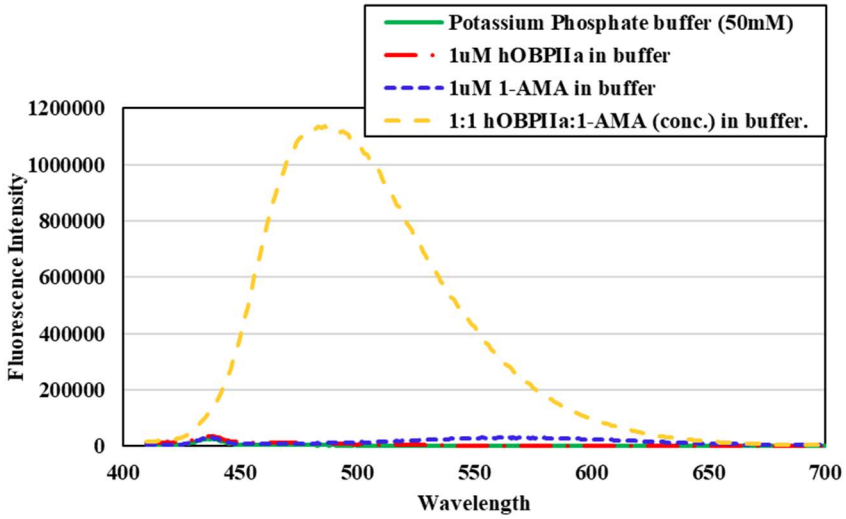

Figure 19: Spectrofluorometric emission spectra of the biosensor solution and corresponding components individually. The complete biosensor solution (mixture of hOBPIIa and 1-AMA in the buffer) showed a sharp emission peak (greater than 1,100,000 counts per second or cps) near 485 nm wavelength (yellow line) which is 2 orders of magnitude larger than the fluorescence intensity obtained for 1-AMA solution alone in the buffer (blue line)

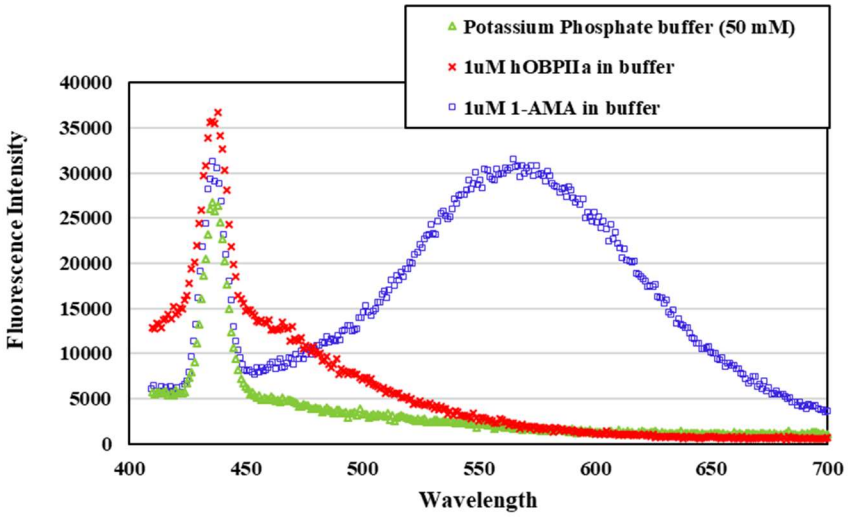

Figure 20: Close-up of the fluorescence intensity curves of the individual components of the biosensor complex, except the complete biosensor (Note that the scale of the y-axis is different for the two graphs) (Rahman 2020)

Earlier work (Roblyer 2017; Rahman 2020) found that the emission intensity of the biosensor complex decreased as it was exposed to the odorant gases. A number of commonly found odorant gases in landfills, including hydrogen sulfide, ammonia, methyl mercaptan, etc. as well as mixtures of gases (Mixture 1: hydrogen sulfide, methane, and carbon monoxide; Mixture 2: ammonia and methane), were tested with the biosensor complex. For each of the gases tested, three different flow rates were used (0.5 standard liters per minute or SLPM, 0.7 SLPM, and 0.9 SLPM). Each odorant gas and the gas mixtures showed a unique pattern of decreasing trend in peak fluorescence intensity, which may be useful in building a library for identifying the type and quantity of the odorants in an unknown mixture for example. **Figure 21** is the fluorescence intensity vs. wavelength graph of the biosensor complex exposed to hydrogen sulfide at a 0.5 SLPM flow rate, which shows that the peak emission intensity (obtained at 485 nm wavelength) of the biosensor complex decreases with time up to a certain point (up to around 120 seconds) after which it remains nearly unchanged (the intensities are shown in relative terms, which allows for better comparison of the results).

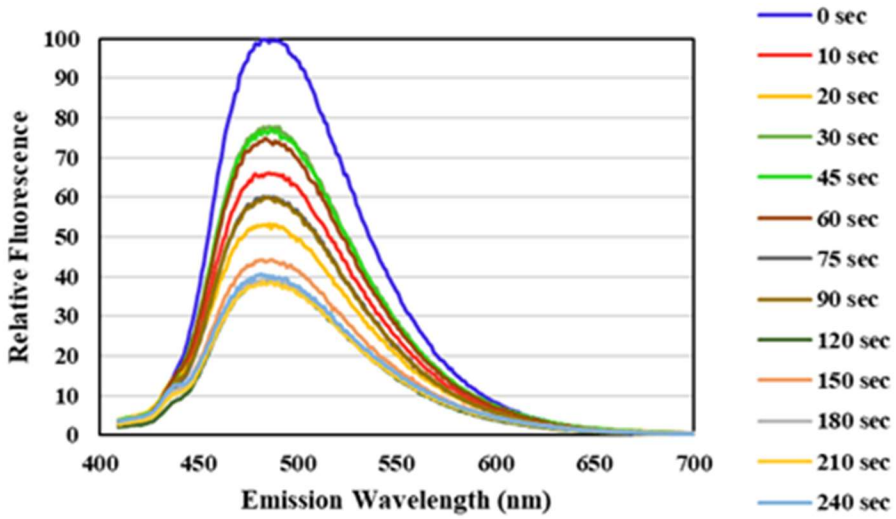

Figure 21: Spectrofluorometric emission spectra of the biosensor complex for excitation taking place at 380 nm for 0.5 SLPM H_2S (hydrogen sulfide). The intensity decreases as time of gas exposure increases

Figure 22 is the plot of peak emission intensities against time for all three flow rates used for hydrogen sulfide. From the graph, it was observed that the duration of the inverse relationship between the peak emission intensities and time of odorant gas exposure varies according to the flow rate. This duration, i.e., the time up to which the biosensor complex shows an inverse relationship between emission intensity and exposure time, is called the saturation limit or the quantification range (QR) for that particular flow rate of the gas.

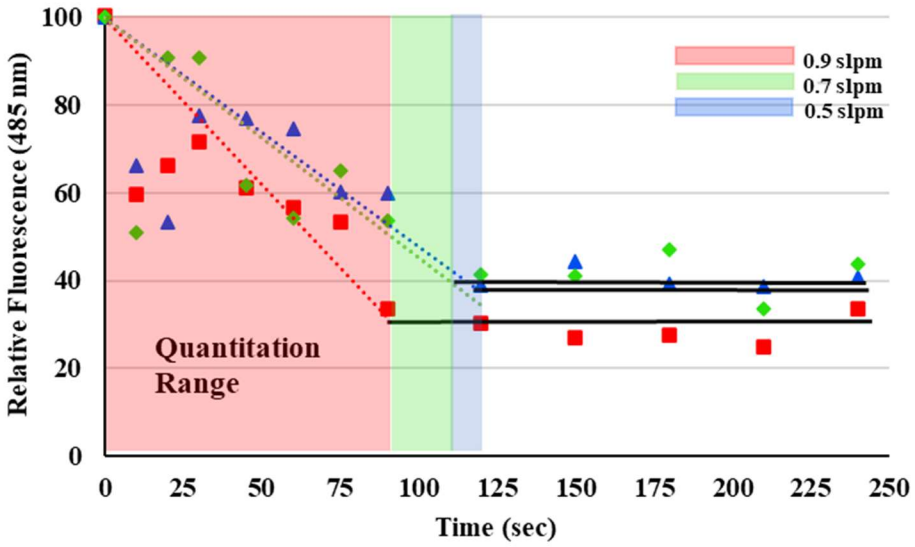

Figure 22: Fluorescence response curve for H_2S for three different flow rates used. The higher the flow rate, the lower the time of saturation (lower QR) (Rahman 2020)

In general, it was observed (as expected) that the biosensor complex saturates faster (shorter QR) with an increased gas flow rate for all the odorant gases tested. For hydrogen sulfide, the saturation time was around 120 seconds for the lower flow rate (0.5 SLPM) and around 90 seconds for the higher flow rate (0.9 SLPM) as shown in **Figure 22**. Also, the decrease in intensity was faster for the higher flow rate as observed by a steeper slope due to increased mass flux of hydrogen sulfide at higher flow rates, which results in increased binding with the biosensor complex within a given exposure time (Rahman 2020).

The biosensor was also found to react with methane (tested with 0.5 SLPM only since a lower flow rate seemed to delay biosensor saturation by the other individual gases tested) even though methane is a non-odorant compound. This is because methane is purely hydrophobic, and OBP has an affinity for hydrophobic ligands (Li et al. 2007; Franks 1975; Briand et al. 2000). Depending on the flow rate, around 180 µg of hOBPIIa in 10 mL biosensor solution was able to detect approximately 35-45 µg of hydrogen sulfide, 12-18 µg of ammonia, 83-95 µg of methyl mercaptan, and 15 µg of methane (**Table 13**). Also, during these experiments, no pH change was observed for any of the odorant gases passed through the biosensor complex, ensuring that the pH did not influence the binding capacity of hOBPIIa.

Table 13: Quantitation ranges and mass ranges of the pure odorant gases tested at different flow rates (Rahman 2020)

Odorant gas	Quantitation Range (seconds)			Mass Range (µg)
	0.5 SLPM	0.7 SLPM	0.9 SLPM	
Hydrogen Sulfide	120	110	90	35-45
Ammonia	90	75	50	10-20
Methyl Mercaptan	95	75	60	80-95
Methane	100	-	-	15

A separate experiment was also conducted by connecting a photoionization detector (PID) at the reactor chamber outlet in that study to ensure that the odorant gases were combining with the biosensor solution and not merely escaping the experimental chamber outlet via short-circuiting. The result showed no presence of gas at the outlet of the chamber. The biosensor was also found to remain essentially unreactive when exposed to non-odorous nitrogen gas at 0.5 SLPM flow rate. The relative peak emission intensity (as shown in **Figure 23**) did not show a noticeable decrease with time during nitrogen gas exposure unlike the other target gases.

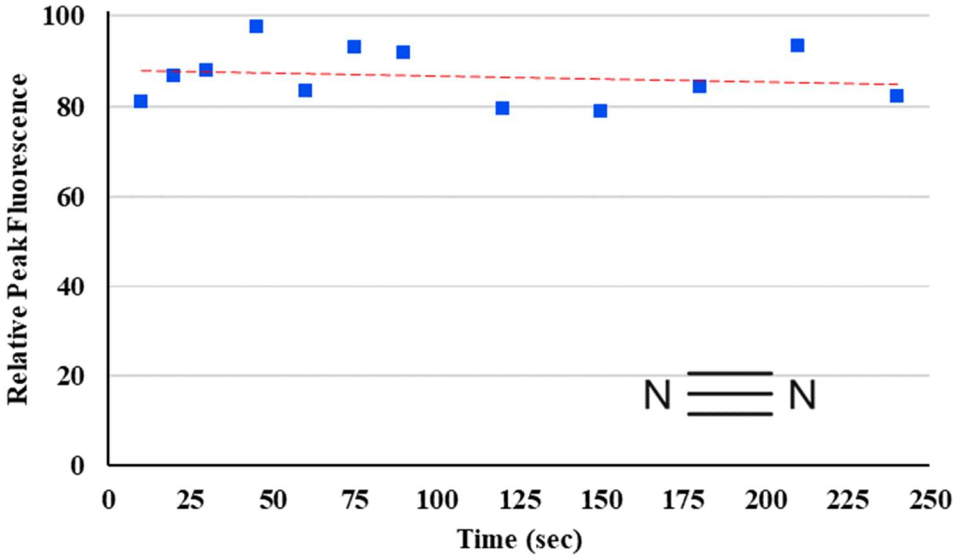

Figure 23: Peak emission intensity against time for non-odorous N_2 passed at 0.5 SLPM flow rate into the biosensor solution (Rahman 2020)

An additional experiment was also carried out to investigate reaction reversibility. The odorant gas (e.g., H_2S) was exposed to the biosensor solution for a time equal to the quantitation range followed by purging with air or pure nitrogen at the same rate to observe if the intensity curve returned to its original intensity. However, during the nitrogen purge, the intensity only showed a slight upward trend after 400 seconds of exposure (**Figure 24**), which indicated that an extended purge time range might be needed.

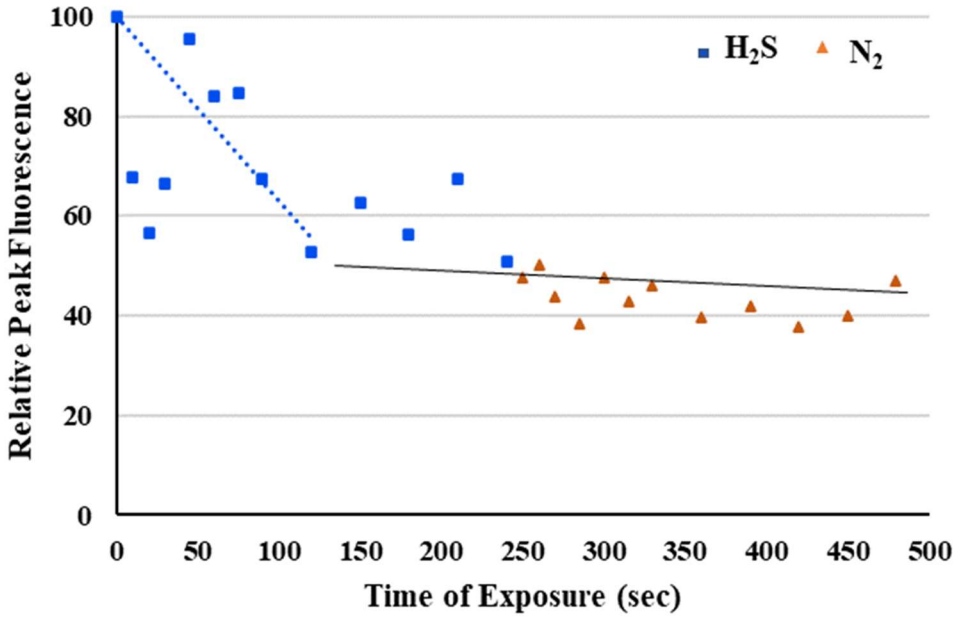

Figure 24: Graph of peak emission intensity against time obtained by passing 0.5 SLPM H_2S gas through the biosensor solution for the first 4 minutes followed by 0.5 SLPM N_2 gas for the final 4 minutes (Rahman 2020)

Further experiments need to be conducted by incorporating a diverse range of odorant gases and gas mixtures in the biosensor complex to allow a deeper understanding of the response time for the biosensor to become saturated. This would increase the spectroscopic library with enough data to analyze the slopes of the odorants tested and possibly identify and quantify the unknown odorants in real-world scenarios down the line. All previous experiments were conducted in batch using subsampling techniques that did not allow for real-time analysis of the odorant-biosensor binding assays. It is necessary to upgrade the prototype reactor design to include flow-through analysis in real-time. In addition, further testing is required to explore the possibilities of the reversibility of the protein-odorant bond. Pelosi et al. (2018) identified that the binding site of bovine OBP contains a gated chemical entrance in the form of a benzene ring of phenylalanine, which greatly slows down the process of dissociation of the odorant-protein binding. This idea suggests that the OBP regeneration may take longer than the initial binding time.

1.11 Objectives

The main objectives of this research are:

1. To explore the reversibility of the protein-odorant bond to determine if the biosensor can be deployed in a multiple-use configuration allowing for reuse in the field for multiple readings or single-use with replacement of the biosensor after each reading.
2. To redesign the prototype reactor chamber as a flow-through system for increased accuracy and real-time measurement using a highly sensitive and portable spectrofluorometer.
3. To build on previous results obtained from the preliminary study conducted by Rahman (2020) by carrying out further spectrofluorometric analyses of the biosensor complex with a wider range of landfill odorants and mixtures.

2 MATERIALS AND METHODS

2.1 Materials

A high-performance QE Pro-FL fluorescence spectrophotometer with individual light source module at 385 nm wavelength along with single channel touchscreen controller, and a Square One cuvette holder (SQ1-ALL) were all procured from Ocean Insight as well as the OceanView spectroscopy software (OceanView 2.0 software). A flow cell (Catalog Number "71F-Q-10") was procured from the Starna Cells. A flowmeter (MilliporeSigma™ Supelco™ Rotameter with Needle Valve) having a flow range 0 to 33 mL/min was obtained from Fisher Scientific. The fluorophore, 1-AMA (1-aminoanthracene, technical grade, 90%) was obtained from Sigma Aldrich in powdered form. The following calibration gas cylinders were procured from the company Cal Gas Direct Inc. (CA, USA):

- Ammonia, 25 ppm gas balanced with nitrogen
- Formaldehyde, 25 ppm gas balanced with nitrogen
- Hydrogen sulfide, 25 ppm gas balanced with nitrogen
- Methyl mercaptan, 50 ppm gas balanced with nitrogen
- Tert-butyl mercaptan, 3 ppm gas balanced with nitrogen
- Toluene, 24 ppm gas balanced with air

2.2 Purified hOBPIIa

Aliquots of purified human odorant binding protein (hOBPIIa) were produced under the supervision of Dr. David Binninger, Associate Professor in the Department of Biological Sciences at FAU, by his research team following the protocol described by Roblyer (2017). Earlier in 2015, the bacterial expression plasmid containing the coding sequence for the recombinant protein variant hOBPIIa was obtained from Dr. Artur Ribeiro, a Professor in the Biological Engineering Department at the University of Minho, Portugal. Later, Dr. Binninger's research team induced and cultured *E. coli* containing the human odor binding protein gene. The protein was then isolated from the batch, and a Bradford assay analysis (Bradford 1976) was conducted to determine the concentration of the induced, purified protein samples (**Figure 25**).

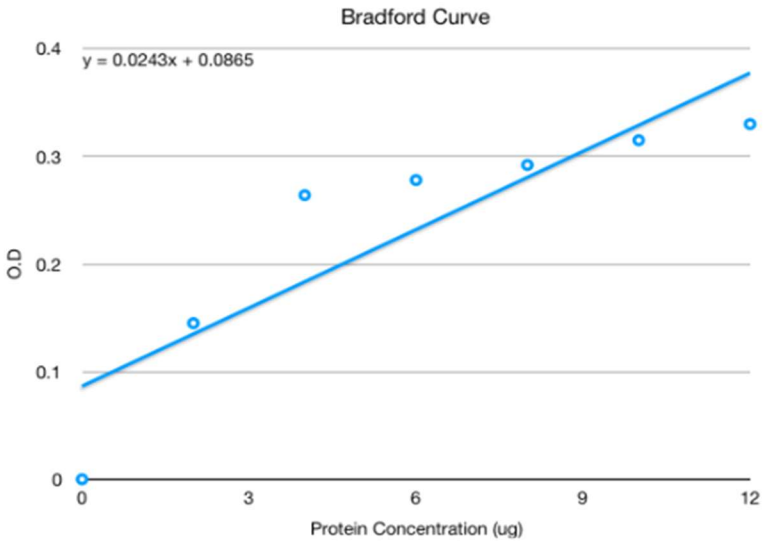

Sample	O.D
Induced Sample (2uL)	0.278
Un-induced Sample	0

Figure 25: Bradford curve showing a clear increase in protein concentration between induced and uninduced samples

After obtaining a positive result from the Bradford assay, an SDS-PAGE (Sodium Dodecyl Sulfate Polyacrylamide Gel Electrophoresis) was conducted following the method of Gallagher (2012) to verify the base-pair size of the purified protein (**Figure 26**).

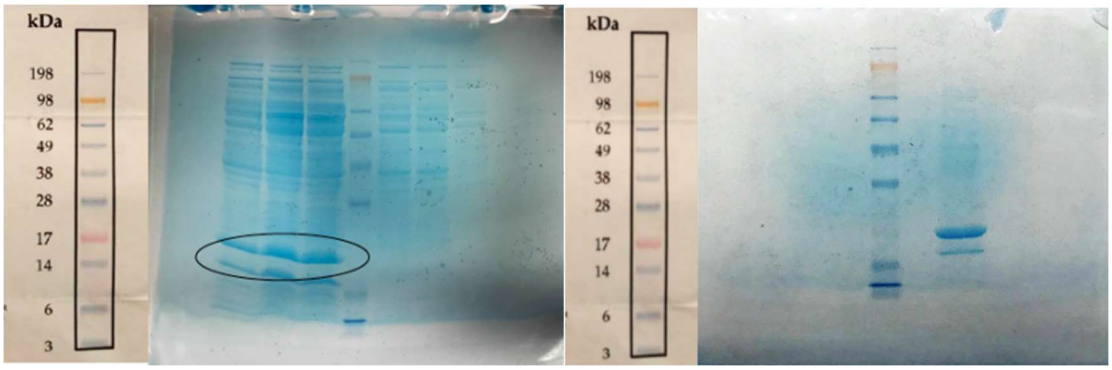

Figure 26: 12.5% SDS-PAGE Gel of crude protein (Circle shows the molecular weight determined for the purified protein from the marker) (left) and 12.5% SDS-PAGE Gel of purified protein (right)

A linear regression equation was used to estimate the amount of isolated protein based on the measured optical density (OD). **Table 14** shows the concentration of the protein samples (mg/mL) in 50 mM Tris–HCl, pH 7.4 solution having a molecular weight of around 17 kDa (Dal Monte et al. 1991; Roblyer 2017). A total of 8 mg of hOBPIIa divided in 11 samples were purified and stored in a -20°C freezer.

Table 14: Estimated concentrations of the purified hOBPIIa in the laboratory

Sample Number	Estimated Concentration (mg/mL)
1	1.95
2	1.47
3	1.56
4	1.79
5	2.35
6	2.96
7	3.00
8	3.49
9	4.16
10	1.20
11	0.54

2.3 Preparation of the Biosensor Complex

1-aminoanthracene (1-AMA) is used as a fluorophore to prepare the biosensor complex. 1-AMA forms a complex with OBPs and has an effective role in understanding the interaction between OBPs and odorants as explained in **section 1.8.4**. 1-AMA is a fluorophore whose quantum yield increases when it remains in a hydrophobic environment. OBPs contain a hydrophobic cavity inside their β-barrel (Briand 2002), and this explains the increased quantum yield when 1-AMA forms a complex with these proteins. 1-AMA in an aqueous solution by itself does not have the same high quantum yield (Briand 2000). Since 1-AMA is hydrophobic, it was first dissolved in 100% methanol, and then deionized water was added to the solution to achieve a final methanol concentration of 10%. Methanol is used as a solvent for 1-AMA, since it displaces the fluorophore from the protein in lower amounts compared to other options such as ethanol or dimethyl sulfoxide (mentioned in **section 1.8.4**). This, in turn, allows a better measurement of the effect of odorant displacement of 1-AMA. Due to light sensitivity, 1-AMA was stored in the dark in an amber colored glass bottle when not in use. Previously, in an experiment conducted by Roblyer (2017) followed by a verification test by Rahman (2020), it was evaluated that the optimal ratio of hOPBIIa to 1-AMA is approximately 1:1. Following up on that experiment, to prepare the biosensor complex, 1 μM hOBPIIa was mixed with 1 μM 1-AMA (1:1 ratio of protein to fluorophore) solution in 50 mM potassium phosphate-KOH, pH 7.5 buffer solution. The buffer solution keeps the pH of the system at a constant level of 7.5, so that the properties of the solution remain unchanged when combined with acidic or basic odorant gases that were analyzed later in the fluorescence binding assay.

2.4 Experimental Setup

The prototype reactor chamber was used to conduct the initial set of experiments where several new ways to regenerate the spent biosensor were explored as a continuation of the previous study conducted by Rahman (2020). However, this experimental setup does not allow for real-time fluorescence analysis of the odorant-biosensor binding assays since subsamples were extracted from the reactor chamber at specific time intervals for the fluorescence analysis. Thus, a modified experimental setup was established later using a flow-through reactor chamber for real-time fluorescence measurement that eliminates the

need to remove any of the biosensor molecules from the reaction chamber. This modification was done to increase the accuracy of the results. In the following subsections, both the prototype and the modified experimental setups are discussed in detail.

2.4.1 Prototype Experimental Setup

The reactor chamber used in the prototype experimental setup was built using a modified 50 mL centrifuge tube as shown in **Figure 30**. The biosensor complex in the buffered solution is located at the bottom of this reaction chamber. The total volume of the biosensor solution was limited to 15 mL in the chamber. A flowmeter (0.1-1 L/min capacity) connects a pressurized gas cylinder with a specialized regulator (**Figure 27**) to the reactor chamber with a one-way check valve, to prevent backflow, using quarter-inch flexible pipe tubing. Another flexible pipe tubing section leads from the inflow check valve into the top of the reaction chamber and ends in an aquarium-grade pumice stone bubbler used to increase the surface area of exposure to the dispersed influent gas.

Figure 27: 29L, 34L, and 58L aluminum gas cylinders used in the experiments (left) and both C-10 and CGA-600 connections/regulators are used in the cylinders depending on the threads (male/female) of the opening (right)

By means of a second one-way check valve to prevent reverse contamination of the reaction zone with the outside atmosphere, the uncombined gas escapes through the top of the reactor chamber. The use of a narrow centrifuge tube as the reactor chamber increases the efficiency of the process by exposing a reduced surface area of the biosensor complex to the headspace above. Due to this, the amount of odorant escaping the reaction chamber is theoretically reduced. Another benefit comes from the tube being elongated in the vertical dimension, which improves the likelihood of successful binding with the protein complex as the target odorant gas must travel a greater distance to reach the air-water interface. This design minimizes short-circuiting of odorant gas in the reaction chamber. The experimental

setup schematic is shown in **Figure 28**, and a labeled photograph showing all the components is shown in **Figure 29**.

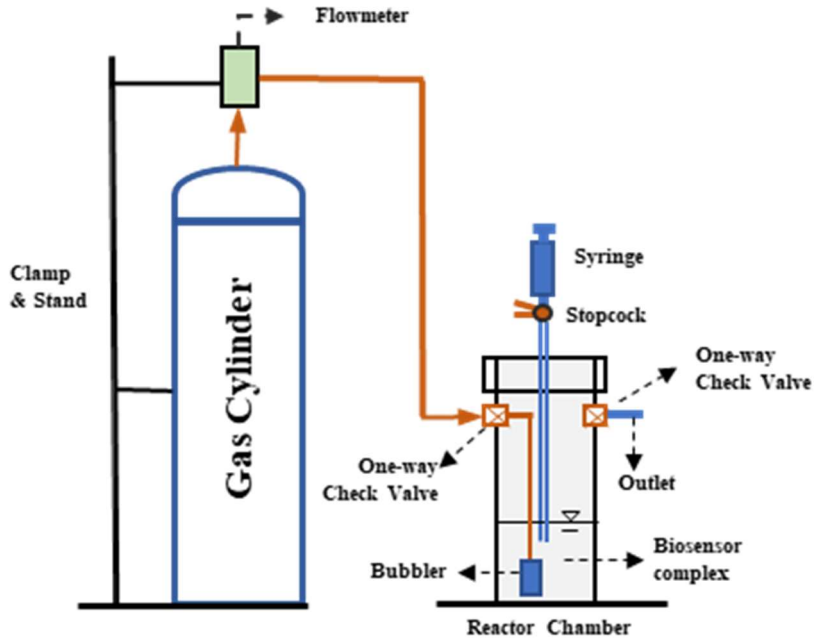

Figure 28: Schematic diagram of the experimental setup

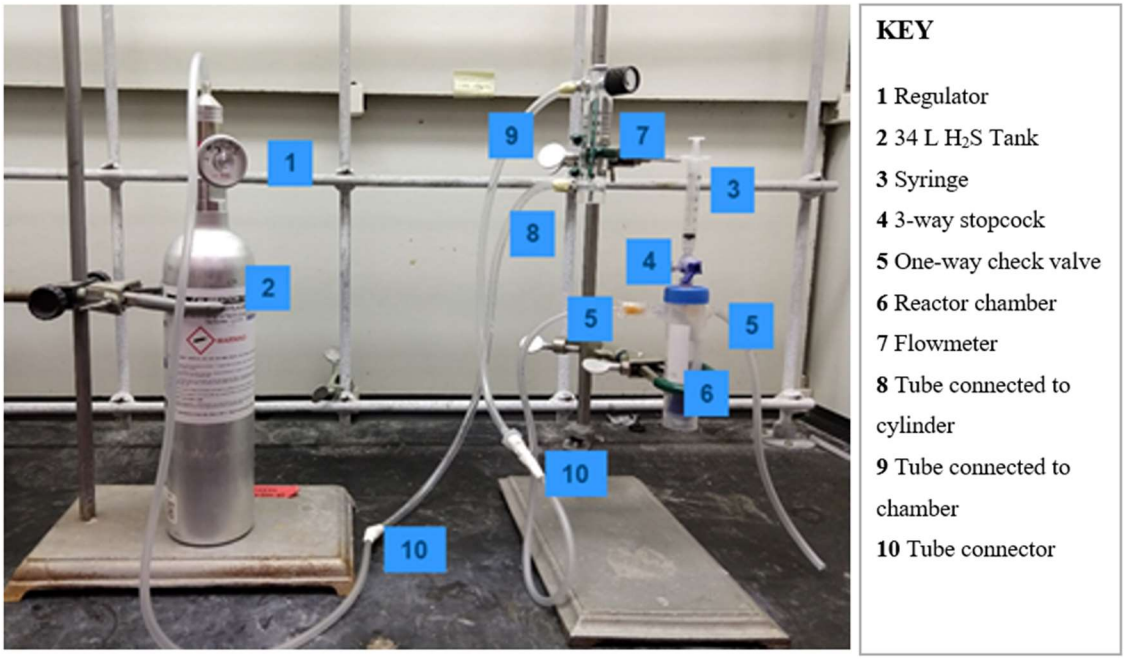

Figure 29: Labeled photograph of the experimental setup

To collect subsamples for fluorometry, a 3-way stopcock was inserted into the cap of the centrifuge tube (**Figure 30**-left). One of the ports (labeled as #4 in **Figure 30**-right) of the stopcock was only opened to draw a sample of the solution from the chamber using a gas-

tight syringe, which was screwed on using a Luer-lok mechanism. Each time after collecting the sample, an empty new syringe was substituted for the old one containing the sample. The other port (shown as #5 in **Figure 30**-right) was kept closed for the duration of the experiment. This setup ensures that the inside of the reaction chamber is never exposed to the external environment, thus eliminating the introduction of any possible contaminants. The experimental apparatus was set up under a fume hood to safely exhaust the odorant gases after passing through the reaction chamber.

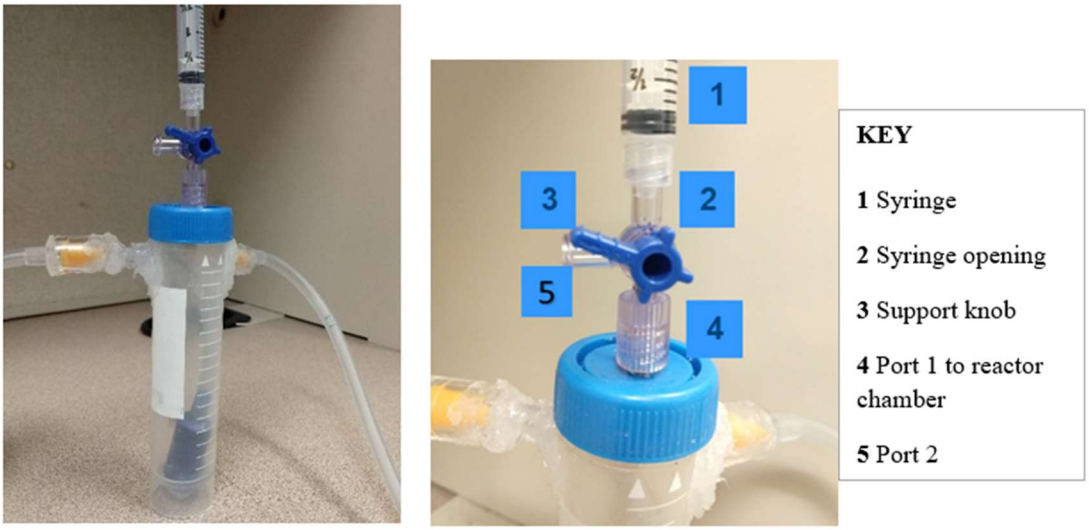

Figure 30: Reactor chamber using a centrifuge tube (left) 3-way stopcock used on the lid of the exposure chamber and the different ports and other parts on the lid are labeled (right)

2.4.1.1 Biosensor Regeneration Experiments Using Prototype Reactor Chamber

As mentioned in **section 1.10**, Rahman (2020) previously conducted several experiments to analyze the competitive binding assay of the biosensor complex with a number of odorants including hydrogen sulfide, ammonia, methyl mercaptan, etc. where each of the odorant gases showed a unique pattern of decreasing trend in peak fluorescence intensity up to a certain time (known as the saturation limit, as mentioned in **section 1.10**) upon reacting with the biosensor complex. Afterwards, using the same prototype reactor chamber, a biosensor regeneration experiment was conducted in an attempt to reverse the protein binding after its initial use of detecting an odorant to explore whether the same protein can be reused multiple times before it is spent. Initially, in that study, it was hypothesized that passing an odorless, inert gas (either pure nitrogen or zero air which is 20.9% oxygen balanced with nitrogen) through the spent biosensor reactor chamber would regenerate the sensor by inducing reversal of the initial reaction and purging the odorants. To that end, an experiment was conducted by Rahman (2020) where hydrogen sulfide (25 ppm balanced with nitrogen) was first passed through the biosensor solution (15 mL solution containing 270 ug of hOBPIIa) for 4 minutes at a flow rate of 0.5 SLPM followed by purging the system with pure nitrogen for another 4 minutes at the same flow rate to observe if the intensity curve returns to its original height (i.e., initial peak intensity), indicating that the biosensor has been regenerated. Initially, zero air was considered first

as the most desirable purge gas since it can be readily available in the field. However, the presence of carbon dioxide may affect the pH of the solution, and thus pure nitrogen was subsequently used as the purge gas, while hydrogen sulfide was selected as the target odorant gas for this experiment. Also, pure nitrogen was already shown to not appreciably react with the biosensor complex itself in the previous study by Rahman (2020) (refer to **Figure 23**). However, initial experiments indicated that full regeneration might take longer than initially anticipated. In this study, additional experiments were conducted to explore a number of other possible ways to regenerate the sensor as follows:

I. Repeating the reversibility experiment conducted by Rahman (2020), while increasing the nitrogen purging time to 15 minutes (i.e., passing 25 ppm hydrogen sulfide gas through the biosensor solution for the first 4 minutes followed by 99.998% nitrogen gas for the final 15 minutes, both at 0.5 SLPM flow rate) and measuring the fluorescence of the subsamples collected at selected time intervals throughout the entire period of the experiment.
II. Repeating the previous experiment while adjusting the temperature of the solution to the human body temperature of 37°C and then purging the solution with pure nitrogen gas for 15 minutes, to replicate temperatures typically found in the human nose. The measurement of fluorescence was conducted as described in the previous experiment.

Temperature adjustment to 37°C was achieved using a Corning hotplate as shown in **Figure 31** (left). Initially, a water bath of 37°C was created in a beaker, which was then used to immerse the reactor chamber containing the odorant-infused biosensor solution before any nitrogen purge gas was passed through it. Once the target temperature was achieved (as measured using a certified laboratory thermometer), nitrogen gas was passed into the solution for a 15-minute purge, while collecting subsamples for fluorescence measurements as shown in **Figure 31** (right).

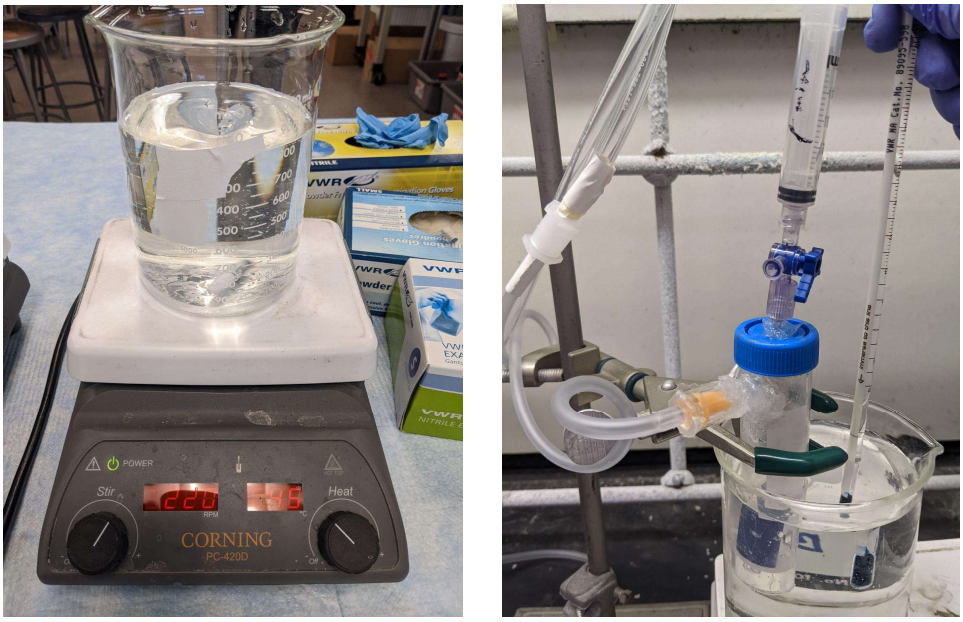

Figure 31: Creation of water bath using Corning hotplate (left) and collection of subsamples at 37°C while purging with nitrogen gas for 15 minutes (right)

III. Saturating the biosensor solution with hydrogen sulfide for the first 4 minutes followed by purging the system with pure nitrogen for the same period of time and recording the fluorescence. Afterwards, adding an additional aliquot of 1-AMA in the remaining biosensor solution to take advantage of Le Châtelier's principle by introducing an additional reactant to the solution at the reaction equilibrium point to shift the equilibrium back to the reactants and regenerate the protein-fluorophore bond.

In Experiment III, the additional 1-AMA was added to the biosensor solution in such a way that the concentration of 1-AMA in the biosensor solution remaining after subsample collection up to the nitrogen purging time reaches 2 µM (the initial concentration of 1-AMA was 1 µM in the biosensor solution). The same experiment was also repeated by adding 2 µM of additional 1-AMA (resultant concentration of 1-AMA being 3µM) at the reaction equilibrium point. Since only a few µL of 1-AMA solution was additionally put into the remaining biosensor solution, the total volume of the solution barely increased, keeping the concentration of the protein practically unchanged.

In each set of the above-mentioned regeneration experiments, at periodic intervals of gas exposure time (30 seconds to 1 minute), 100 µL subsamples were drawn separately from the reaction chamber by means of disposable syringes for fluorescence analysis. The samples were then transferred to a 100 µL capacity (nominal volume) fluorometric quartz cuvette having "Z" Dim 15 mm (the distance from the bottom of the cuvette chamber floor to the center of its light beam) and 10 mm path length (**Figure 32**) for spectrofluorometric analysis. Between sample collections in the cuvette, care was taken to wash the cuvette properly using diluted ethanol and deionized water so that no residue remains in the cuvette that could cause cross-contamination.

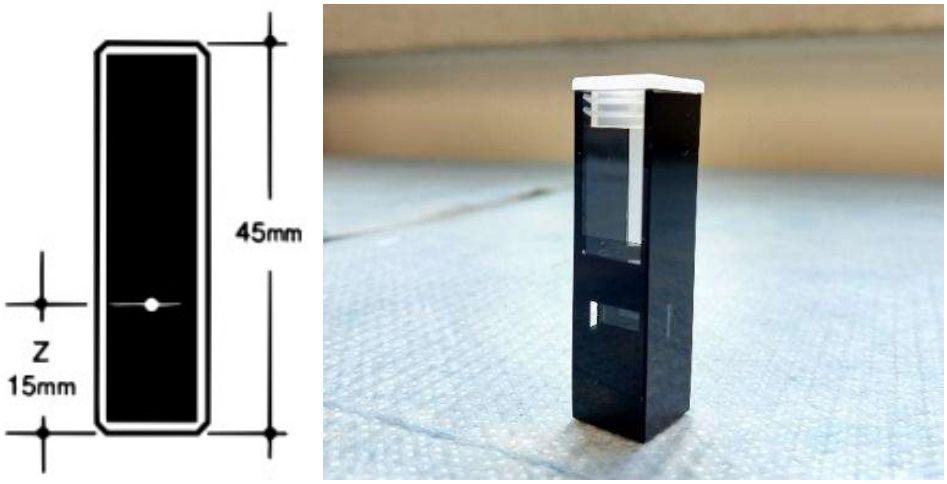

Figure 32: 'Z' dimension (distance from the base to the center of the sample chamber window) of the quartz cuvette (left) and a 100 µL capacity quartz cuvette containing 100 µL of sample each time (right)

2.4.1.2 Fluorescence Measurements in the Regeneration Experiments

Spectrofluorometry is used to assess the binding assay between hOBPIIa and different odorant gases. Fluorescence spectroscopy (i.e., spectrofluorometry) was conducted using a Horiba Jobin Yvon FluoroMax-4 spectrofluorometer (Horiba-Jobin Yvon, Longjumeau, France) (**Figure 33**-left). Two hours prior to starting the experiments, the spectrofluorometer was powered up so that ample warm-up time was provided to the instrument. The fluorescence emission spectra were recorded using FluorEssence software (**Figure 33**-right) at room temperature using an excitation wavelength of 380 nm. The emission spectrum was recorded between 410 and 700 nm at 1 nm intervals. Slit widths were set to 5 nm in both excitation and emission stages.

Figure 33: Horiba Jobin Yvon FluoroMax-4 spectrofluorometer (left) and the Fluorescence software screenshot (right)

2.4.2 Modified Experimental Setup for Real-time Fluorescence Analysis Using QE Pro-FL Spectrometer

The prototype reactor chamber was used for the initial set of experiments in Rahman (2020) as well as for the regeneration tests in this study. The previous reactor chamber required extracting subsamples at specific time intervals for the fluorescence analysis. Thus, there is an obvious time gap between when the sample is collected and when the fluorescence reading is taken. Thus, the goal of modifying the prototype experimental setup was to perform real-time fluorescence analysis to observe the odorant-biosensor interaction without removing any of the biosensor molecules from the reaction chamber. This is achieved by utilizing the cuvette (which is the flow cell in this study as shown in **Figure 37**-left), itself as the reactor chamber while placing it in a specialized cuvette holder (**Figure 34**-right) and establishing a flow-through setup with the entire system. The fluorescence spectroscopy data were collected using a highly sensitive, portable spectrofluorometer, QE Pro-FL (QE Pro spectrometer preconfigured for fluorescence) (**Figure 34**-left), that further miniaturizes the whole setup, thus taking the technology one step closer towards the ultimate goal of deploying the biosensor in a handheld device in real-world scenarios.

Figure 34: QE Pro-FL high-performance spectrofluorometer from Ocean Insight (left) and the SQUARE ONE (SQ1-ALL) Cuvette Holder used with QE Pro-FL for the flow-through system (right) (Ocean Insight 2022)

QE Pro has a number of unique features that makes it more sensitive than the unit used in previous experiments. The integration time (the time taken to collect a single reading) of the QE Pro can be as low as 8 ms and can be up to 60 minutes (Horiba Jobin Yvon's upper limit was only 160 sec (Horiba Scientific, n,d)), which greatly enhances the detection limit in low light level applications (Ocean Insight 2022). Also, the thermoelectric cooling (TEC) feature in QE Pro can precisely control the temperature of the detector, which minimizes the effect of thermal noise and maximizes the signal to noise ratio (SNR), increasing the accuracy of results. The most important advantage of QE Pro for this study is its portability, even allowing it to be carried on-site for field measurements. Most currently available spectrofluorometers on the market cannot be used in a flow-through configuration and are not portable. The fluorescence data can be recorded continuously in the Ocean View software and are saved at a user-defined time interval on the computer. Also, with its high quantum efficiency detector, it considerably increases the accuracy of the experiments.

An individual light source module at 385 nm wavelength was used with the QE Pro spectrometer to illuminate the sample for fluorescence analysis. The light source comes with a touchscreen controller (**Figure 35**-left) where the magnitude of the incoming current, the pattern of the source light emission, as well as its frequency can be controlled. The intensity of the incoming current and the frequency were set as 100% and 0 Hz respectively in the touchscreen controller for the light source in each set of experiments

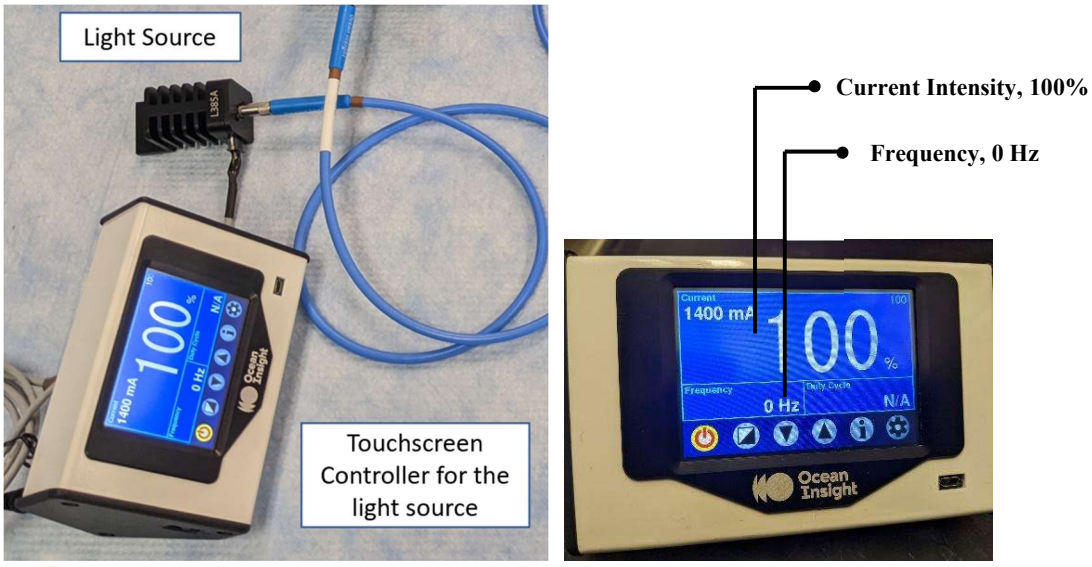

Figure 35: Individual light source module at 385 nm wavelength along with the LED touchscreen controller (left) and the parameters for the incoming current preset for each of the experiments (right)

The light source and the QE Pro spectrometer were connected to the cuvette holder (SQ1-ALL) containing the flow cell, at a 90-degree angle relative to each other for obtaining maximum sensitivity for the fluorescence measurements as shown in **Figure 36**. The connections were made using premium grade UV-Visible optical fiber obtained from Ocean Insight. The spectrometer was finally connected with a laptop to record the fluorescence readings through Ocean View software. To establish the flow-through system by allowing the odorant gas to enter and exit the flow cell, the lid of the cuvette holder has to be kept open while taking the fluorescent measurements. This can be done without incorporating any inaccuracy in the analysis due to the following reasons:

1. The cuvette holder has collimating lenses on both sides, so it only accepts light from a very specific angle.
2. Even if potentially interfering ambient light does make its way into the system, it would be subtracted out in the software when the dark measurement is taken.

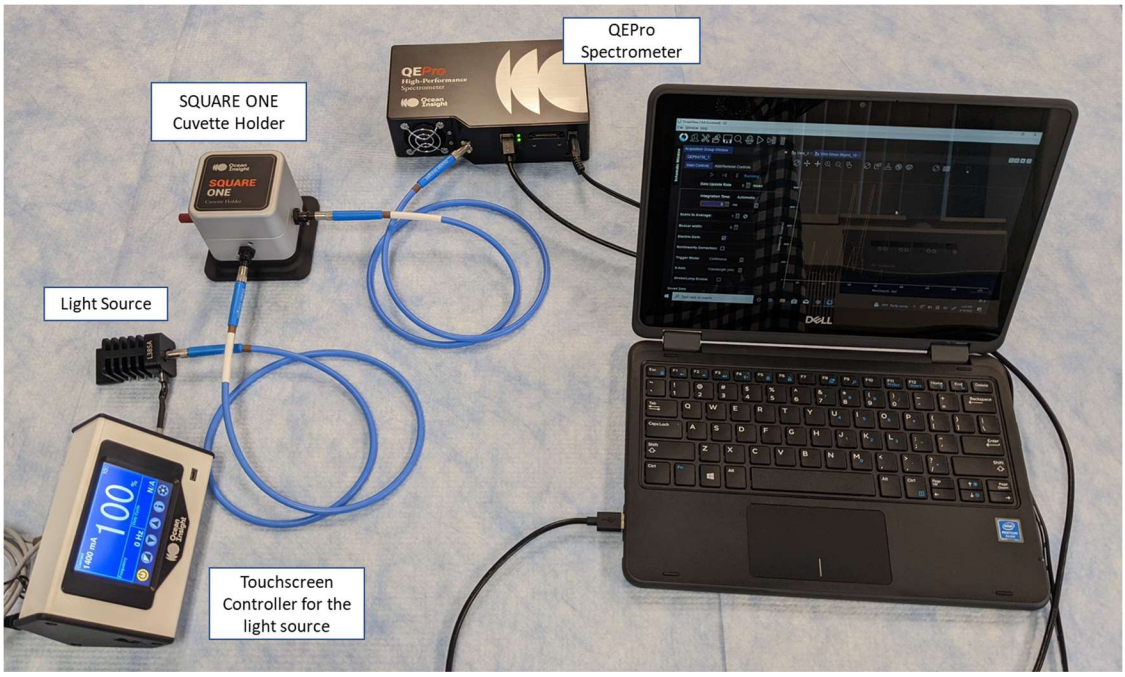

Figure 36: The QE Pro-FL spectrometer and the light source connected with the SQUARE ONE cuvette holder at a 90-degree angle

2.4.2.1 Flow Cell

The 3 mL flow cell cuvette (shown in **Figure 37**-left) used as the reactor chamber in the new modified setup has two protruding tubes at its top that is used as an inlet and outlet during the experiment. The flow cell has long, clear windows on its three sides and so can be used with instruments of any 'Z' dimension. The biosensor complex solution was put into the flow cell through the inlet by means of a pipette. A vacuum air duster as shown in **Figure 37**-right was used to dry out the flow cell following a thorough washing after conducting each set of experiments.

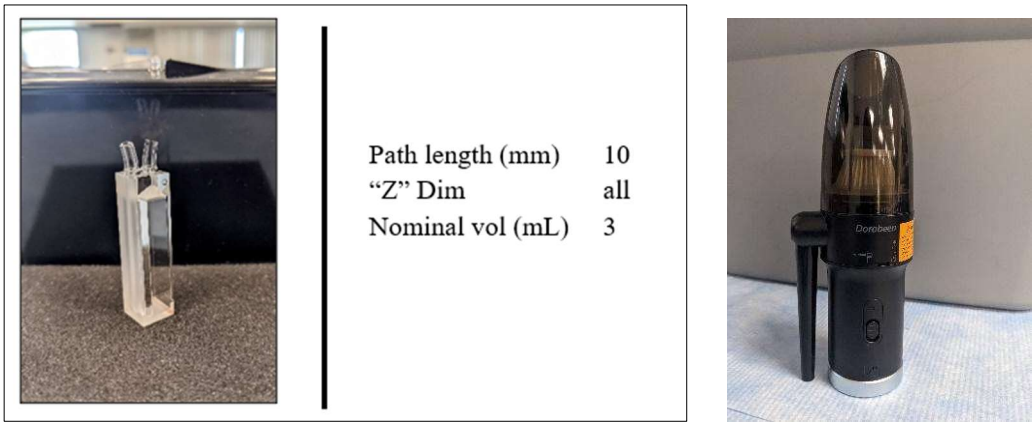

Figure 37: Flow cell used as the reactor chamber in the modified experimental setup (left) and the vacuum air duster used for cuvette drying (right)

2.4.2.2 Establish Flow-through System in the Modified Setup

In the new modified setup, the odorant gases were delivered from specialty pressurized gas cylinders to the flow cell containing the biosensor solution in a similar way as the previous setup. Two-thirds of the flow cell (2 mL) was filled with the biosensor solution, and the remaining volume was kept empty to allow the headspace gas to escape from the chamber so that the uncombined gas would not exert unnecessary pressure on the cell housing. The decision to allow for 2 mL of the solution was to ensure that there was enough volume in the flow cell to enable a clean reading without gas bubbles artificially fooling the detector as well as to ensure that the volume is not high enough to cause liquid overflow when the gas is bubbled into the flow cell.

The odorant gas cylinder uses a calibration gas regulator (0.1 SLPM constant flow rate) connected to a highly sensitive flowmeter (Flowmeter 2 in **Figure 40**) that controls gas flow to the flow cell at a very low rate (0-33 mL/min.). The gas to be measured enters at the bottom of the tube of the flowmeter, passes upwards and exits at the top. This flowmeter comes with four different interchangeable floats, allowing for four different upper limits of flow rates as follows:

- Glass Float: 6 mL/min
- Sapphire Float: 8 mL/min
- Stainless Steel Float: 17 mL/min
- Carboloy Float: 33 mL/min

With the different floats, the flow rate of the odorant gases can be carefully controlled more accurately. The flowmeter was shipped with the Sappihre float installed within the device. However, to increase the range of flows that can be measured, the float needed to be switched to Carboloy. The front plastic shield was removed at first to access the glass tube scale inside. Following this, the tube was detached by unscrewing the nut at the top (**Figure 38**-left). There are two plastic plugs at both ends of the tube. Once the tube was detached (**Figure 38**-right), one of those plugs was pushed in using a long, thin steel probe so that it could push out both the float and the plug at the other end out of the tube. One of the plugs was then replaced back at one end and after that, the Carboloy float was put into the tube. The other plug was then fitted back. Care must be taken while doing this so that on the 0 end of the tube, the float rests on the plug such that without any airflow, the reading shows a perfect 0. The tube was then reassembled back into its case.

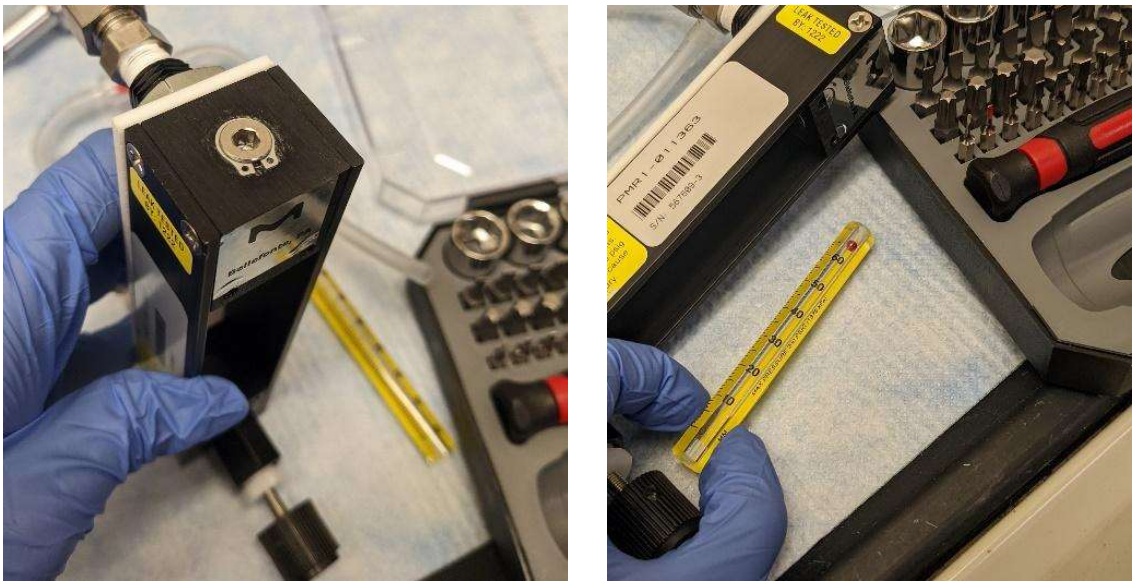

Figure 38: The nut at the top of the flowmeter was unscrewed to access the glass tube scale inside it (left) and the glass tube scale was detached to substitute the float (right)

Brass pipe fitting adapters were used at the NPT (National Pipe Taper) connections of the flowmeter and the rest of the connections with the flow cell use flexible silicone tubing. The extra gas (difference in flow rate between cylinder regulator and flowmeter) coming from the cylinder was diverted through a Y-connector by means of another flowmeter (Flowmeter 1 in **Figure 40**) and exhausted in the fume hood. Check valves were attached on both sides of the Y-connector to prevent backflow and a third check valve was attached at the outlet of the flow cell that would allow the uncombined gas to escape from the chamber to prevent reverse contamination of the reaction zone with external air. The whole experimental apparatus was set up under a fume hood to exhaust the gas safely. The schematic of the modified setup is illustrated in **Figure 39**.

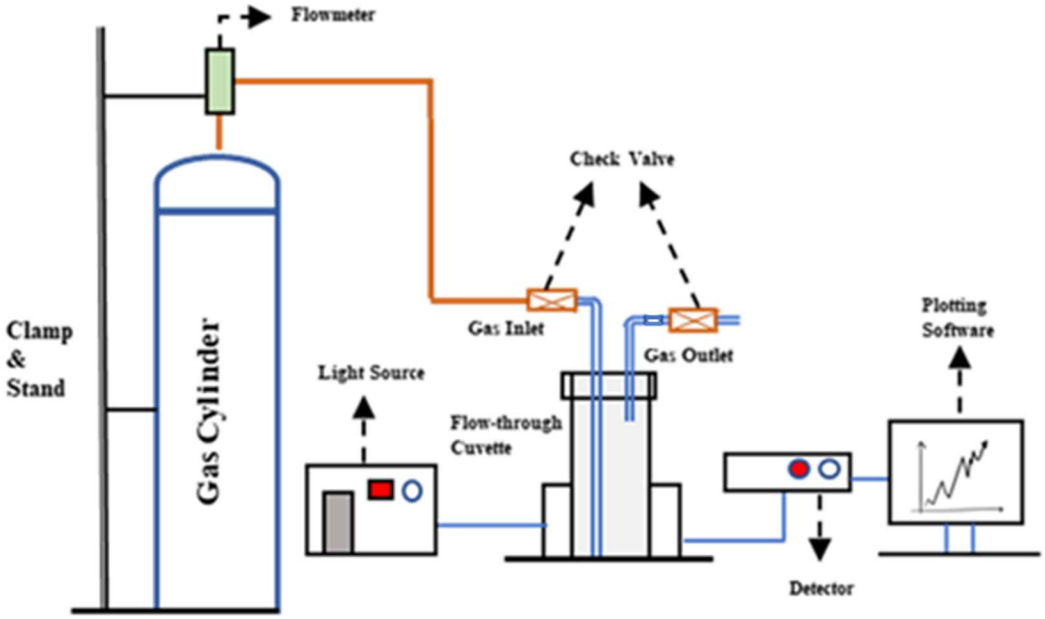

Figure 39: Schematic diagram for experimentation with a flow-through system for real-time fluorescence analysis

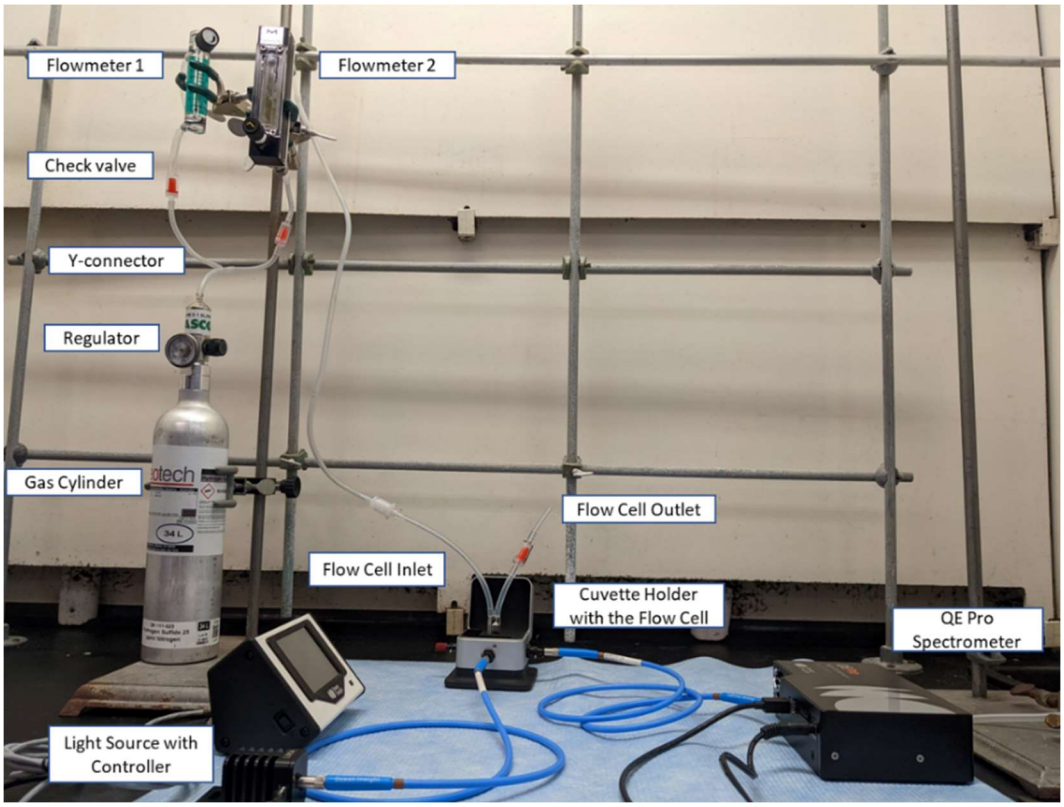

Figure 40: Complete experimental setup to analyze protein-odorant binding assay with real-time fluorescence measurement using a flow-through system

For experiments with odorant gas mixtures supplied through two cylinders, a Y-connector was used to combine the two streams of gas from their sources and then passed through the flowmeter, eventually leading to the flow cell as shown in **Figure 41**-right.

Figure 41: Single gas cylinder used in the pure odorant gas experiments (left) and two cylinders containing two different gases used in the gas mixtures experiments. The cylinders are connected through a Y-connector tube before the entrance of the flowmeters (right)

2.4.2.3 Verifying Gas Compatibility throughout the Entire System with a Photoionization Detector (PID)

Once the setup was established, a MiniRAE Lite photoionization detector (PID) (Gastech n.d.) was used to check the compatibility of the gas concentration in the entire setup as shown in **Figure 42** (left). The PID can measure the presence of volatile substances in the range of 0-5,000 ppm (RAE Systems Inc. 2013), and thus can identify if there is any leakage throughout the system or if any amount of gas escapes through the outlet of the flow cell. Hydrogen sulfide was selected as the model odorant for this experiment in part because its presence can be detected by PID (Honeywell, 2021). The PID was used at two separate locations in the setup to detect the concentration of the hydrogen sulfide. At first, the concentration of the gas coming from the cylinder directly was measured and recorded. In case of no leakage in the system, all the gas entering the flowcell will escape through its outlet given that there is no biosensor in the cell. Upon connecting the PID at the outlet of the flow cell (shown in **Figure 42**-right), it was seen that the same amount of gas was escaping from the cell, which ensures that the system is gas leak proof.

Figure 42: MiniRAE Lite photoionization detector (PID) to check the compatibility of the gas concentration in the entire setup (left) and in case of no leakage, all the gas entering into the flowcell placed in the SQ1-ALL cuvette holder will escape through the outlet when the cell is empty (not filled with biosensor solution) (right)

2.4.2.4 Analyzing Protein-Odorant Binding Assay

To analyze the competitive binding assay, the following pure gases and gas mixtures were tested with the biosensor complex using the new modified flow-through setup for real-time fluorescence measurements:

- Hydrogen sulfide (25 ppm gas balanced with nitrogen)
- Ammonia (25 ppm gas balanced with nitrogen)
- Methyl mercaptan (50 ppm gas balanced with nitrogen)
- Toluene (24 ppm gas balanced with air)
- Formaldehyde (10 ppm gas balanced with nitrogen)
- Tert-butyl mercaptan (3 ppm gas balanced with nitrogen)
- Mixture 1: Toluene (24 ppm gas balanced with air) and ammonia (25 ppm gas balanced with nitrogen)
- Mixture 2: Toluene (24 ppm gas balanced with air) and tert-butyl mercaptan (3 ppm gas balanced with nitrogen)

All gases tested in this study are considered to be hazardous air pollutants and can be found in landfill air in varying amounts. Also, all of them have a very distinctive odor even at very low concentration levels (low ODT), as mentioned in **Table 15**. The concentrations of the gases were selected in such a way as to keep them as close as possible to real-world scenarios. In each of the experiments, the gas flow rate was kept constant at 25 mL/min (0.025 SLPM) into the flow cell containing 2 mL of biosensor solution (36 µg of hOBPIIa). As mentioned earlier in **section 1.10**, Rahman (2020) already conducted experiments with the most commonly found landfill odorants including hydrogen sulfide, ammonia, and methyl mercaptan where the gas flow rates were varied in the range of 0.5-0.9 SLPM and the volume of the biosensor solution was 10 mL (containing 180 µg of

hOBPIIa) in each set of experiments. Depending on the flow rates, about 35-45 µg of hydrogen sulfide, 12-18 µg of ammonia, 83-95 µg of methyl mercaptan were found to combine with 180 µg of hOBPIIa until the gases reached the saturation limit in the reactor. This study uses a gas flow rate that is approximately 20 times lower than that used in the previous study, while the protein usage was also lowered by 5 times in order to simulate practical usage in real-world scenarios and minimize reagent use and response time. In this case, the quantitation ranges (QRs) would be expected to increase by a factor of 4 for these gases compared to the QR values found in Rahman (2020) for the 0.5 SLPM flow rate. For example, 2 mL of biosensor solution containing 36 µg of hOBPIIa would combine with around 7 µg of hydrogen sulfide, 3 µg of ammonia and 16 µg of methyl mercaptan before reaching the saturation limit.

Also, previously in Rahman (2020), prior to conducting the actual experiments with the odorant gases, a separate experiment was also conducted with pure nitrogen gas (as mentioned in **section 1.10**) to check whether nitrogen has any effect on the fluorescence measurement since the odorant gases were balanced with nitrogen in the cylinder. Similar to that, using the new flow-through setup, an experiment was conducted with nitrogen gas at 25 mL/min flow rate prior to testing with the odorant gases to compare with the previous results. Also, since the toluene cylinder used in this study was balanced with air, a separate experiment was conducted for zero air using the same flow rate prior to testing with the toluene gas.

Table 15: Molecular structure, odor threshold, and health effects of the gases tested

Gas Tested	Molecular Structure	Odor Description	Odor Detection Threshold (ODT, ppm)	Health Effects
Hydrogen Sulfide	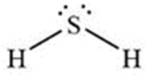	Rotten eggs	0.0005-0.3	Irritation to the eyes and respiratory system, apnea, coma, convulsions, dizziness, headache, weakness, irritability, insomnia, stomach upset (CDC 2019)

Gas Tested	Molecular Structure	Odor Description	Odor Detection Threshold (ODT, ppm)	Health Effects
Ammonia	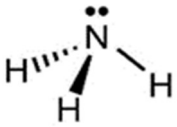	Sweat or urine like	5-50	Immediate burning of the eyes, nose, throat and respiratory tract that might result in blindness, lung damage or death (NYSDOH 2011)
Methyl Mercaptan	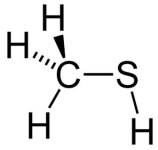	Rotten cabbage	0.002	Highly irritant when it contacts moist tissues such as the eyes, skin, and upper respiratory tract. It can also induce headache, dizziness, nausea, vomiting, coma, and death. (ATSDR 2017)
Toluene	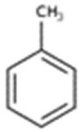	Sweet, pungent benzene like	0.16-100	Eye and nose irritation, tiredness, confusion, euphoria, dizziness, headache, dilated pupils, anxiety, muscle fatigue, insomnia, nerve damage, and liver and kidney damage (CDC 2019)

Gas Tested	Molecular Structure	Odor Description	Odor Detection Threshold (ODT, ppm)	Health Effects
Formaldehyde	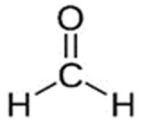	Strong pickle	0.5-1.0	Watery eyes; burning sensations in the eyes, nose, and throat; coughing; wheezing; nausea; skin irritation, cancer (NIH 2011)
Tert-butyl Mercaptan	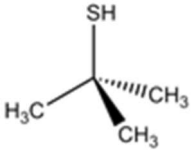	Spoiled cabbage or rotten eggs	0.0001-0.001	Irritation of nose, throat and lungs causing coughing, wheezing and shortness of breath; high concentrations cause weakness, nausea, dizziness, headaches, confusion and coma (NJDOH 2003)

2.4.2.5 Recording Fluorescence Measurements Using Ocean View Software

To analyze the odorant-protein binding assay, the flow cell containing the biosensor complex exposed to an odorant gas was excited by means of the light source at 385 nm when the spectrometer starts continuously recording the fluorescence data. At the beginning of each experiment, before taking any fluorescence measurement, a background/dark measurement was recorded in the Ocean View software (**Figure 43**). The background measurements are automatically subtracted from each fluorescence reading obtained from a sample to reduce the impact of background noise. The software shows data for both pre and post subtraction of the dark measurements (a View Minus Background tab). The integration time was set as 8 ms in the software for each of the experiments. The fluorescence data obtained from the software were updated continually (5 ms intervals) to provide an uninterrupted real-time fluorescence measurement.

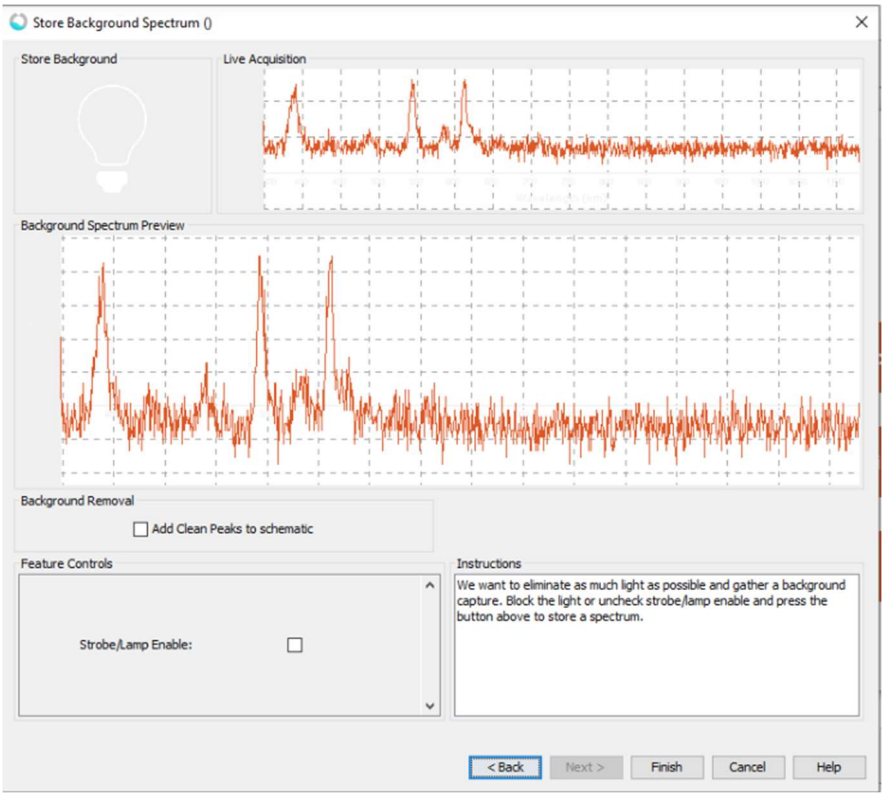

Figure 43: Background fluorescence signal being recorded in the Ocean View software before each set of experiments. The x-axis represents wavelength (nm), while the y-axis represents fluorescence intensity (count)

2.4.2.6 Alternate Flow-through Setup Using Peristaltic pump

As described in **section 2.4.2**, the modified setup was designed so that the odorant gas was passed into the flow cell directly to react with the biosensor solution, which also acts as the chamber for analyzing fluorescence readings. The gas passed into the flow cell inevitably leads to bubble formation in the cell, which can potentially interfere with the readings. Therefore, an alternate setup was also established using two reactor chambers at the same time, which allows for the reaction to take place in one chamber and fluorescence measurements to be recorded from the other chamber, which is the flow cell in this case, without the impact of bubble formation directly within the cell. Only hydrogen sulfide was tested using this setup to understand whether there was actually an impact of the gas bubbles interfering with the instrument readings.

In the alternate setup, the odorant gas was passed in the prototype reaction chamber (modified 50 mL centrifuge tube) in the same way as described in **section 2.4.1**. This chamber was connected to the flow cell by means of a peristaltic pump as shown in **Figure 44**. The process works in such a way that biosensor solution would be circulated within the system constantly by the pump. As the odorant gas mixes with the solution in the prototype chamber, the resultant solution flows into the flow cell where the readings were continuously recorded by the spectrofluorometer. This way, the bubble formation was limited to the reaction chamber and only the solution was moved to the flow cell for

measurement without the bubbles getting in the way. The total volume of biosensor solution in the reaction chamber was 10 mL containing 180 µg of hOBPIIa as used before in the previous study in Rahman (2020) and not just 2 mL as used when the flow cell was acting as the reaction chamber for all other experiments in this study. This is because a continuous flow of solution would be necessary throughout the system, and the flow cell by itself would need to be kept full so that gas bubbles were not formed there. This requires a larger volume of solution than that for filling just the flow cell.

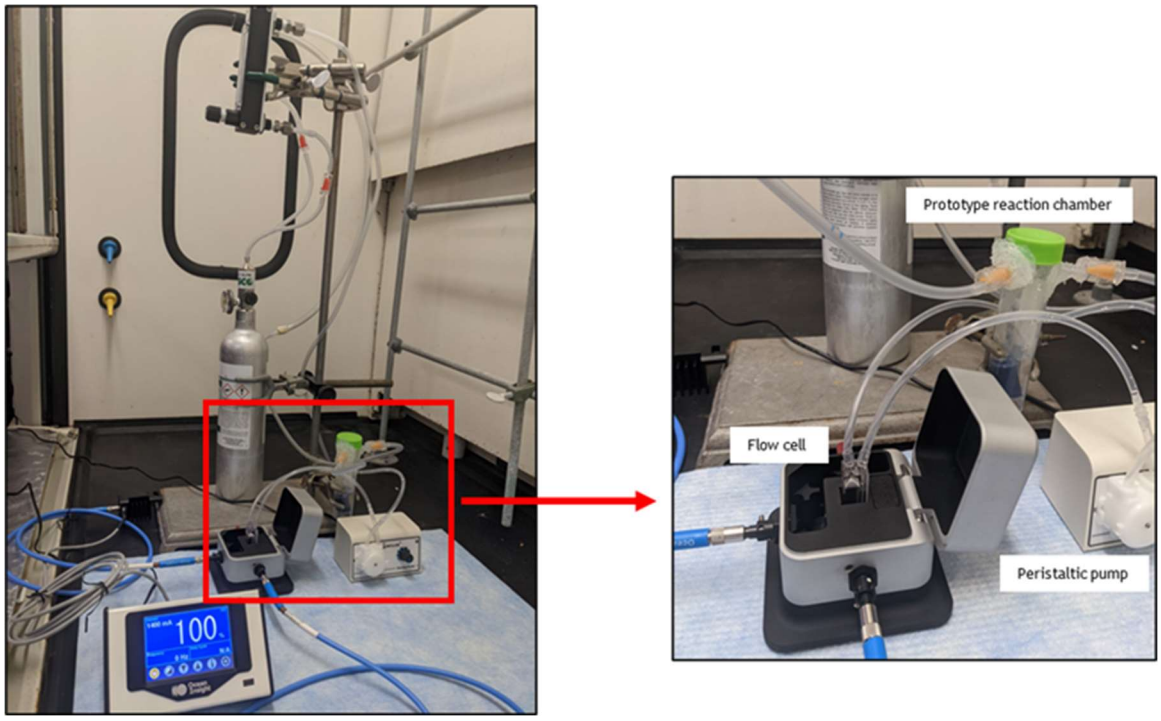

Figure 44: Alternate flow-through setup for real-time fluorescence analysis. The protein-odorant interaction takes place in the protype reaction chamber from where it is transferred to the flow cell through a peristaltic pump in a clockwise direction, creating a loop

3 RESULTS AND DISCUSSION

3.1 Biosensor Regeneration Experiments

One of the main objectives of this research was to explore possible ways to make the odorant-protein binding reaction reversible as a continuation of the previous study conducted by Rahman (2020). Reusing the protein multiple times after it initially binds with the odorant will allow the technology to be much less expensive to produce. The expected result is represented by a concept graph (**Figure 45**), which is a plot of the peak emission intensity (obtained at 485 nm wavelength) of the biosensor complex upon exciting at 380 nm wavelength as it is introduced to an odorant gas versus time.

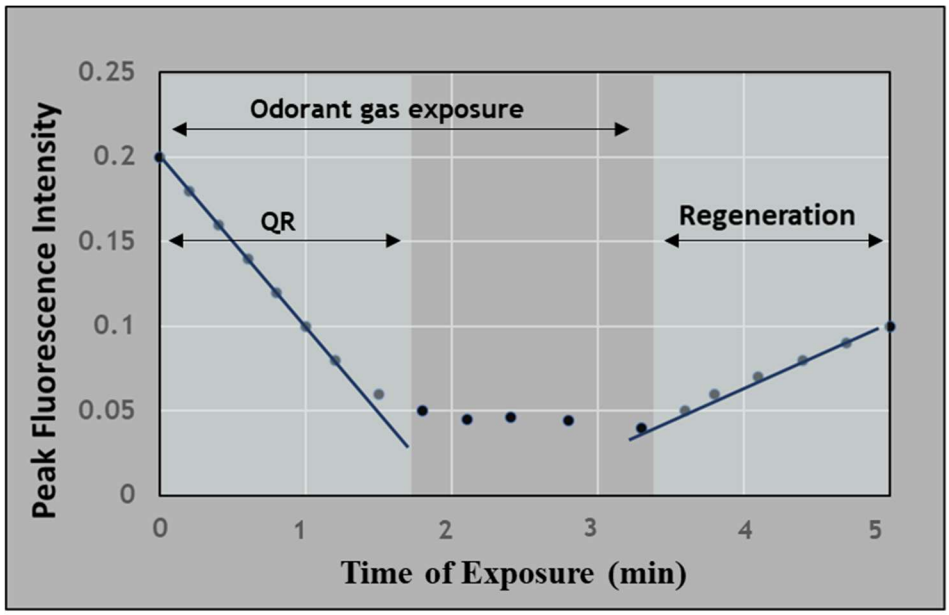

Figure 45: Concept graph indicating successful regeneration shown by a bounce-back of the intensity at the last part of the graph

The decreasing intensity of the biosensor solution during the initial portion of the graph is due to the odorant (in this case hydrogen sulfide gas) displacing the protein-fluorophore bond to bind with the protein (discussed in **section 1.10**). Within two minutes of gas exposure to the biosensor solution, the saturation point (also known as QR) is reached, after which the intensity remains somewhat unchanged as the sensor no longer reacts with additional odorant gas with the curve remaining flat. This signal indicates that the biosensor is spent and would need to be regenerated by some means to get the fluorescent intensity back to nearly the initial position in order to obtain another odorant reading.

As mentioned in **section 1.10**, one of the ways to make the protein-odorant reaction reversible was already investigated in Rahman (2020) where a selected odorant gas (hydrogen sulfide) was first passed through the biosensor at 0.5 SLPM flow rate for 4 minutes (saturation occurs after around 2 minutes) followed by purging the system with air or pure nitrogen (another 4 minutes) at the same flow rate. However, the outcome of that initial experiment with nitrogen purging over a 4-minute window showed that the intensity

did not return to its original level (**Figure 46**). Here, the peak emission intensities (obtained at 485 nm wavelength) first decreased for about 2 minutes as the sensor reacted with the hydrogen sulfide gas passing at 0.5 SLPM flow rate, and then the signal became somewhat constant for the next 2 minutes after the sensor reached its saturation limit (blue points). At this point, around 270 µg of hOBPIIa combined with 35 µg of hydrogen sulfide before the sensor reached its saturation limit. During the final 4 minutes of nitrogen purging at the same flow rate, the spectroscopic signal remained relatively unchanged (brown points), indicating that using nitrogen as the purge gas in the already spent biosensor was not able to regenerate the signal. However, after 400 seconds, there was a slight upward trend of the intensity for the last three points collected, which was a promising result that indicated that an extended purge time range beyond 4 minutes might be required.

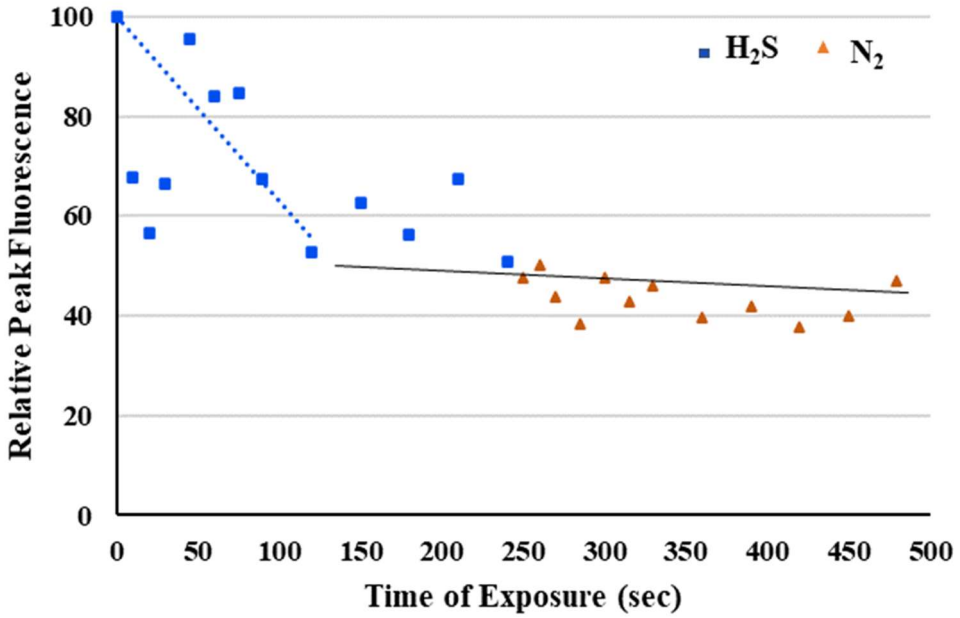

Figure 46: Graph of peak emission intensity against time obtained by passing 0.5 SLPM H_2S gas through the biosensor solution for the first 4 minutes followed by 0.5 SLPM N_2 gas for the final 4 minutes (Rahman 2020)

The preliminary experiments suggest that this purging time might be in excess of 4 minutes for a 15 mL sample pre-saturated with hydrogen sulfide. Other possible alternatives to determine appropriate regeneration conditions included elevated temperature and addition of excess fluorophore, as discussed in the following subsections.

3.1.1 Increasing Nitrogen Purging Time

As a first attempt to conduct the biosensor regeneration experiment, the nitrogen purging time was increased from 4 minutes to 15 minutes after the sensor was exposed and became saturated to hydrogen sulfide for the first 4 minutes. The graph obtained by plotting the peak emission intensity over time (**Figure 47**) shows that the peak intensity first decreases with time for the first few minutes as the biosensor was exposed to the hydrogen sulfide gas at 0.5 SLPM flow rate, and then the signal remains flat throughout the entire period of

nitrogen purging time (final 15 minutes, orange points) in the spent biosensor solution, instead of returning back to a relative fluorescence near 100, as expected.

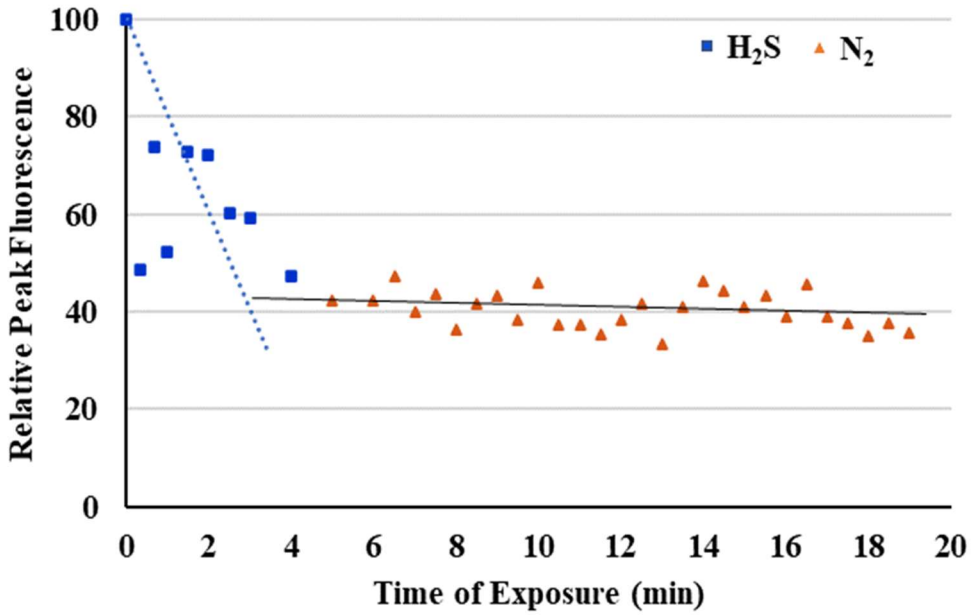

Figure 47: Graph of peak emission intensity against time obtained by passing 0.5 SLPM H_2S gas through the biosensor solution for the first 4 minutes followed by 0.5 SLPM N_2 gas for the final 15 minutes

3.1.2 Adjusting Temperature During Nitrogen Purging

In the next experiment, while purging the system (biosensor already combined with the hydrogen sulfide gas) with nitrogen gas, the temperature of the solution was adjusted to the human body temperature of 37°C. However, adjusting the temperature also seemed to have no impact in the regeneration of the sensor as shown in **Figure 48**. Here also, the intensity first decreases for about 2 minutes while the sensor was exposed to hydrogen sulfide gas and then becomes unchanged for the next 2 minutes as the saturation occurs (blue points) and then it remains somewhat constant during the final 15 minutes of nitrogen purging (orange points) as before while the solution was kept at a temperature of 37°C.

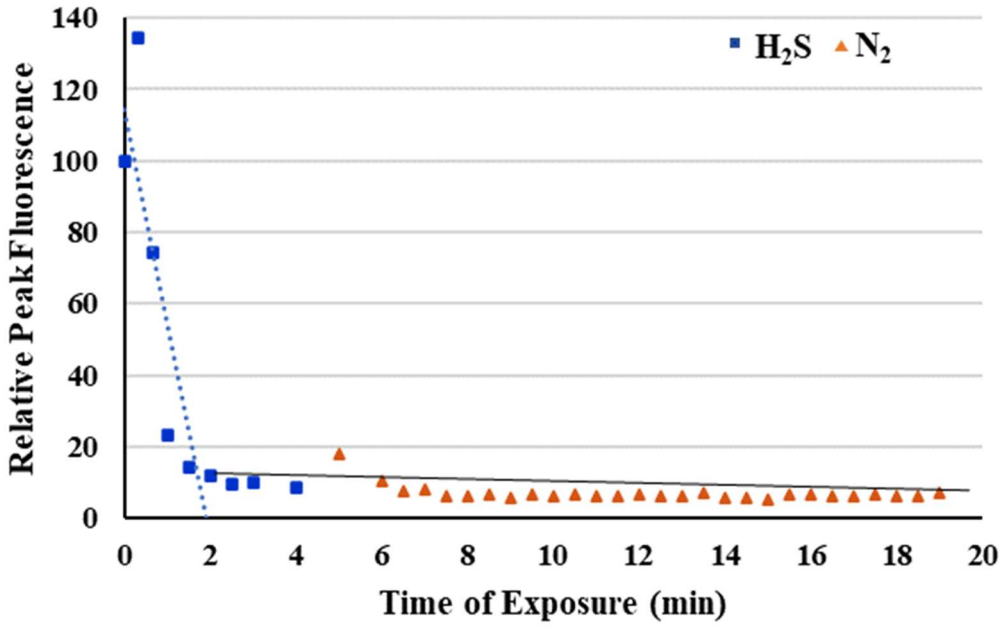

Figure 48: Graph of peak emission intensity against time obtained by passing 0.5 SLPM H2S gas through the biosensor solution for the first 4 minutes followed by 0.5 SLPM N2 gas for the final 15 minutes temperature while maintaining a temperature of 37°C

3.1.3 Applying Le Châtelier's principle

One of the findings from these fluorescence curves obtained from the previously-mentioned regeneration tests was that, in all cases the reaction seems to reach an equilibrium or saturation point (after around 2 minutes), which means that after this point, the intensity does not change appreciably. Keeping this in mind, an experiment was conducted to take advantage of Le Châtelier's principle by introducing additional fluorophore (1-AMA) at the reaction equilibrium point to attempt to regenerate the biosensor. According to Le Châtelier's principle, if a dynamic equilibrium of a reversible reaction is disturbed by changing the conditions (pressure, temperature, or concentration), the position of equilibrium shifts to counteract the change to reestablish an equilibrium (Atkins 1993). This means, in the case of a truly reversible reaction, adding excess quantities of one of the products (i.e., fluorophore 1-AMA in this case) at the reaction equilibrium point, may shift the reaction equilibrium to the left and regenerate the protein-fluorophore bond again as shown in **Figure 49**. Hypothetically, this would be expected to release the odorant from its protein binding and allow the free odorant molecules to be purged from the system.

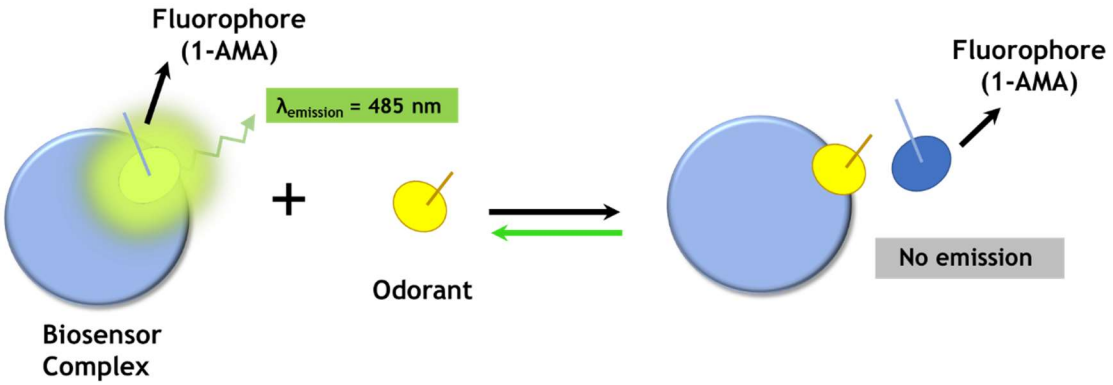

Figure 49: Adding more 1-AMA at the reaction equilibrium will favor more reactant formation (protein-fluorophore complex) to regenerate the sensor if the reaction is reversible

The result of testing this hypothesis is presented in **Figure 50**. Here, the intensity of the biosensor solution first decreases for around 2 minutes and then remains unchanged for the next 2 minutes (blue points) as well as during the 4 minutes of nitrogen purging time (orange points).

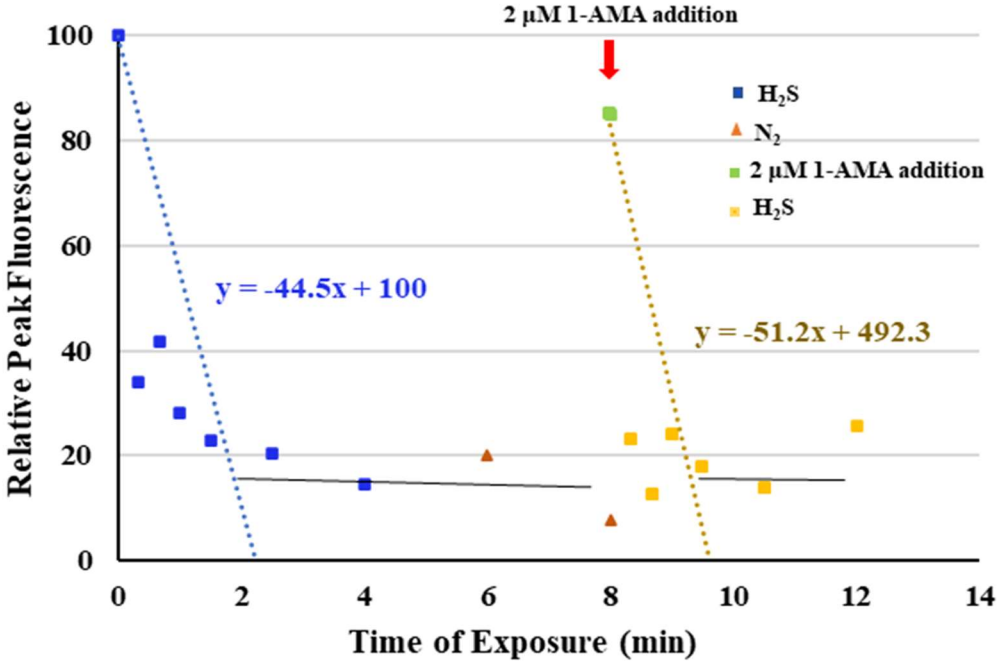

Figure 50: Graph of peak emission intensity against exposure time obtained by passing 0.5 SLPM H_2S gas through the biosensor solution for the first 4 minutes followed by 0.5 SLPM N_2 gas for the next 4 minutes and then the additional passage of H_2S gas in cycle 2 after successful regeneration of the biosensor by adding 2 µM additional 1-AMA

Only two samples were collected for spectrofluorometry during the nitrogen purging time since nitrogen does not significantly change the fluorescence intensity as observed from

the previous experiments (refer to **Figure 47** and **Figure 48**). Afterward, the intensity returns back to almost 90% (green point) when an additional 2 µM of 1-AMA in the remaining biosensor solution was added, leading to successful regeneration of the sensor. Afterward, when another cycle of hydrogen sulfide was passed into the regenerated sensor for a second round of detection for 4 more minutes, it caused a similar pattern of decrease in the peak fluorescence intensity as of the initial cycle (yellow points). Similar to the first cycle, here the intensity decreases for the first few minutes until it remains nearly unchanged for the rest of the experiment. The slopes of the lines generated for the two cycles were within 15% of each other. Here for the two cycles combined, around 70 µg of hydrogen sulfide reacts with 270 µg of hOBPIIa up to the saturation points. When the same experiment was conducted by adding 1µM of additional 1-AMA at the reaction equilibrium, it resulted in a slight increase in the peak fluorescence intensity (graph not shown). No attempt was made to optimize the amount of additional fluorophore added in this experiment as doubling the concentration showed only a minimal effect but tripling the concentration of the fluorophore resulted in near complete regeneration.

3.2 Analysis of the Fluorescence Binding Assay for Nitrogen

Figure 52 shows the results obtained from passing nitrogen purge gas at 25 mL/min flow rate into the biosensor solution using the new flow-through setup. The experiment was run for 4 minutes to compare the results obtained for the same experiment but using a 0.5 SLPM flow rate in Rahman (2020) and the prior setup (refer to **Figure 51**). The new results show a similar trend as the older ones, the fluorescence intensity remaining nearly the same over the course of the experiment, and the biosensor seems to be non-reactive with the inert nitrogen purge gas. There is significantly less noise in the latest iteration as seen by comparing the new setup (**Figure 51**) and the previous one (**Figure 52**).

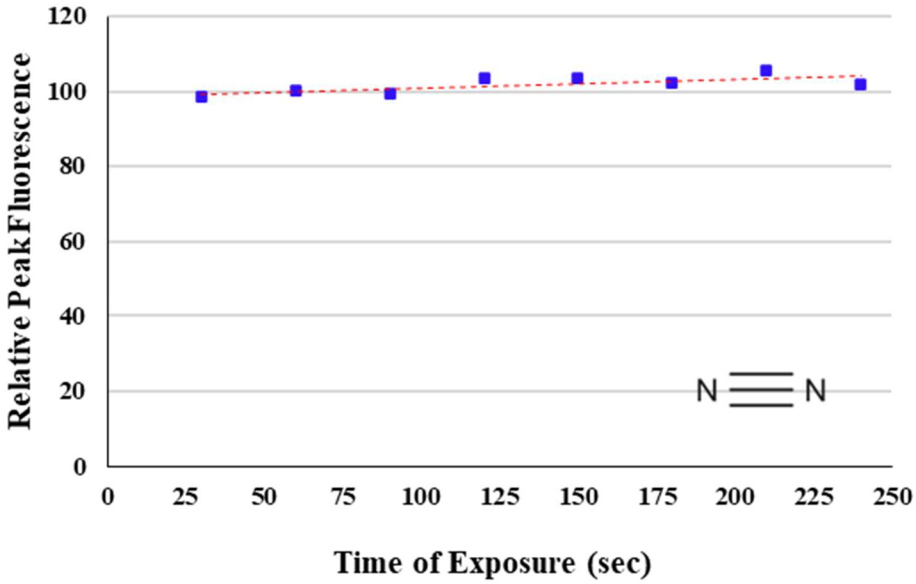

Figure 51: Peak emission intensity against time for non-odorous N_2 passed at 25 mL/min (0.025 SLPM) flow rate into the biosensor solution using the new flow-through setup

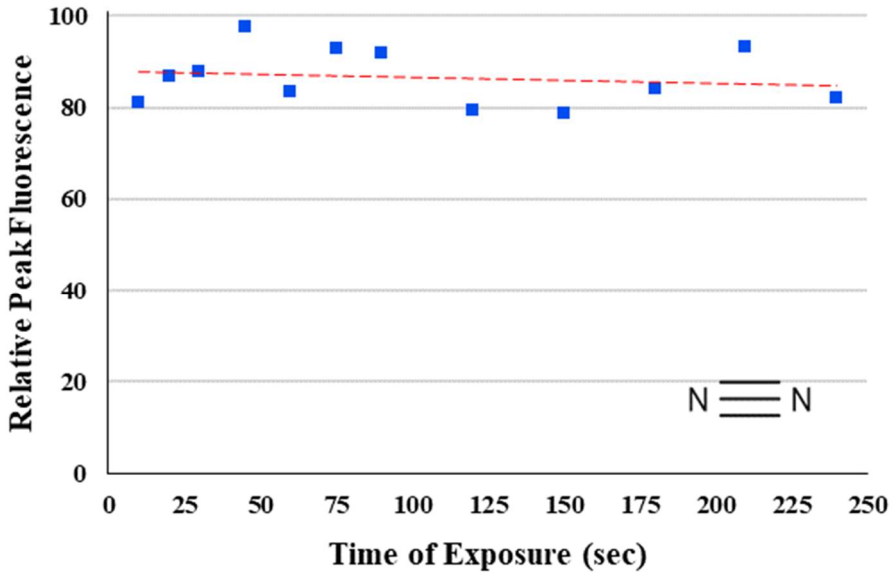

Figure 52: Peak emission intensity against time for non-odorous N_2 passed at 0.5 SLPM flow rate into the biosensor solution using the previous experimental setup (Rahman 2020)

3.3 Analysis of the Fluorescence Binding Assay for Pure Odorant Gases

In the previous study (Rahman 2020), binding assays were performed for pure odorants including hydrogen sulfide, methyl mercaptan, and ammonia, where the fluorescence intensity was found to decrease up to the QR for each, depending on the flow rates used. The ranges for hydrogen sulfide were 90-120 seconds for a flow rate of 0.5-0.9 SLPM. For ammonia and methyl mercaptan, the ranges were 50-90 seconds and 60-95 seconds, respectively for the same range of flow rates. It was also seen that for a specific gas, a certain mass would bind with the biosensor before the QR was reached.

For the current set of experiments, the flow rate was lowered to approximately 20 times the previous value (0.025 SLPM vs. 0.5 SLPM), while the protein amount was decreased by a factor of 5. This means that the QR should be expected to increase by approximately 4 times for each these gases. However, while testing these gases for real-time fluorescence analysis with the flowthrough system, it was observed that none of the gases showed any decrease in fluorescence intensity even for an experiment duration of 8 minutes. Afterwards, the experiment duration was extended to 1 hour to check for a decrease in fluorescence intensity. Nitrogen was passed for the first few minutes in each experiment to ensure that no air was in the system to impact the reaction with the odorants in any way. However, no appreciable change in intensity was observed during this 1-hour period for any of the three gases tested. **Figure 53**, **Figure 55** and **Figure 57** show the intensity vs. wavelength plot obtained at different time intervals for hydrogen sulfide, ammonia, and methyl mercaptan, respectively during this 1-hour period, while **Figure 54**, **Figure 56**, and **Figure 58** show the plot of relative peak emission intensities against time for the same gases, respectively during the same time intervals.

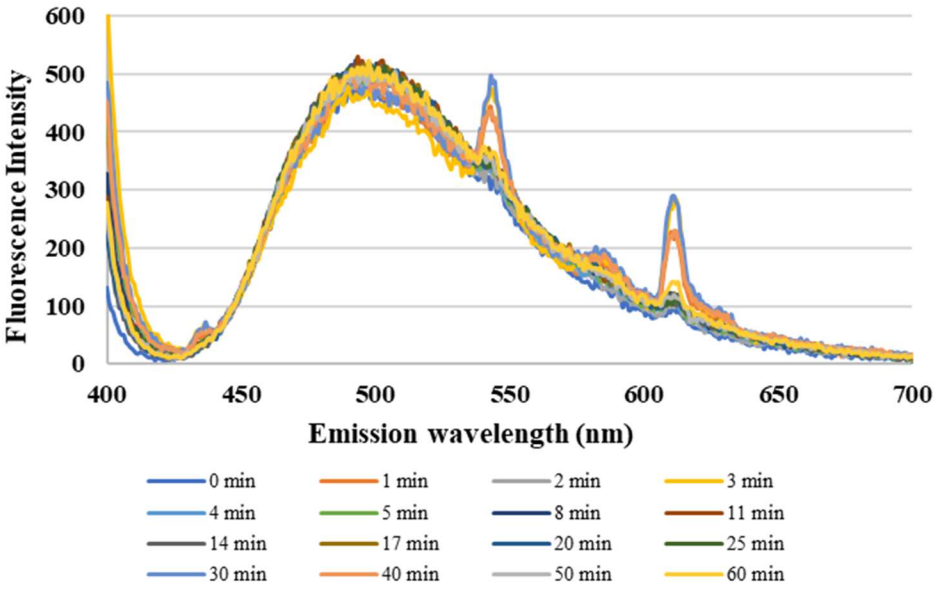

Figure 53: Spectrofluorometric emission spectra for 25mL/min H_2S

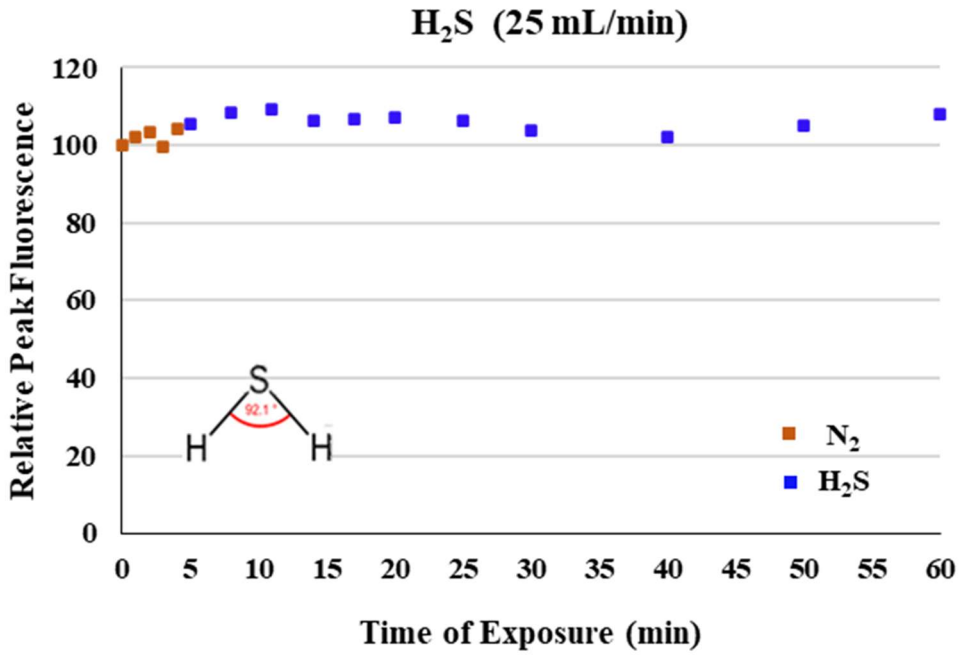

Figure 54: Relative peak emission intensity against time of gas exposure for 25mL/min H_2S for real-time fluorescence measurement (First 4 minutes purging with N_2)

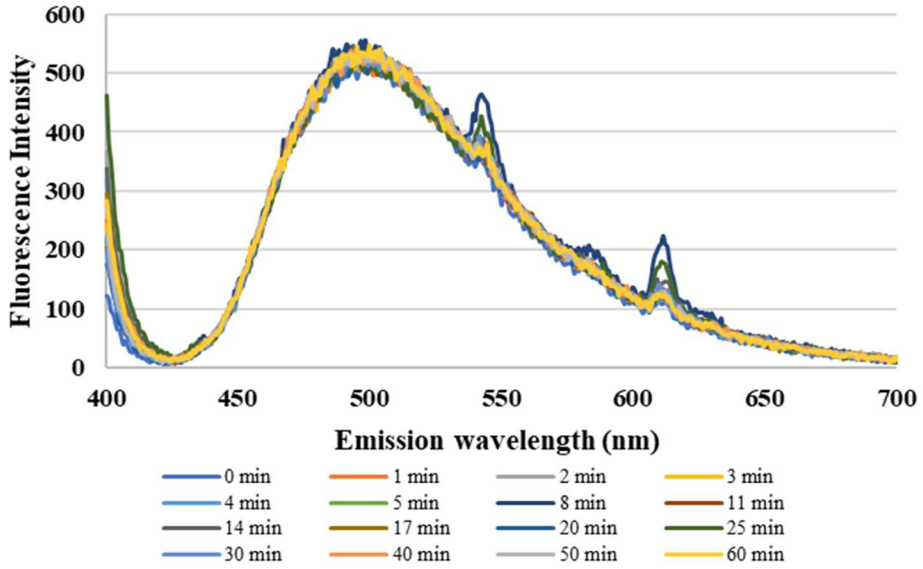

Figure 55: Spectrofluorometric emission spectra for 25mL/min NH_3

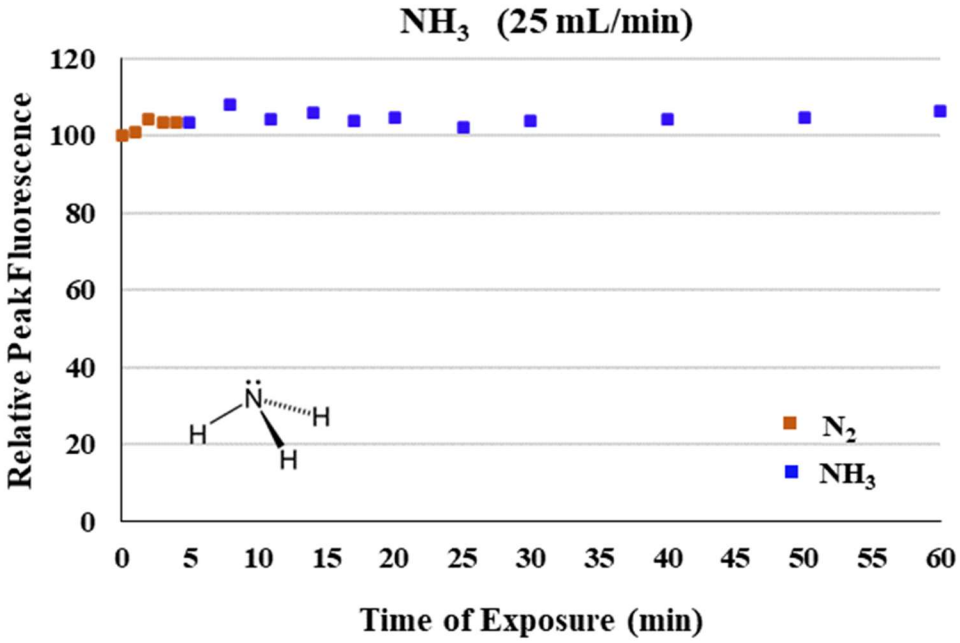

Figure 56: Relative peak emission intensity against time of gas exposure for 25mL/min NH_3 for real-time fluorescence measurement (First 4 minutes purging with N_2)

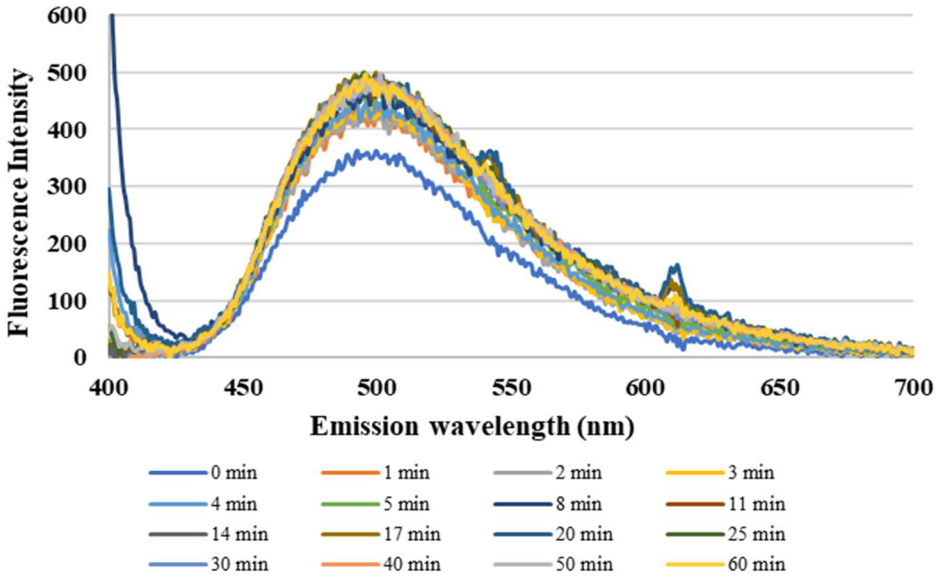

Figure 57: Spectrofluorometric emission spectra for 25mL/min CH_3SH (methyl mercaptan)

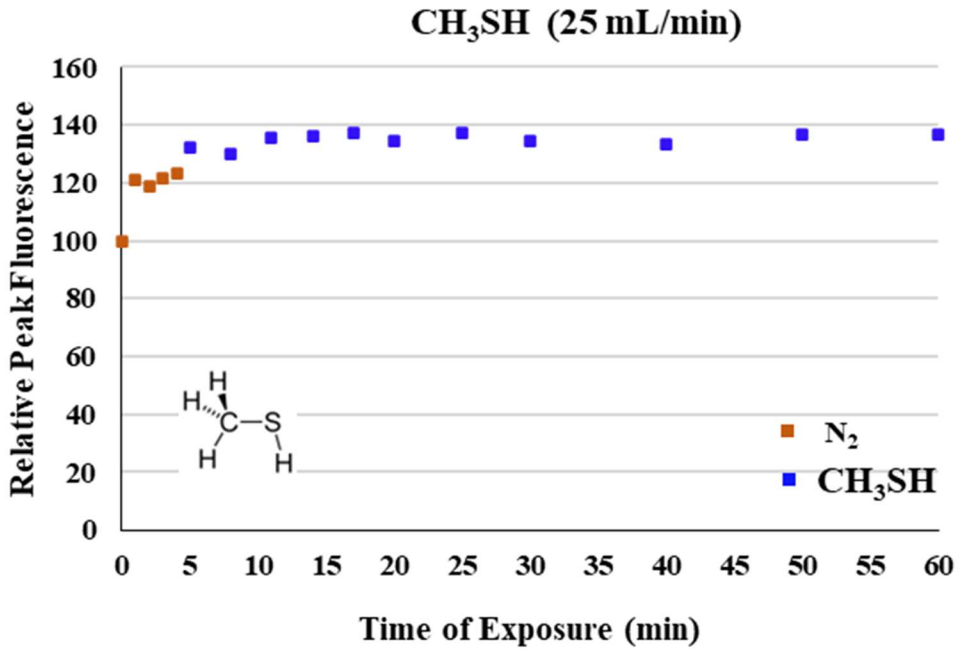

Figure 58: Relative peak emission intensity against time of gas exposure for 25mL/min CH_3SH (methyl mercaptan) for real-time fluorescence measurement (First 4 minutes purging with N_2)

Because of the lack of change in fluorescence intensity in the experiments, it was important to rule out the impact of bubble formation on the readings. To that end, three separate experiments were designed and conducted for hydrogen sulfide, as follows:

I. Using a peristaltic pump to separate the reactor chamber (**section 2.4.2.6**), so that bubbles would be formed in a separate chamber and not interfere with the fluorescence reading
II. Saturating the buffer solution with odorant gas before adding the protein to rule out mass transfer limitations
III. Using a syringe to draw samples and measure fluorescence in a separate cuvette to mimic the previous experimental procedure

For Experiment I, an alternate flowthrough setup with a peristaltic pump was established to separate the reactor chamber from the flow cell where the measurement takes place. The fluorescence intensity dropped for the first 6 minutes when the pump was active even without the introduction of the odorant gas (shown in **Figure 59**).

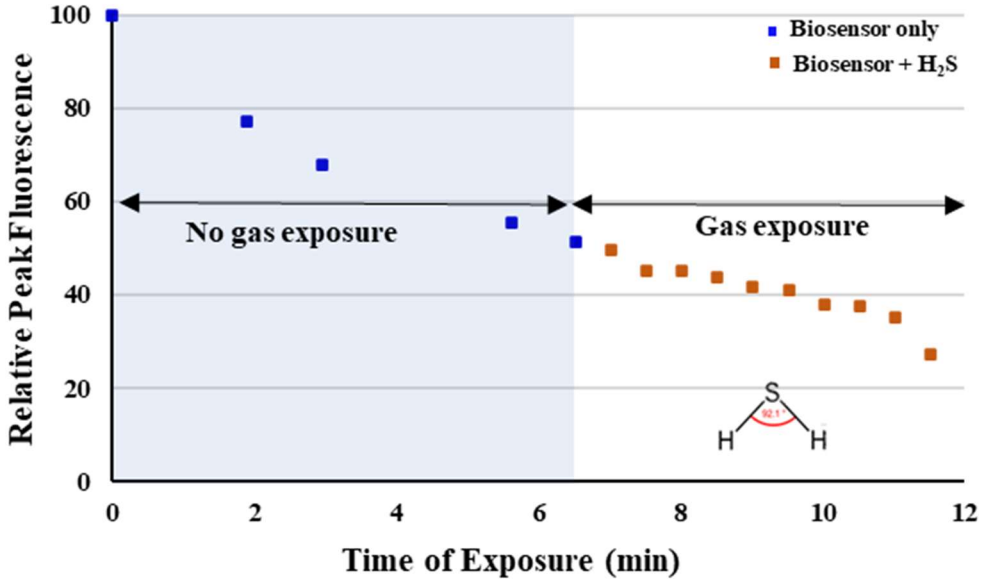

Figure 59: Relative peak emission intensity against time for the biosensor solution while the peristaltic pump is active (blue points) followed by an exposure to 0.025 SLPM H_2S (orange points)

After hydrogen sulfide was introduced, the intensity kept falling at the same rate, signifying that the odorant gas may not have been responsible for the drop in intensity in this case. One explanation might be that the biosensor accumulates in different parts of the system while it is circulated, leading to a steady decrease in intensity throughout the whole experiment. Also, it is possible that the molecules are colliding more during circulation, leading to a decrease in energy levels and thus, fluorescence intensity (Hardwick 1957).
A separate experiment where the biosensor solution was circulated with the pump without adding any odorant gas was conducted to verify the falling intensity. **Figure 60** shows the result where the intensity keeps decreasing with time during the entire time of the

experiment while the transfer takes place. If complete mixing conditions were achieved, the signal intensity with no added gas would be expected to be flat over time. Therefore, the bubble effect was not able to be tested in this configuration.

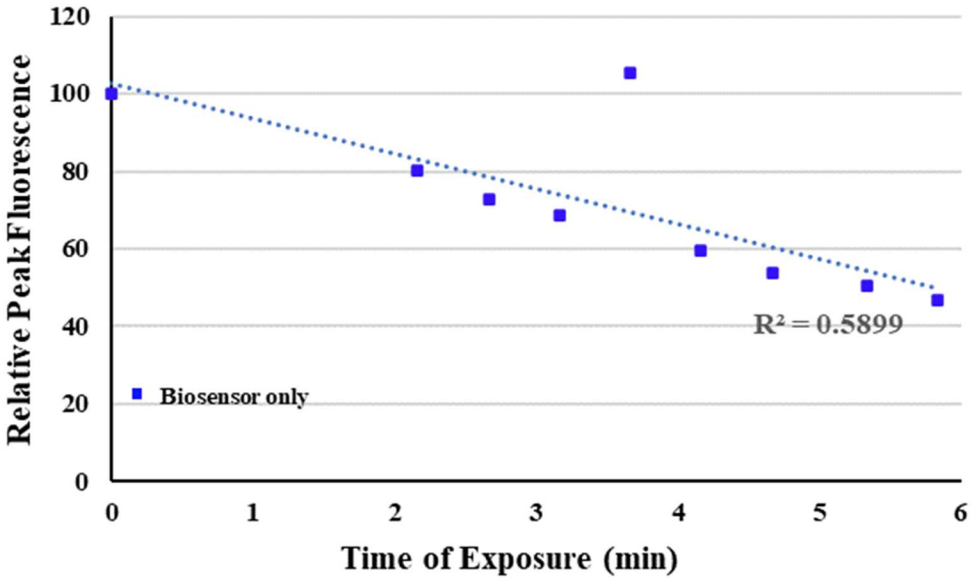

Figure 60: Relative peak emission intensity against time for the biosensor solution while the peristaltic pump is active

Experiment II was designed where the buffer solution was initially saturated with hydrogen sulfide gas by passing it for 5 minutes before the protein and 1-AMA mixture was added to it. The intention was to prevent the biosensor itself from coming in contact with the odorant bubbles that might interfere with the readings. The expectation was that once the protein is introduced, the intensity reading will fall. This is not intended to be a continuous fluorescence analysis; rather the goal was to collect a one-time reading to ensure that a decrease in intensity is actually observed once the odorant combines with the biosensor. For this experiment, three concentrations of protein-fluorophore were used (1 µM, 1.5 µM, and 2 µM). Although the regular experiments were conducted at a concentration of 1 µM, two separate concentrations were used here to check whether any decrease in intensity was observed in the presence of an increased amount of protein.

Figure 61 shows the results of this experiment. Readings were collected for each set of biosensor concentrations just by itself and then also after the biosensor was added to the buffer solution previously saturated by the odorant gas. There was no measurable difference between the two readings for the concentrations of 1 µM and 1.5 µM, as shown in **Figure 61**. However, a promising decrease in reading was observed for the 2 µM concentration. This provides evidence that the bubble formation might not have interfered with the previous results obtained.

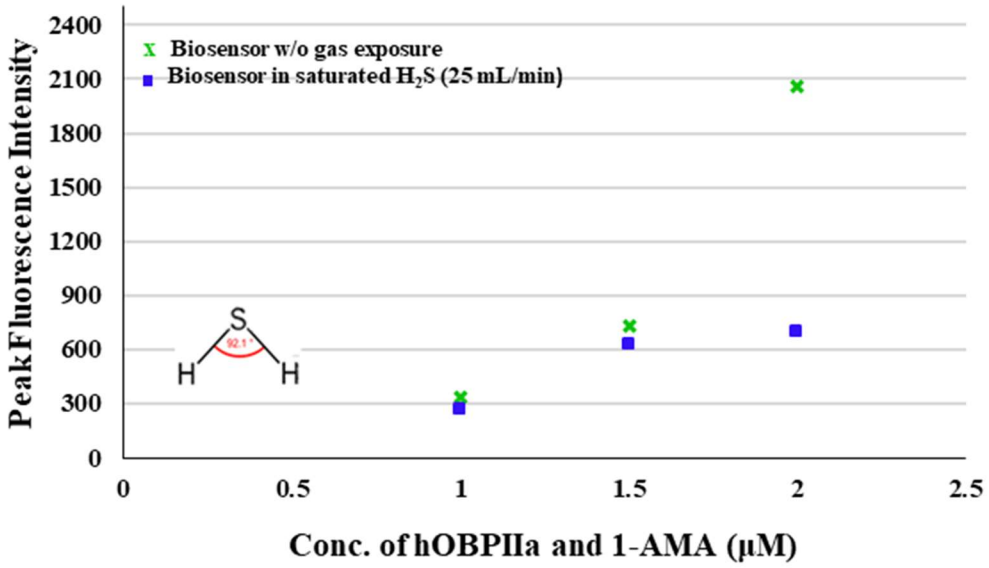

Figure 61: Peak emission intensity against time for the biosensor solution only at different concentrations of protein-1-AMA (green points) and biosensor in saturated H_2S at the same concentrations (blue points)

To further test whether a 2 µM concentration of protein and 1-AMA yields a decrease in fluorescence intensity for continuous real-time measurements, the flow-through system was again used to pass hydrogen sulfide gas into the biosensor solution for 4 minutes. **Figure 62** is plot of relative peak emission intensity against time of gas exposure for that particular experiment. Although there is some decrease in the intensity overall (80% of initial reading), there is no clear pattern that replicates previous results from Roblyer (2017) or Rahman (2020).

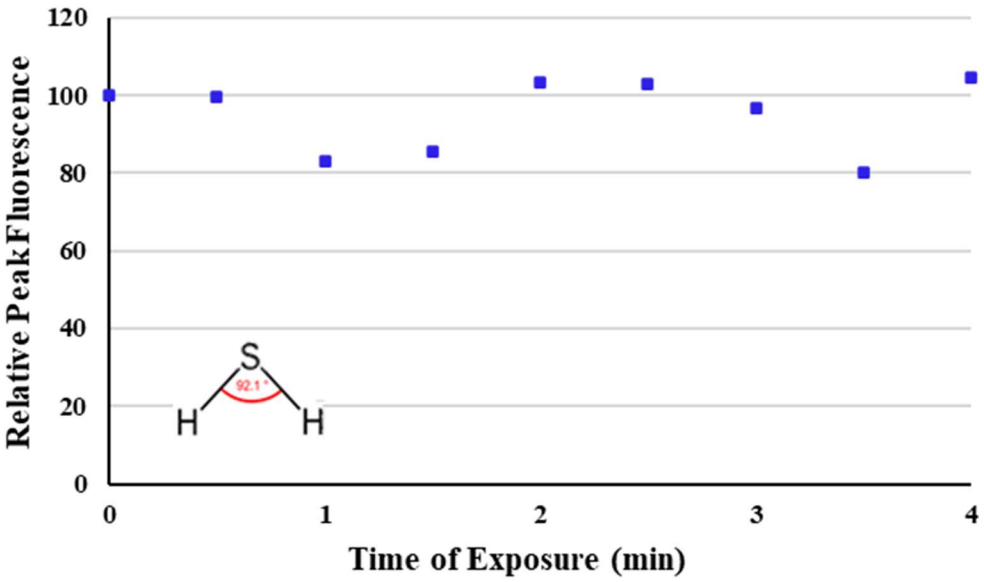

Figure 62: Relative peak emission intensity against time of gas exposure for 0.025 SLPM H_2S for real-time fluorescence measurement (using 2 µM conc. of protein and 1-AMA)

Because Experiment II did not provide conclusive results, Experiment III was conducted where the flow cell was used for combining the odorant gas with the biosensor and then samples were collected using syringes at certain time intervals similar to how the regeneration experiments were conducted. The goal was to rule out whether the previous decrease in intensities was merely due to the gradual mass loss of the biosensor solution as samples were collected throughout the entire length of the experiment. The fluorescence measurements themselves were obtained using a separate cuvette (refer to **Figure 32**), which was the same one used in the regeneration experiments and previous experiments from Rahman (2020).

Here, hydrogen sulfide was passed into the biosensor solution for 3.5 minutes. **Figure 63** is the plot of relative peak emission against time of gas exposure for this experiment. As seen from the graph, there is a clear pattern of decrease in this case, although the intensity does not decrease past the 80% mark. Additionally, this final intensity level seemed to be achieved rather quickly and not gradually as was the case with the previous experiments conducted by Rahman (2020). This is evidence that the measured decrease in fluorescence intensity in the previous study (Rahman 2020) may not have been entirely due to potential mass loss of the biosensor during the measurement of readings. But it might still be possible that mass loss is partially the cause since the intensity did actually decrease in Experiment III.

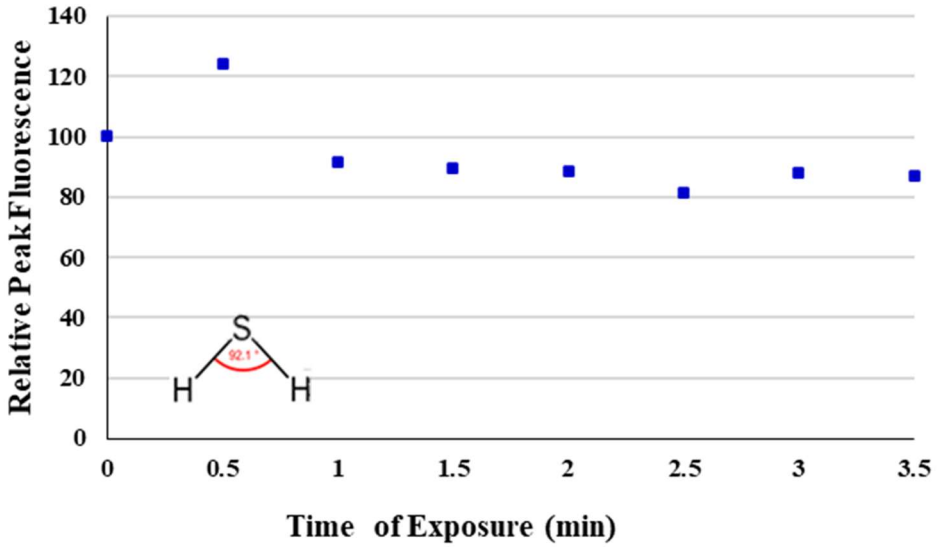

Figure 63: Relative peak emission intensity against time of gas exposure for 25 mL/min H_2S while samples are collected using syringes from the flow cell (not real-time analysis)

The previous three experiments did not conclusively show that the odorant gas bubbles in the cuvette chamber led to an inability to detect any changes in measurable fluorescence intensity. So, the next step was to conduct the same experiment for an extended period of time using three new odorant gases to check whether any decrease is observed. Real-time fluorescence analysis was conducted for 1 hour for toluene, formaldehyde, and tert-butyl mercaptan, individually, as well as a test with zero-air to make sure that the balancing gas in toluene does not interfere with the result. **Figure 64** is a plot of relative peak fluorescence intensity versus time for the zero air. There seems to be some initial increase in intensity that remains mostly constant for much of the 10-minute duration of the experiment. Results for toluene, formaldehyde, and tert-butyl mercaptan are shown in **Figure 65**, **Figure 66** and **Figure 67**, respectively. With toluene, the reading remains nearly constant for the first 20 minutes of the experiment, but decreases steadily thereafter, ultimately reaching almost 75% of its initial intensity at the 60-minute mark. The reduction in intensity is linear, as shown by the plotted trendline on the graph (**Figure 65**). However, for the other two gases, i.e., formaldehyde and tert-butyl mercaptan, the intensity remains nearly constant for the duration of the experiment.

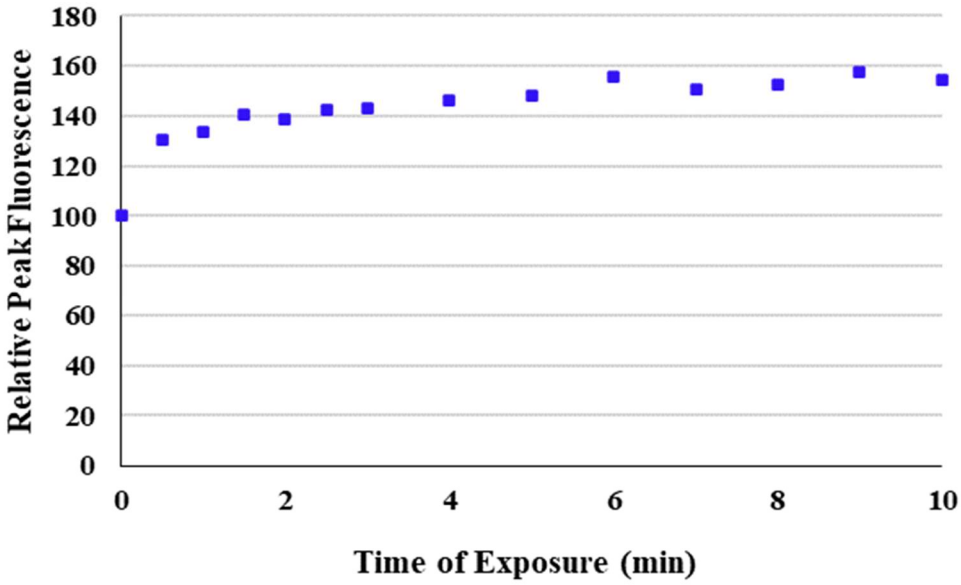

Figure 64: Relative peak emission intensity against time for zero air exposure at 25 mL/min for real-time fluorescence measurement

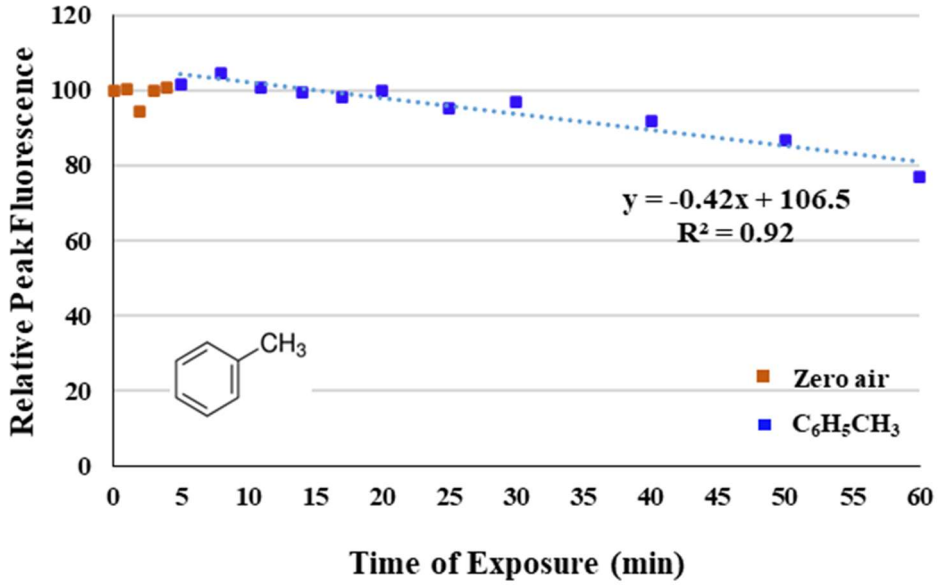

Figure 65: Relative peak emission intensity against time of gas exposure for 25 mL/min $C_6H_5CH_3$ (toluene) for real-time fluorescence measurement

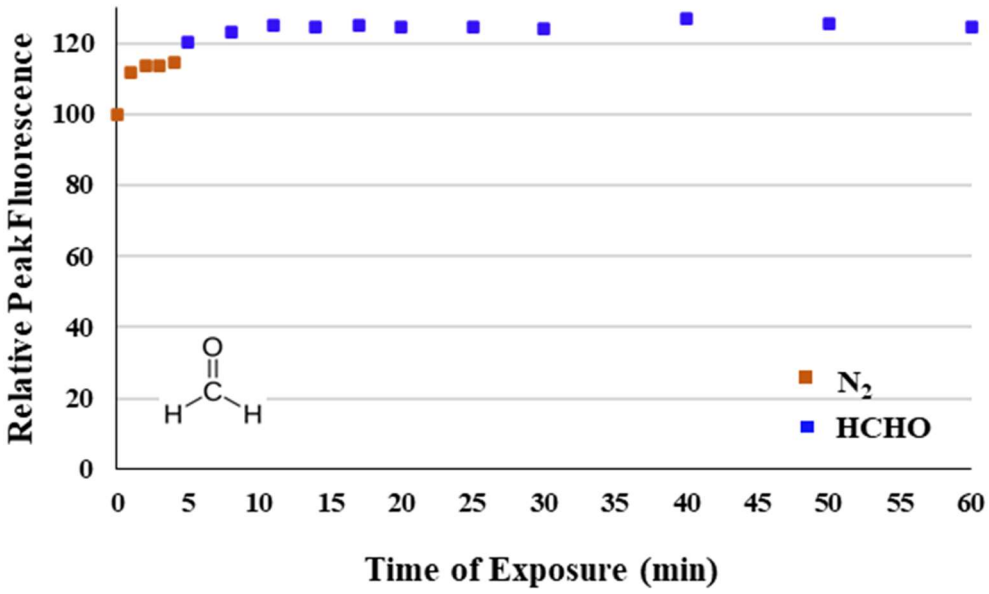

Figure 66: Relative peak emission intensity against time of gas exposure for 25 mL/min HCHO (formaldehyde) for real-time fluorescence measurement

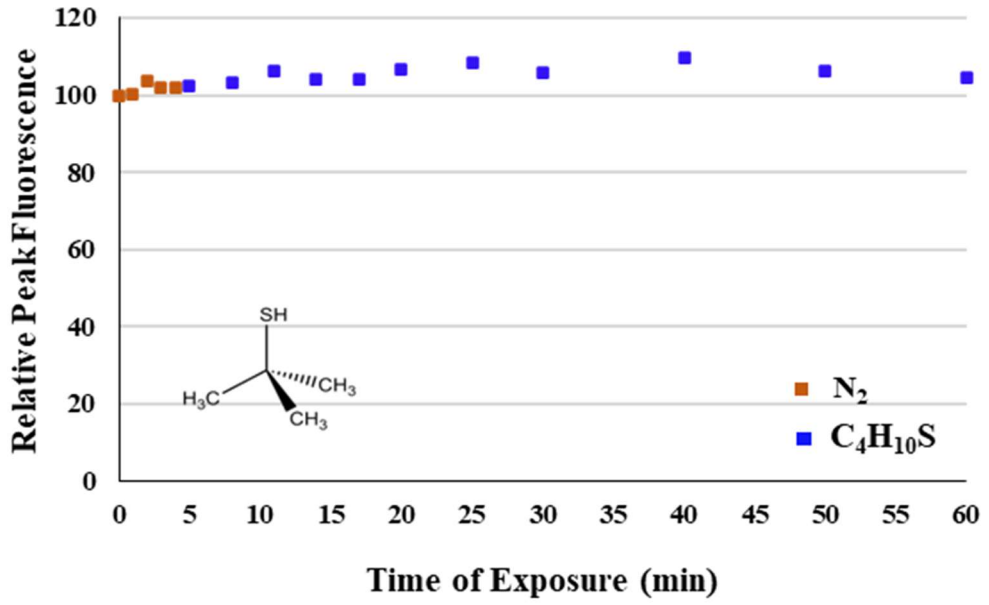

Figure 67: Relative peak emission intensity against time of gas exposure for 25 mL/min $C_4H_{10}S$ (tert-butyl mercaptan) for real-time fluorescence measurement

The difference in results can be explained by the difference in binding energies as found by Castro et al. (2021). As can be seen in **Table 16**, the binding energy ($\Delta G_{binding}$) of toluene with hOBPIIa has a higher magnitude than the other gases. Coupled with a higher hydrophobicity, this would allow toluene to combine with hOBPIIa more easily than the other odorants tested, since hOBPIIa tends to bind more readily with hydrophobic

molecules (Briand et al. 2002). Around 136 µg of toluene was passed in 36 µg of hOBPIIa within the 1-hour experiment. Tert-butyl mercaptan, while having a comparatively high hydrophobicity, has a lower binding energy, which may explain it failing to decrease the fluorescence intensity. Also, the concentration of commercially available specialty gas cylinders of tert-butyl mercaptan (3 ppm) used in this study was 8 times lower than that of toluene (24 ppm), which may play a part in the tert-butyl mercaptan not combining with the biosensor to generate a measurable signal (below detection), under the experimental conditions. The binding energies ($\Delta G_{binding}$) as well as the hydrophobicity (log P) for hydrogen sulfide and ammonia are also lower, as mentioned in **Table 16**, indicating their reluctance to chemically combine with the protein to decrease the fluorescence intensity of the biosensor. These molecules are also smaller in size and have a very high Vp (vapor pressure) value, meaning they are the most volatile odorants tested in this study, another factor that may influence or inhibit binding with the protein as found by Castro et al. (2021). In the case of formaldehyde, Castro et al. (2021) has not provided any data. However, based on the low hydrophobicity and high vapor pressure (OECD 2002, National Academics Press 2022) as documented in **Table 16**, it is expected that formaldehyde would not combine with the protein to an appreciable extent.

Table 16: The level of hydrophobicity (log P), vapor pressure (Vp) and the binding energy ($\Delta G_{binding}$) of several pure odorant gases (Castro et al. 2021, OECD 2002, National Academics Press 2022)

Name	Formula	log P (Hydrophobicity level)	Vp (Vapor pressure, mmHg)	$\Delta G_{binding}$ (kcal/mol)
Hydrogen sulfide	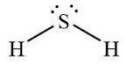	-1.38	13,376	-0.6
Methyl Mercaptan	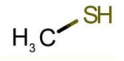	0.78	1510	-1.1
Ammonia	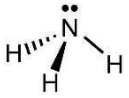	-2.66	7500	-1.4
Butyl mercaptan	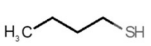	2.28	45.5	-3.3
Toluene	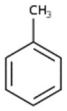	2.73	28.4	-5.7

Name	Formula	log P (Hydrophobicity level)	Vp (Vapor pressure, mmHg)	$\Delta G_{binding}$ (kcal/mol)
Formaldehyde	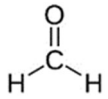	0.35	3890	-

In the previous experiment with toluene (as shown in **Figure 65**), since the intensity was lowered by more than 20%, one conclusion might be that the biosensor might have mostly been spent, leading to a slow rate of change in intensity in that experiment. To test this, another experiment was run with double the concentration of the biosensor (2µM hOBPIIa and 1-AMA having 72 µg of hOBPIIa) and the same flowrate of toluene for 1 hour (25 mL/min containing a total of 136 µg of toluene). **Figure 68**, which is a plot of fluorescence intensity versus time, shows that the intensity was lowered by around 15% in this experiment. This refutes the argument that the biosensor was mostly spent in the previous experiment, since even with double the concentration, the rate of decrease in intensity with toluene remains nearly the same, which means that toluene in general combines at a slow rate with the biosensor.

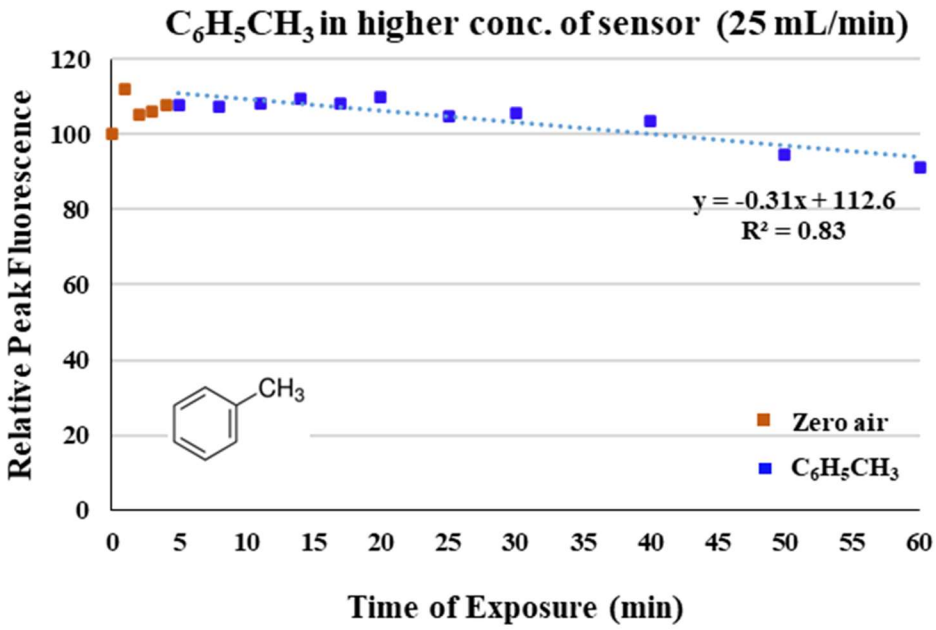

Figure 68: Relative peak emission intensity against time of gas exposure for 25mL/min $C_6H_5CH_3$ (toluene) for real-time fluorescence measurement while using a higher concentration of the sensor

In the previous study, Rahman (2020) found a decrease in fluorescence intensity for experiments with all odorants, including hydrogen sulfide and ammonia. A reason for this

might be the higher flowrate of gas used during those experiments compared to the current study (approximately 20 times higher). This higher flowrate and corresponding higher mass flux of the odorant gases may have forced the odorant molecules to combine with the biosensor more rapidly with a visible decrease in intensity. However, for this study, the miniaturized flow cell and setup will not support such a high odorant flowrate. The odorant molecules that fail to show a decrease in fluorescence intensity at such a low flow rate in this study may not bind with hOBPIIa in the human nose. Rather, being hydrophilic, they simply diffuse themselves in the mucus to be transported over to the olfactory neurons, as mentioned in Castro et al (2021).

3.4 Analysis of the Fluorescence Binding Assay for Mixture of Odorant Gases

The experiments with pure odorant gases show that the highly hydrophobic toluene (based on **Table 16**) combines with the biosensor while the other less hydrophobic odorants do not change the spectrofluorometric intensity in a measurable amount. Thus, it was decided for testing with mixtures, two other gases should be mixed with toluene separately based on their hydrophobicity in **Table 16**. The first experiment was with a combination of ammonia and toluene keeping a combined flow rate of 25 mL/min. The goal is to investigate whether a mixture of the two hydrophobic gases can lower the fluorescence intensity even further. **Figure 69** shows intensity versus time plot of this experiment. As can be seen, the intensity was lowered by around just more than 20% of the original value. Since this is the same result obtained with toluene alone and the slope of the intensity trendline is also similar to that of the experiment with only toluene (as shown in **Figure 65**), the presence of ammonia does not seem to affect the outcome in the current experimental configuration.

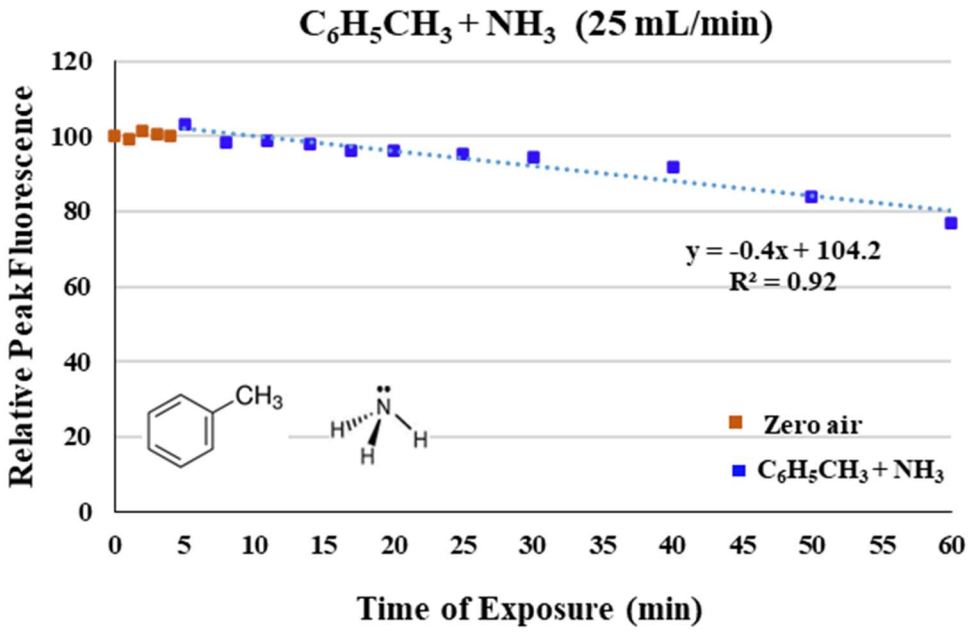

Figure 69: Relative peak emission intensity against time for a mixture of $C_6H_5CH_3$ (toluene) and NH_3 (ammonia) at 25 mL/min for real-time fluorescence measurement

The next experiment was conducted with a mixture of toluene and tert-butyl mercaptan. The intensity versus time plot is shown in **Figure 70**. The outcome is almost the same as in the case of the previous mixture (refer to **Figure 69**), the intensity being lowered by just more than 20% with a nearly similar gradient of the slope. This shows that just like the previous experiment, there was no additional lowering of intensity due to the mixture of toluene and tert-butyl mercaptan, with toluene most likely playing the leading role behind the change in intensity. These two experiments with the gas mixtures demonstrate the ability of hOBPIIa to indicate the presence of hydrophobic gases within a mixture of odorants under these specific experimental conditions.

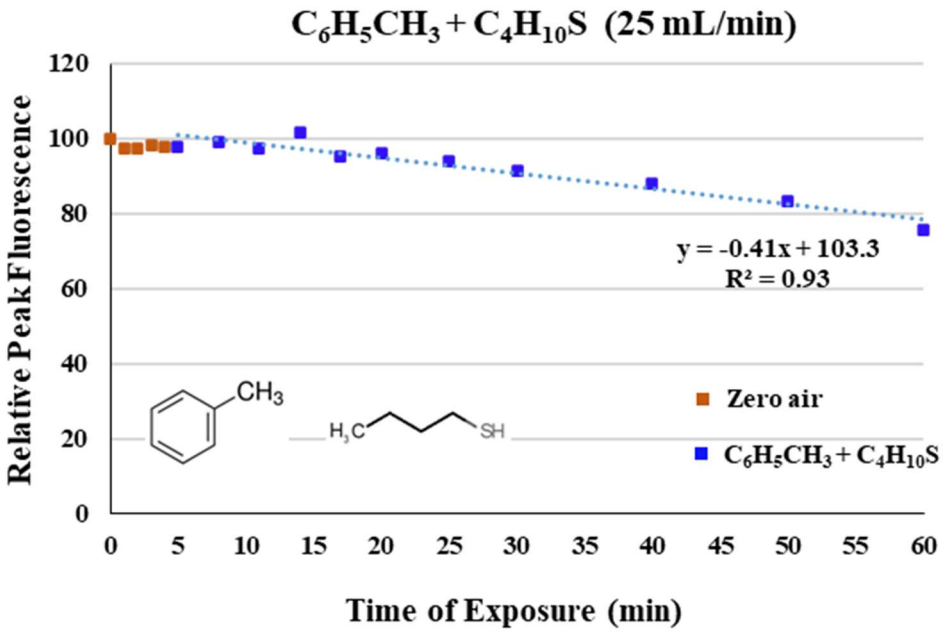

Figure 70: Relative peak emission intensity against time for mixture of $C_6H_5CH_3$ (toluene) and $C_4H_{10}S$ (tert-butyl mercaptan) at 25 mL/min for real-time fluorescence measurement

4 CONCLUSIONS AND RECOMMENDATIONS

4.1 Major Findings

One of the most important objectives of this research was to explore the regeneration of the biosensor solution after initial usage with an odorant gas. As a continuation of the previous study from Rahman (2020), a number of methods were tested to bring back the initial protein fluorescent signal in the biosensor after its reaction with an odorant gas. Successful results were obtained by following Le Châtelier's principle, where additional fluorophore was injected into the used biosensor after its initial odorant reaction, causing the equilibrium to shift to the left and regenerate most of the original protein fluorescent signal. Experimentally, almost 90% of the initial protein was regenerated, and the resultant protein was shown to follow the same reaction behavior with the odorant gas as the initial batch of reactant protein.

An important aspect of the current research has been the miniaturization of the experimental setup from the previous study of Rahman (2020). This has been accomplished by using a highly-sensitive, high-precision spectrofluorometer (QE Pro-FL) obtained from Ocean Insight, which allows a flow-through setup, enabling the flow cell cuvette to be used as the reaction chamber to collect real-time fluorescence readings. The advantages to this setup are manyfold. Using the cuvette as the reaction chamber has substantially lowered the protein usage to run each experiment, while allowing for continuous logging of the spectrofluorometric measurements as the experiments progress. This enables an increase in accuracy by ensuring that the samples are never taken out of the reactor chamber or exposed to potentially contaminated ambient air for fluorescence measurements as in the procedure followed by Rahman (2020), which otherwise causes the protein mass to decrease gradually with each additional sample, resulting in potential inaccurate fluorescence readings. The new QE Pro-FL spectrofluorometer also allows for automatic logging of results after specific intervals and up until a predetermined point in time, largely automating the procedure and cutting down on the time required to run an experiment. Additionally, each reading is collected in real-time, as opposed to the nearly 15 seconds required to collect a single reading using the previous spectrofluorometer in Rahman (2020). An added advantage of using this spectrofluorometer is its portability being modular and small in size, which allows it to be effectively used for taking field measurements.

As part of the current research, a number of landfill odorants tested in Rahman (2020) as well as a batch of new odorants were tested with the biosensor solution to observe their spectrofluoroscopic response using the newly designed experimental setup. These odorants tested included hydrogen sulfide, ammonia, methyl mercaptan, toluene, formaldehyde, and tert-butyl mercaptan (Appendix B documents the amount of mass detected for all the tested gases with the biosensor complex). Of these odorants, the biosensor solution showed the strongest response towards toluene, which is shown by a decrease to nearly 80% of the original fluorescence intensity. This can be explained by the higher magnitude of binding energy of toluene with hOPBIIa compared to the other odorants as mentioned in Castro (2021) for the higher level of hydrophobicity of toluene, which makes it easier to combine with hOBPIIa. An explanation as to why the other reactant odorants (which are also

hydrophilic in nature) showed a less-than-expected lowering of fluorescence intensity would be the lower flowrates used for the gases in the new experimental setup for reducing the impact of bubbles on the fluorescence readings. The experiments with the gas mixtures demonstrate the ability of hOBPIIa to indicate the presence of hydrophobic odorants within a mixture of hydrophobic and hydrophilic odorants.

4.2 Recommendations

In the current experimental setup, the flowrate has been minimized compared to the prior batch of experiments with the prototype chamber. Although this has allowed the adoption of a more efficient flow-through system, the response curves have a less-than-expected decrease in fluorescence intensity. It would be informative to run the experiment with the previous procedure used in Rahman (2000) but with the lower flowrate and biosensor concentration of this study to see if a similar result is obtained. Additional experiments should be conducted using higher flowrates reflecting previous experiments as conducted in Rahman (2020), while ensuring that the higher flowrate does not lead to overflow of the new smaller reactor chamber, i.e., the flow cell. The target will be to replicate the results obtained by Rahman (2020). An argument can be made to increase the concentration of the gas rather than increasing the flowrate. However, this does not reflect the real-world scenario in landfills where the actual concentrations of the gases are relatively low but the intensity of the odorant and the windspeed (corresponding to the flowrate in the experiments) can vary.

In the next set of experiments, a larger range of targeted odorant categories should be included as part of the experiments. This will include hydrophobic odorants since those have been known to bind well with hOBPIIa as well as hydrophobic compounds that are non-odorous and can be found in landfill gas e.g., methane, ethane, propane, butane, nitrous oxide, carbon dioxide, etc. (Scheutz et al. 2008). These non-odorous hydrophobic gases will be potential interferents in odor measurements in landfill air and so it is important to investigate the response of the biosensor to these gases. Hydrophobic mixtures should also be included in future experiments.

Since a low flow rate of the hydrophilic odorant gas does not show a signal with the biosensor in this study, future experiments can be designed to find out whether the hydrophilic odorants combine with the protein under certain conditions (e.g., change in temperature, increasing gas flowrates, or adding certain additives). A promising line of research would be modifying the binding site or the binding characteristics of the protein for the hydrophilic odorants. Since the binding site is being targeted, this would also open the door to modifying the affinity of the protein towards certain odorants and perhaps even detect specific odorants from a mixture of gases. Additionally, it might be the case that if the binding affinity of the fluorophore towards the protein is reduced, the hydrophilic odorants might find it easier to combine with the protein. This can be accomplished by changing the structure of the protein to reduce the affinity for the fluorophore (van den Noort et al. 2021) or even controlling external factors to affect this affinity (Oliva et al. 2020).

From the outset of this research, the goal has been to extend this theoretical concept of quantifying odors using hOBPIIa and gradually develop this to be used in the field for detecting landfill odors. One step towards this direction will be capturing the spectrofluorometric response of the protein to environmental air (i.e., landfill air). In order to accomplish this, a prototype setup can be created that will pump in ambient air to the reactor chamber at a flowrate comparable to what is used in the laboratory experiments. Additionally, field samples can also be collected for testing in the laboratory using Tedlar bags of varying capacities (e.g., a 1.0 L Tedlar bag can support an experiment for 40 minutes if a flowrate of 25mL/min is used). This will allow for a way of detecting and quantifying environmental odors in field experiments.

As part of this study, the biosensor has been successfully regenerated through Le Châtelier's principle by adding more fluorophore at the reaction equilibrium. However, there was no effort to find out the optimum volume of fluorophore required for this regeneration process. As a next step, further investigation should be done to optimize the volume of this additional fluorophore as well as study the number of regeneration cycles to determine biosensor lifetime before it is spent. Potentially, this can be many cycles because the protein is known to be stable under many denaturing conditions.

The research so far has focused on quantifying unpleasant odors. As a next step, additional experiments can be run using pleasant odors to compare results against those obtained for unpleasant odors. Comparing the rate of fluorescence decrease of pleasant odors against the unpleasant ones, will allow an understanding of which pleasant odors are more susceptible to combining with hOBPIIa, and thus potentially helping to mask specific unpleasant odors.

So far, all the experiments have been with odorants that have been procured through specialty gas cylinders in their gaseous form. With the exception of formaldehyde, all the odorants naturally exist in their gaseous state. Future experiments can be undertaken to investigate whether liquid odorants can be detected using the biosensor through the same principle. One way of accomplishing this would be to use a combination of a syringe pump (shown in **Figure 71**) and air stream for converting the liquid odorant to gaseous form and then going through the same process as in the current set of experiments.

Figure 71: Single and multiple syringe infusion pump

APPENDICES

Appendix A: Amount of Gas Detected at Different Flow Rates from Rahman (2020) and this Study Combined

Name	Formula	Mass Detected at 0.5 SLPM (µg)	Mass Detected at 0.7 SLPM (µg)	Mass Detected at 0.9 SLPM (µg)	Mass Detected at 0.025 SLPM (25 mL/min) (µg)
Nitrogen	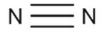	No signal	-	-	No signal
Zero Air	-	-	-	-	No signal
Methane		15	-	-	-
Hydrogen sulfide	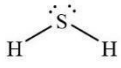	35	45	43	No signal
Methyl Mercaptan	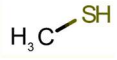	95	83	85	No signal
Ammonia	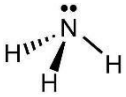	12	18	15	No signal
Butyl mercaptan		-	-	-	No signal
Toluene	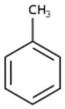	-	-	-	136 (up to 1 hour)
Formaldehyde	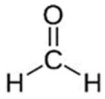	-	-	-	No signal

Appendix B: Fluorescence Measurement

A. Relative peak fluorescence intensity obtained at different time intervals for regeneration experiment (4 min hydrogen sulfide + 15 min nitrogen) (Refer to Figure 47)

Time (min)	Relative Peak Fluorescence Intensity
0	100.0
0.3	48.5
0.7	73.9
1.0	52.4
1.5	72.9
2.0	72.1
2.5	60.3
3.0	59.1
4.0	47.2
5	42.5
6	42.3
6.5	47.3
7	40.0
7.5	43.8
8	36.4
8.5	41.5
9	43.2
9.5	38.5
10	45.8
10.5	37.4
11	37.5
11.5	35.4
12	38.4
12.5	41.6
13	33.5
13.5	41.1
14	46.2
14.5	44.4
15	41.1
15.5	43.4
16	39.0
16.5	45.5
17	39.0
17.5	37.8

18	35.1
18.5	37.5
19	35.7

B. Relative peak fluorescence intensity obtained at different time intervals for regeneration experiment at 37°C (4 min hydrogen sulfide + 15 min nitrogen) (Refer to Figure 48)

Time (min)	Relative Peak Fluorescence Intensity
0	100.0
0.3	48.5
0.7	73.9
1.0	52.4
1.5	72.9
2.0	72.1
2.5	60.3
3.0	59.1
4.0	47.2
5	42.5
6	42.3
6.5	47.3
7	40.0
7.5	43.8
8	36.4
8.5	41.5
9	43.2
9.5	38.5
10	45.8
10.5	37.4
11	37.5
11.5	35.4
12	38.4
12.5	41.6
13	33.5
13.5	41.1
14	46.2
14.5	44.4
15	41.1
15.5	43.4
16	39.0
16.5	45.5
17	39.0
17.5	37.8
18	35.1

Time (min)	Relative Peak Fluorescence Intensity
18.5	37.5
19	35.7

C. Relative peak fluorescence intensity obtained at different time intervals for regeneration experiment while adding additional 1-AMA (4 min hydrogen sulfide + 4 min nitrogen + 1-AMA addition + 4 min hydrogen sulfide) (Refer to Figure 49)

Time (min)	Relative Peak Fluorescence Intensity
0	100.0
0.33	34.1
0.67	41.6
1	28.0
1.5	23.0
2.5	20.5
4	14.4
6	20.0
8	7.7
8 (1-AMA)	85.1
8.33	23.1
8.67	12.7
9	24.0
9.5	18.0
10.5	13.8
12	25.6

D. Relative peak fluorescence intensity obtained at different time intervals for hydrogen sulfide at 25mL/min flow rate for 1hour (First 4 min nitrogen) (Refer to Figure 54)

Time (min)	Relative Peak Fluorescence Intensity
0	100.0
1	102.2
2	103.5
3	99.5
4	104.2
5	105.6
8	108.4
11	109.4
14	106.5

17	106.7
20	107.1
25	106.2
30	104.0
40	102.0
50	105.2
60	108.2

E. Relative peak fluorescence intensity obtained at different time intervals rate for ammonia at 25mL/min flow for 1hour (First 4 min nitrogen) (Refer to Figure 56)

Time (min)	Relative Peak Fluorescence Intensity
0	100.0
1	101.0
2	104.2
3	103.6
4	103.5
5	103.5
8	108.0
11	104.2
14	106.1
17	103.7
20	104.8
25	102.3
30	103.7
40	104.3
50	104.5
60	106.3

F. Relative peak fluorescence intensity obtained at different time intervals rate for methyl mercaptan at 25mL/min flow for 1hour (First 4 min nitrogen) (Refer to Figure 58)

Time (min)	Relative Peak Fluorescence Intensity
0	100
1	121.143
2	118.7008
3	121.4867
4	123.035
5	132.0747
8	130.1139
11	135.4766
14	135.9249
17	137.1982
20	134.7231

25	137.5062
30	134.5141
40	133.5515
50	136.6812
60	136.8517

G. Relative peak fluorescence intensity obtained at different time intervals for zero air at 25mL/min flow rate for 10 minutes (Refer to Figure 64)

Time (min)	Relative Peak Fluorescence Intensity
0	100
0.5	130.829
1	133.3853
1.5	140.4139
2	138.5271
2.5	142.3007
3	143.4254
4	145.9817
5	148.0828
6	155.8125
7	150.4857
8	152.3116
9	157.8819
10	154.381

H. Relative peak fluorescence intensity obtained at different time intervals for toluene at 25mL/min flow rate for 1hour (First 4 min zero air) (Refer to Figure 65)

Time (min)	Relative Peak Fluorescence Intensity
0	100.0
1	100.6
2	94.5
3	99.9
4	100.9
5	101.6
8	104.7
11	100.6
14	99.7
17	98.5
20	100.0
25	95.4
30	97.0
40	91.9

50	86.9
60	77.1

I. Relative peak fluorescence intensity obtained at different time intervals for formaldehyde at 25mL/min flow rate for 1hour (First 4 min nitrogen) (Refer to Figure 66)

Time (min)	Relative Peak Fluorescence Intensity
0	100.0
1	111.9
2	113.6
3	113.6
4	114.5
5	120.5
8	123.0
11	125.1
14	124.5
17	125.0
20	124.6
25	124.7
30	124.2
40	126.8
50	125.3
60	124.5

J. Relative peak fluorescence intensity obtained at different time intervals at 25mL/min flow rate for tert-butyl mercaptan for 1hour (First 4 min nitrogen) (Refer to Figure 67)

Time (min)	Relative Peak Fluorescence Intensity
0	100.0
1	100.1
2	103.5
3	102.1
4	102.0
5	102.2
8	103.4
11	106.0
14	104.0
17	104.0
20	106.6
25	108.2
30	106.0

40	109.5
50	106.2
60	104.6

K. Relative peak fluorescence intensity obtained at different time intervals at 25mL/min flow rate for toluene in an increased amount of sensor for 1hour (First 4 min zero air) (Refer to Figure 68)

Time (min)	Relative Peak Fluorescence Intensity
0	100.0
1	112.2
2	105.1
3	106.0
4	107.7
5	107.7
8	107.2
11	108.2
14	109.7
17	108.5
20	110.0
25	105.0
30	105.6
40	103.4
50	94.8
60	91.1

L. Relative peak fluorescence intensity obtained at different time intervals at 25mL/min flow rate for a mixture of toluene and ammonia for 1hour (First 4 min zero air) (Refer to Figure 69)

Time (min)	Relative Peak Fluorescence Intensity
0	100.0
1	99.5
2	101.7
3	100.6
4	100.1
5	103.2
8	98.4
11	98.8
14	98.1
17	96.1
20	96.4
25	95.4
30	94.4
40	92.1

Time (min)	Relative Peak Fluorescence Intensity
50	84.2
60	76.8

M. Relative peak fluorescence intensity obtained at different time intervals at 25mL/min flow rate for a mixture of toluene and tert-butyl mercaptan for 1hour (First 4 min zero air) (Refer to Figure 70)

Time (min)	Relative Peak Fluorescence Intensity
0	100.0
1	97.3
2	97.7
3	98.2
4	97.8
5	97.8
8	99.4
11	97.6
14	101.6
17	95.4
20	96.0
25	93.9
30	91.7
40	87.9
50	83.2
60	75.9

REFERENCES

Abdurachim, K., & Ellis, H. R. (2006). Detection of protein-protein interactions in the alkanesulfonate monooxygenase system from Escherichia coli. Journal of bacteriology, 188(23), 8153-8159.

Agency for Toxic Substances and Disease Registry (ATSDR). (2014). Toxic Substances Portal – Methyl Mercaptan. Retrieved from https://www.atsdr.cdc.gov/MMG /MMG.asp?id=221&tid=40

Agency for Toxic Substances and Disease Registry (ATSDR). (2015). Toxic Substances Portal - Ammonia. Retrieved from https://www.atsdr.cdc.gov/PHS/PHS.asp?id=9&tid=2

Agency for Toxic Substances and Disease Registry (ATSDR). (2016). Landfill Gas Safety and Health Issues. Retrieved from Agency for Toxic Substances & Disease Registry: https://www.atsdr.cdc.gov/hac/landfill/html/ch3.html

Atkins, P.W. (1993). The Elements of Physical Chemistry (3rd ed.). Oxford University Press.

Agency for Toxic Substances and Disease Registry (ATSDR). 2016. Toxicological Profile for Hydrogen Sulfide and Carbonyl Sulfide. Atlanta, GA: U.S. Department of Health and Human Services, Public Health Service.

ATSDR. (2017). U.S. Department of Health & Human Service. Medical Management Guidelines for Methyl Mercaptan. Retrieved from https://wwwn.cdc.gov/TSP/MMG/MMGDetails.aspx?mmgid=221&toxid=40#:~:text=Acute%20exposure%20to%20methyl%20mercaptan,staggering%20gait%20can%20also%20occur.

Baker, B. P. (1982). Land Values Surrounding Waste Disposal Facilities (No. 639-2016-42174).

Baltrėnas, P., Andrulevičius, L., & Zuokaitė, E. (2013). Application of Dynamic Olfactometry to Determine Odor Concentrations in Ambient Air. Polish Journal of Environmental Studies, 22(2).

Bax, C., Sironi, S., & Capelli, L. (2020). How Can Odors Be Measured? An Overview of Methods and Their Applications. Atmosphere, 11(1), 92.

Belgiorno, V., Naddeo, V. & Zarra, T. (2013). Odour Impact Assessment Handbook. A John Wiley & Sons, Ltd., Publication

Bernhard, B. (2014, August 12). More odor lawsuits filed against Bridgeton Landfill owner. Retrieved from https://www.stltoday.com/lifestyles/health-med-fit/health/more-odor-lawsuits-filed-against-bridgeton-landfill-owner/article_c059212f-0385-5124-a3bf-fc67e9aa6c99.html

Blizzard, N. (2018, December 3). NEW DETAILS: $4.1 million settlement approved in Dayton landfill odor lawsuit. Retrieved from https://www.daytondailynews.com/news/new-details-million-settlement-approved-dayton-landfill-odor-lawsuit/r4HZKBL7rGD9M4ctJkaD7M/

Bokowa, A. H. (2011). The effect of sampling on the measured odour concentration. Chemical Engineering Transactions, 23, 43-48. https://doi.org/10.3303/CET1123008

Boudreau, M. D., Taylor, H. W., Baker, D. G., & Means, J. C. (2006). Dietary exposure to

2-aminoanthracene induces morphological and immunocytochemical changes in pancreatic tissues of Fisher-344 rats. Toxicological Sciences, 93(1), 50-61. https://doi.org/10.1093/toxsci/kfl033

Brattoli, M., De Gennaro, G., De Pinto, V., Demarinis Loiotile, A., Lovascio, S., & Penza, M. (2011). Odour detection methods: Olfactometry and chemical sensors. Sensors, 11(5), 5290-5322. https://doi.org/10.3390/s110505290

Briand, L., Eloit, C., Nespoulous, C., Bézirard, V., Huet, J. C., Henry, C., ... & Pernollet, J. C. (2002). Evidence of an odorant-binding protein in the human olfactory mucus: location, structural characterization, and odorant-binding properties. Biochemistry, 41(23), 7241-7252. https://doi.org/10.1021/bi015916c

Briand, L., Nespoulous, C., Perez, V., Rémy, J. J., Huet, J. C., & Pernollet, J. C. (2000). Ligand-binding properties and structural characterization of a novel rat odorant-binding protein variant. European journal of biochemistry, 267(10), 3079-3089. https://doi.org/10.1046/j.1432-1033.2000.01340.x

Bushdid, C., Magnasco, M. O., Vosshall, L. B., & Keller, A. (2014). Humans can discriminate more than 1 trillion olfactory stimuli. *Science*, *343*(6177), 1370-1372.

CalRecycle. (2019). Odor Characteristics of Compostable Materials. Retrieved from https://www.calrecycle.ca.gov/swfacilities/compostables/odor/characteris

Capo, A., Pennacchio, A., Varriale, A., D'Auria, S., & Staiano, M. (2018). The porcine odorant-binding protein as molecular probe for benzene detection. PloS one, 13(9), e0202630

Carannante I., Marasco A. (2018) Olfactory Sensory Neurons to Odor Stimuli: Mathematical Modeling of the Response.

Carlson, C. A., Lloyd, J. A., Dean, S. L., Walker, N. R., & Edmiston, P. L. (2006). Sensor for fluorene based on the incorporation of an environmentally sensitive fluorophore proximal to a molecularly imprinted binding site. Analytical chemistry, 78(11), 3537-3542. https://doi.org/10.1021/ac051375b

Castro, T. G., Silva, C., Matamá, T., & Cavaco-Paulo, A. (2021). The structural properties of odorants modulate their association to human odorant binding protein. Biomolecules, 11(2), 145.

Cave, J. W., Kenneth, J., & Mitropoulos, A. N. (2019). Progress in the development of olfactory-based bioelectronic chemosensors. Biosensors and Bioelectronics, 123, 211-222.

Centers for Disease Control and Prevention (2019). The National Institute for Occupational Safety and Health (NIOSH). Hydrogen Sulfide. Retrieved from https://www.cdc.gov/niosh/topics/hydrogensulfide/default.html

Centers for Disease Control and Prevention (2019). The National Institute for Occupational Safety and Health (NIOSH). Toluene. Retrieved from https://www.cdc.gov/niosh/topics/toluene/default.html

Charlier, L., Cabrol-Bass, D., & Golebiowski, J. (2009). How does human odorant binding protein bind odorants? The case of aldehydes studied by molecular dynamics. Comptes Rendus Chimie, 12(8), 905-910.

Chiriac, R., Carre, J., Perrodin, Y., Fine, L., & Letoffe, J. M. (2007). Characterisation of VOCs emitted by open cells receiving municipal solid waste. Journal of hazardous materials, 149(2), 249-263. https://doi.org/10.1016/j.jhazmat.2007.07.094

Choi, S. H., Lee, J. W., & Sim, S. J. (2004). Enhancement of the sensitivity of surface plasmon resonance (SPR) immunosensor for the detection of anti-GAD antibody by changing the pH for streptavidin immofadelbilization. Enzyme and microbial technology, 35(6-7), 683-687.

Curren, J., Hallis, S. A., Snyder, C. C. L., & Suffet, I. M. H. (2016). Identification and quantification of nuisance odors at a trash transfer station. Waste management, 58, 52-61. https://doi.org/10.1016/j.wasman.2016.09.021

Davoli, E. (2004). I recenti sviluppi nella caratterizzazione dell'inquinamento olfattivo. Tutto sugli odori, Rapporti GSISR.

Davoli, E., Gangai, M. L., Morselli, L., & Tonelli, D. (2003). Characterisation of odorants emissions from landfills by SPME and GC/MS. Chemosphere, 51(5), 357-368. https://doi.org/10.1016/S0045-6535(02)00845-7

De Feo, G., De Gisi, S., & Williams, I. D. (2013). Public perception of odour and environmental pollution attributed to MSW treatment and disposal facilities: A case study. Waste management, 33(4), 974-987.

Delahunty, C. M., Eyres, G., & Dufour, J. P. (2006). Gas chromatography-olfactometry. Journal of Separation Science, 29(14), 2107-2125.

Di Lena, M., Porcelli, F., & Altomare, D. F. (2016). Volatile organic compounds as new biomarkers for colorectal cancer: a review. *Colorectal Disease*, *18*(7), 654-663.

Dincer, F., Odabasi, M., & Muezzinoglu, A. (2006). Chemical characterization of odorous gases at a landfill site by gas chromatography–mass spectrometry. Journal of chromatography A, 1122(1-2), 222-229.

Du Preez, M., & Lottering, T. (2009). Determining the negative effect on house values of proximity to a landfill site by means of an application of the hedonic pricing method. South African Journal of Economic and Management Sciences, 12(2), 256-262.

El-Fadel, M., Findikakis, A. N., & Leckie, J. O. (1997). Environmental impacts of solid waste landfilling. Journal of environmental management, 50(1), 1-25.

Ekathimerini. (2019, December 19). Corfu police arrest four over landfill vandalism. Retrieved from https://www.ekathimerini.com/news/238193/corfu-police-arrest-four-over-landfill-vandalism/

El-Fadel, M., Findikakis, A. N., & Leckie, J. O. (1997). Environmental impacts of solid waste landfilling. Journal of environmental management, 50(1), 1-25. https://doi.org/10.1006/jema.1995.0131

Elliott, P., Richardson, S., Abellan, J. J., Thomson, A., De Hoogh, C., Jarup, L., & Briggs, D. J. (2009). Geographic density of landfill sites and risk of congenital anomalies in England: authors' response. Occupational and environmental medicine, 66(2), 140-140.

"Energy and Environmental Affairs." (2016). Mass.gov. Retrieved from http://www.mass.gov/eea/docs/dep/recycle/laws/lfgasapp.pdf.

Epstein, E. (2011). Industrial composting: environmental engineering and facilities management. CRC Press.

Fang, J. J., Yang, N., Cen, D. Y., Shao, L. M., & He, P. J. (2012). Odor compounds from different sources of landfill: characterization and source identification. Waste Management, 32(7), 1401-1410. https://doi.org/10.1016/j.wasman.2012.02.013

Flower, D. R. (1995). Multiple molecular recognition properties of the lipocalin protein

family. Journal of Molecular Recognition, 8(3), 185-195. https://doi.org/10.1002/jmr.300080304
Fisher, R. M., Alvarez-Gaitan, J. P., & Stuetz, R. M. (2019). Review of the effects of wastewater biosolids stabilization processes on odor emissions. *Critical Reviews in Environmental Science and Technology*, *49*(17), 1515-1586.
Fisher, R., Hayes, J., Alvarez-Gaitan, J. P., Aurisch, R., Vitanage, D., & Stuetz, R. (2018). Influence of biosolids processing on the production of odorous emissions at wastewater treatment plants. *Proceedings of the Water Environment Federation*, *2018*(2), 57-61.
Franks, F. (1975). The hydrophobic interaction. In Water a comprehensive treatise (pp. 1-94). Springer, Boston, MA. https://doi.org/10.1073/pnas.0610945104
Freeman, T., & Cudmore, R. (2002). Review of odour management in New Zealand. New Zeal. Minist. Environ. Air Qual. Tech. Rep, 24.
Gallagher, S. R. (2012). SDS-polyacrylamide gel electrophoresis (SDS-PAGE). *Current Protocols Essential Laboratory Techniques*, *6*(1), 7-3.
Ganni, M., Garibotti, M., Scaloni, A., Pucci, P., & Pelosi, P. (1997). Microheterogeneity of odorant-binding proteins in the porcupine revealed by N-terminal sequencing and mass spectrometry. Comparative Biochemistry and Physiology Part B: Biochemistry and Molecular Biology, 117(2), 287-291.
Gastech (n.d.). MiniRAE Lite. Retrieved from https://gastech.com/products/gas-detectors-portable/single-gas/minirae-lite
Gao, A., Wang, Y., Zhang, D., He, Y., Zhang, L., Liu, Y., ... & Li, T. (2020). Highly sensitive and selective detection of human-derived volatile organic compounds based on odorant binding proteins functionalized silicon nanowire array. Sensors and Actuators B: Chemical, 309, 127762.
Gonçalves, F., Silva, C., Ribeiro, A., & Cavaco-Paulo, A. (2018). 1-Aminoanthracene Transduction into Liposomes Driven by Odorant-Binding Protein Proximity. ACS applied materials & interfaces, 10(32), 27531-27539. Gonçalves, F., Silva, C., Ribeiro, A., & Cavaco-Paulo, A. (2018). 1-Aminoanthracene Transduction into Liposomes Driven by Odorant-Binding Protein Proximity. ACS applied materials & interfaces, 10(32), 27531-27539.
Gostelow, P., Parsons, S. A., & Stuetz, R. M. (2001). Odour measurements for sewage treatment works. Water Research, 35(3), 579-597. https://doi.org/10.1016/S0043-1354(00)00313-4
Heaney, C. D., Wing, S., Campbell, R. L., Caldwell, D., Hopkins, B., Richardson, D., & Yeatts, K. (2011). Relation between malodor, ambient hydrogen sulfide, and health in a community bordering a landfill. Environmental research, 111(6), 847-852. https://doi.org/10.1016/j.envres.2011.05.021
Henry, C. G., Meyer, G. E., Schulte, D. D., Stowell, R. R., Parkhurst, A. M., & Sheffield, R. E. (2011). Mask scentometer for assessing ambient odors. Transactions of the ASABE, 54(2), 609-615.
Heydel, J. M., Coelho, A., Thiebaud, N., Legendre, A., Bon, A. M. L., Faure, P., ... & Briand, L. (2013). Odorant-binding proteins and xenobiotic metabolizing enzymes: implications in olfactory perireceptor events. The Anatomical Record, 296(9), 1333-1345. https://doi.org/10.1002/ar.22735
Hirsch, A. R. (2009). Parkinsonism: the hyposmia and phantosmia connection. Archives

of neurology, 66(4), 538-542. doi:10.1001/archneurol.2009.38
Hite, D., Chern, W., Hitzhusen, F., & Randall, A. (2001). Property-value impacts of an environmental disamenity: the case of landfills. The Journal of Real Estate Finance and Economics, 22(2-3), 185-202.
Horiba Scientific. (n.d). Fluoromax. Retrieved from https://www.horiba.com/int/scientific/products/detail/action/show/Product/fluoromax-1576/
Howard, J. (2001). Nuisance flies around a landfill: patterns of abundance and distribution. Waste management & research, 19(4), 308-313.
Jasper, S. (2013). The Nervous System. Retrieved from http://www.zo.utexas.edu/faculty/sjasper/bio301L/nervous.html
Jedra, Christina. (2022). Future Of Oahu Landfill Is Uncertain After Committee Rejects Alternatives. Honolulu Civil Beat Inc. Retrieved from https://www.civilbeat.org/2022/04/future-of-oahu-landfill-is-uncertain-after-committee-rejects-alternatives/?fbclid=IwAR1LED5sYZtHduQBDpUVWdJWyi9l89pCHMvqgvxIkVl6YaCVy6Fs3y93tq0
Jiang, J. K. (1996). Concentration measurement by dynamic olfactometer. Water environment & technology, 8(6), 55-59.
Jin, P. C. (2015). "Characteristics of Gas Emissions in Landfill Site in Recent Years." International Journal of Environmental Science and Development, 6(5).
Kang, C. D., Lee, S. W., Park, T. H., & Sim, S. J. (2006). Performance enhancement of real-time detection of protozoan parasite, Cryptosporidium oocyst by a modified surface plasmon resonance (SPR) biosensor. Enzyme and microbial technology, 39(3), 387-390. https://doi.org/10.1016/j.enzmictec.2005.11.039
Kazakov, A. S., Markov, D. I., Gusev, N. B., & Levitsky, D. I. (2009). Thermally induced structural changes of intrinsically disordered small heat shock protein Hsp22. Biophysical chemistry, 145(2-3), 79-85.
Kim, K.-H. H., Choi, Y., Jeon, E., and Sunwoo, Y. (2005b). "Characterization of malodorous sulfur compounds in landfill gas." Atmospheric Environment, Pergamon, 39(6), 1103–1112.
Kim, S. U., Kim, Y. J., Yea, C. H., Min, J., & Choi, J. W. (2008). Fabrication of functional biomolecular layer using recombinant technique for the bioelectronic device. Korean Journal of Chemical Engineering, 25(5), 1115-1119.
Kim, T. H., Lee, S. H., Lee, J., Song, H. S., Oh, E. H., Park, T. H., & Hong, S. (2009). Single-carbon-atomic-resolution detection of odorant molecules using a human olfactory receptor-based bioelectronic nose. Advanced Materials, 21(1), 91-94. https://doi.org/10.1002/adma.200801435
Kmiecik, D., & Albani, J. R. (2010). Effect of 1-aminoanthracene (1-AMA) binding on the structure of three lipocalin proteins, the dimeric β lactoglobulin, the dimeric odorant binding protein and the monomeric α 1-acid glycoprotein. Fluorescence spectra and lifetimes studies. Journal of fluorescence, 20(5), 973-983.
Kobayashi, H., Ogawa, M., Alford, R., Choyke, P. L., & Urano, Y. (2009). New strategies for fluorescent probe design in medical diagnostic imaging. Chemical reviews, 110(5), 2620-2640.

Ko, H. J., Lee, S. H., Oh, E. H., & Park, T. H. (2010). Specificity of odorant-binding proteins: a factor influencing the sensitivity of olfactory receptor-based biosensors. Bioprocess and biosystems engineering, 33(1), 55.

Ko, H. J., & Park, T. H. (2008). Enhancement of odorant detection sensitivity by the expression of odorant-binding protein. Biosensors and Bioelectronics, 23(7), 1017-1023. https://doi.org/10.1016/j.bios.2007.10.008

Ko, J. H., Xu, Q., & Jang, Y. C. (2015). Emissions and control of hydrogen sulfide at landfills: a review. Critical Reviews in Environmental Science and Technology, 45(19), 2043-2083.

Kulig, A. (2004). Metody pomiarowo-obliczeniowe w ocenach oddziaływania na środowisko obiektów gospodarki komunalnej (Measurement and modelling based methods applicable in environmental impact assessment of municipal utilities). Warsaw University of Technology: Warszawa, Poland.

Lacazette, E., Gachon, A. M., & Pitiot, G. (2000). A novel human odorant-binding protein gene family resulting from genomic duplicons at 9q34: differential expression in the oral and genital spheres. Human Molecular Genetics, 9(2), 289-301. https://doi.org/10.1093/hmg/9.2.289, R. E., Mukhtar, S., Carey, J. B., & Ullman, J. L. (2004). A review of literature concerning odors, ammonia, and dust from broiler production facilities: 1. Odor concentrations and emissions. Journal of Applied Poultry Research, 13(3), 500-508. https://doi.org/10.1093/japr/13.3.500

Laister, G., Stretch, D. D., & Strachan, L. (2002). Managing landfill odour using dispersion modelling and community feedback. Proc. of Wastecon 2002.

Laor, Y., Parker, D., & Pagé, T. (2014). Measurement, prediction, and monitoring of odors in the environment: a critical review. Reviews in Chemical Engineering, 30(2), 139-166. https://doi.org/10.1515/revce-2013-0026

Leal, J., Smyth, H. D., & Ghosh, D. (2017). Physicochemical properties of mucus and their impact on transmucosal drug delivery. International journal of pharmaceutics, 532(1), 555-572. https://doi.org/10.1016/j.ijpharm.2017.09.018

LECHNER, M., WOJNAR, P., & Bernhard, R. E. D. L. (2001). Human tear lipocalin acts as an oxidative-stress-induced scavenger of potentially harmful lipid peroxidation products in a cell culture system. Biochemical Journal, 356(1), 129-135.

Lee, S. H., Jun, S. B., Ko, H. J., Kim, S. J., & Park, T. H. (2009). Cell-based olfactory biosensor using microfabricated planar electrode. Biosensors and Bioelectronics, 24(8), 2659-2664. https://doi.org/10.1016/j.bios.2009.01.035

Lewkowska, P., Dymerski, T., & NamieśNik, J. (2015). Use of sensory analysis methods to evaluate the odor of food and outside air. Critical Reviews in Environmental Science and Technology, 45(20), 2208-2244.

Li, J. L., Car, R., Tang, C., & Wingreen, N. S. (2007). Hydrophobic interaction and hydrogen-bond network for a methane pair in liquid water. Proceedings of the National Academy of Sciences, 104(8), 2626-2630.

Li, J., Zou, K., Li, W., Wang, G., & Yang, W. (2019). Olfactory Characterization of Typical Odorous Pollutants Part I: Relationship Between the Hedonic Tone and Odor Concentration. Atmosphere, 10(9), 524. https://doi.org/10.3390/atmos10090524

Li, R. Y. M., & Li, H. C. Y. (2018). Have housing prices gone with the smelly wind? Big data analysis on landfill in Hong Kong. Sustainability, 10(2), 341.

Liu, C., Furusawa, Y., & Hayashi, K. (2013). Development of a fluorescent imaging sensor

for the detection of human body sweat odor. Sensors and Actuators B: Chemical, 183, 117-123.

Lu, Y., Li, H., Zhuang, S., Zhang, D., Zhang, Q., Zhou, J., ... & Wang, P. (2014). Olfactory biosensor using odorant-binding proteins from honeybee: Ligands of floral odors and pheromones detection by electrochemical impedance. Sensors and Actuators B: Chemical, 193, 420-427. https://doi.org/10.1016/j.snb.2013.11.045

Martuzzi, M., Mitis, F., & Forastiere, F. (2010). Inequalities, inequities, environmental justice in waste management and health. European Journal of Public Health, 20(1), 21-26. https://doi.org/10.1093/eurpub/ckp216

Maulini-Duran, C., Artola, A., Font, X., & Sánchez, A. (2013). A systematic study of the gaseous emissions from biosolids composting: raw sludge versus anaerobically digested sludge. *Bioresource technology*, *147*, 43-51.

McGinley, M. A., & McGinley, C. M. (2004). Comparison of field olfactometers in a controlled chamber using hydrogen sulfide as the test odorant. *Water Science and Technology*, *50*(4), 75-82.

Meeroff, D., & Rahman, S. (2021). Waste 360. Odor management at landfills: Part 1 - the current state of the art. (2021). https://www.waste360.com/landfill-operations/odor-management-landfills-part-1-current-state-art

Meeroff, D., & Rahman, S. (2021). Odor management at landfills: Part 2 - A novel biosensor for measuring odors at landfills. (2021). https://www.waste360.com/landfill-operations/odor-management-landfills-part-2-novel-biosensor-measuring-odors-landfills

Mei, B., Kennedy, M. W., Beauchamp, J., Komuniecki, P. R., & Komuniecki, R. (1997). Secretion of a novel developmentally regulated fatty acid-binding protein into the perivitelline fluid of the parasitic nematode, Ascaris suum. Journal of Biological Chemistry, 272(15), 9933-9941.

Mikhailopulo, K. I., Serchenya, T. S., Kiseleva, E. P., Chernov, Y. G., Tsvetkova, T. M., Kovganko, N. V., & Sviridov, O. V. (2008). Interaction of molecules of the neonicotinoid imidacloprid and its structural analogs with human serum albumin. Journal of Applied Spectroscopy, 75(6), 857.

Millery, J., Briand, L., Bézirard, V., Blon, F., Fenech, C., Richard-Parpaillon, L., ... & Gascuel, J. (2005). Specific expression of olfactory binding protein in the aerial olfactory cavity of adult and developing Xenopus. European Journal of Neuroscience, 22(6), 1389-1399. https://doi.org/10.1111/j.1460-9568.2005.04337.x

Ministry of the Environment. (1995). Offensive Odor Control Law. Retrieved from https://www.env.go.jp/en/laws/air/odor/index.html

Mirmohseni, A., Shojaei, M., & Farbodi, M. (2008). Application of a quartz crystal nanobalance to the molecularly imprinted recognition of phenylalanine in solution. Biotechnology and Bioprocess Engineering, 13(5), 592-597.

Murphy, C., Doty, R. L., & Duncan, H. J. (2003). Clinical disorders of olfaction. In Handbook of olfaction and gustation (pp. 822-849). CRC Press.

Nagata, Y., & Takeuchi, N. (2003). Measurement of odor threshold by triangle odor bag method. Odor measurement review, 118, 118-127.

National Academics Press. (2022). Emergency and Continuous Exposure Guidance Levels for Selected Submarine Contaminants: Volume 1 (2007). Chapter:5 Formaldehyde. Retrieved from https://nap.nationalacademies.org/read/11170/chapter/7#131

National Academies of Sciences, Engineering, and Medicine. 2007. Emergency and Continuous Exposure Guidance Levels for Selected Submarine Contaminants: Volume 1. Washington, DC: The National Academies Press. https://doi.org/10.17226/11170.

National Cancer Institute. (2011). Formaldehyde and Cancer Risk. Retrieved from https://www.cancer.gov/about-cancer/causes-prevention/risk/substances/formaldehyde/formaldehyde-fact-sheet

Nelson, A. C., Genereux, J., & Genereux, M. (1992). Price effects of landfills on house values. Land economics, 359-365. DOI: 10.2307/3146693

New Jersey Department of Health and Senior Services. (2003). Hazardous substance Fact Sheet. Retrieved from https://nj.gov/health/eoh/rtkweb/documents/fs/0290.pdf

New York State Department of Health. (2011). The Facts About Ammonia. Retrieved from https://www.health.ny.gov/environmental/emergency/chemical_terrorism/ammonia_general.

Nicell, J. A. (2009). Assessment and regulation of odour impacts. Atmospheric Environment, 43(1), 196-206. https://doi.org/10.1016/j.atmosenv.2008.09.033

Nicolas, J., Craffe, F., & Romain, A. C. (2006). Estimation of odor emission rate from landfill areas using the sniffing team method. Waste Management, 26(11), 1259-1269. https://doi.org/10.1016/j.wasman.2005.10.013

Norton, J. M., Wing, S., Lipscomb, H. J., Kaufman, J. S., Marshall, S. W., & Cravey, A. J. (2007). Race, wealth, and solid waste facilities in North Carolina. Environmental Health Perspectives, 115(9), 1344-1350. https://doi.org/10.1289/ehp.10161

Ocean Insight. (2022). QE Pro-FL. Retrieved from https://www.oceaninsight.com/products/spectrometers/high-sensitivity/qepro-fl/

Occupational Safety and Health Administration (OSHA). (2005). "OSHA Fact Sheet." Retrieved from https://www.osha.gov/OshDoc/data_Hurricane_Facts/hydrogen_sulfide_fact.pdf

OECD SIDS. (2002). SIDS Initial Assessment Report. Formaldehyde. Retrieved from https://hpvchemicals.oecd.org/ui/handler.axd?id=5525377e-1442-43d0-8c76-f8cacfadf8bb

Oliva, R., Banerjee, S., Cinar, H., Ehrt, C., & Winter, R. (2020). Alteration of protein binding affinities by aqueous two-phase systems revealed by pressure perturbation. *Scientific reports*, *10*(1), 1-12

OSHA. How Smelly is Ammonia? Retrieved from https://www.osha.gov/sites/default/files/2019-03/fs5-howsmelly.pdf

Palmiotto, M., Fattore, E., Paiano, V., Celeste, G., Colombo, A., & Davoli, E. (2014). Influence of a municipal solid waste landfill in the surrounding environment: Toxicological risk and odor nuisance effects. Environment international, 68, 16-24. https://doi.org/10.1016/j.envint.2014.03.004

Paolini, S., Tanfani, F., Fini, C., Bertoli, E., & Pelosi, P. (1999). Porcine odorant-binding protein: structural stability and ligand affinities measured by Fourier-transform infrared spectroscopy and fluorescence spectroscopy. Biochimica et Biophysica Acta (BBA)-Protein Structure and Molecular Enzymology, 1431(1), 179-188. https://doi.org/10.1016/S0167-4838(99)00037-0

Paraskaki, I., & Lazaridis, M. (2005). Quantification of landfill emissions to air: a case

study of the Ano Liosia landfill site in the greater Athens area. Waste management & research, 23(3), 199-208. https://doi.org/10.1177%2F0734242X05054756

Parker, T., Dottridge, J., & Kelly, S. (2002). Investigation of the composition and emissions of trace components in landfill gas. Environment Agency, R&D Technical Report P1-438/TR.

Pearce, T. C., Schiffman, S. S., Nagle, H. T., & Gardner, J. W. (Eds.). (2006). Handbook of machine olfaction: electronic nose technology. John Wiley & Sons.

Pelosi, P. (2001). The role of perireceptor events in vertebrate olfaction. Cellular and Molecular Life Sciences CMLS, 58(4), 503-509. https://doi.org/10.1007/PL00000875

Pelosi, P., Baldaccini, N. E., & Pisanelli, A. M. (1982). Identification of a specific olfactory receptor for 2-isobutyl-3-methoxypyrazine. Biochemical Journal, 201(1), 245-248. https://doi.org/10.1042/bj2010245

Pelosi, P., Mastrogiacomo, R., Iovinella, I., Tuccori, E., & Persaud, K. C. (2014). Structure and biotechnological applications of odorant-binding proteins. Applied microbiology and biotechnology, 98(1), 61-70.

Pelosi, P., Zhu, J., & Knoll, W. (2018). Odorant-binding proteins as sensing elements for odour monitoring. Sensors, 18(10), 3248.

Polyakova, O. V., Mazur, D. M., Artaev, V. B., & Lebedev, A. T. (2016). Rapid liquid–liquid extraction for the reliable GC/MS analysis of volatile priority pollutants. *Environmental Chemistry Letters*, *14*(2), 251-257.

RAE Systems Inc. (2013). The PID Handbook (3rd ed.). Retrieved from https://www.raesystems.com/sites/default/files/content/resources/pid_handbook_1002-02.pdf

Rahman, S. (2020). *Development of a biosensor for objectively quantifying odorants* (Order No. 27962421). Available from Dissertations & Theses @ Florida Atlantic University - FCLA; ProQuest Dissertations & Theses A&I; ProQuest Dissertations & Theses Global. (2414449391). Retrieved from https://go.openathens.net/redirector/fau.edu?url=https://www.proquest.com/dissertations-theses/development-biosensor-objectively-quantifying/docview/2414449391/se-2

Ramoni, R., Bellucci, S., Grycznyski, I., Grycznyski, Z., Grolli, S., Staiano, M., ... & Conti, V. (2007). The protein scaffold of the lipocalin odorant-binding protein is suitable for the design of new biosensors for the detection of explosive components. Journal of Physics: Condensed Matter, 19(39), 395012.

Ready, R. (2010). Do landfills always depress nearby property values? Journal of Real Estate Research, 32(3), 321-339.

Ritzkowski, M., Heyer, K. U., & Stegmann, R. (2006). Fundamental processes and implications during in situ aeration of old landfills. Waste Management, 26(4), 356-372. https://doi.org/10.1016/j.wasman.2005.11.009

Roblyer, J. G. (2017). Development of a Biosensor to Detect Landfill Odors Using Human Odorant Binding Protein (Doctoral dissertation, Florida Atlantic University).

Roebuck, D. U. N. C. A. N., Strecht, D., & Strachan, L. I. N. D. S. A. Y. (2004). Investigating odour sources and odour emission rates from landfills through direct communication with residents. Proc. of Wastecon 2004.

Ruth, J. H. (1986). Odor thresholds and irritation levels of several chemical substances: a review. American Industrial Hygiene Association Journal, 47(3), A-142.

https://doi.org/10.1080/15298668691389595
Saalberg, Y., & Wolff, M. (2016). VOC breath biomarkers in lung cancer. *Clinica Chimica Acta*, *459*, 5-9.
Sakabe, M., Asanuma, D., Kamiya, M., Iwatate, R. J., Hanaoka, K., Terai, T., ... & Urano, Y. (2012). Rational design of highly sensitive fluorescence probes for protease and glycosidase based on precisely controlled spirocyclization. Journal of the American Chemical Society, 135(1), 409-414.
Sakawi, Z., Sharifah, S. A., Jaafar, O., & Mahmud, M. (2011). Community perception of odor pollution from the landfill. Research Journal of Environmental and Earth Sciences, 3(2), 142-145.
Saladin, K. S. (2004). Anatomy & physiology: the unity of form and function.
Salamone, A. (2019, March 11). Second lawsuit alleges 'offensive odors' at Plainfield Township landfill. Retrieved from https://www.mcall.com/business/mc-biz-grand-central-second-lawsuit-20190311-story.html
Sarkar, U., & Hobbs, S. E. (2002). Odour from municipal solid waste (MSW) landfills: A study on the analysis of perception. Environment International, 27(8), 655-662. https://doi.org/10.1016/S0160-4120(01)00125-8
Sarkar, U., Longhurst, P. J., & Hobbs, S. E. (2003). Community modelling: a tool for correlating estimates of exposure with perception of odour from municipal solid waste (MSW) landfills. Journal of environmental management, 68(2), 133-140. https://doi.org/10.1016/S0301-4797(03)00027-6
Sattler, M., & Devanathan, S. (2007). Which meteorological conditions produce worst-case odors from area sources?. Journal of the Air & Waste Management Association, 57(11), 1296-1306. https://doi.org/10.3155/1047-3289.57.11.1296
Scheutz, C., Bogner, J., Chanton, J. P., Blake, D., Morcet, M., Aran, C., & Kjeldsen, P. (2008). Atmospheric emissions and attenuation of non-methane organic compounds in cover soils at a French landfill. *Waste management*, *28*(10), 1892-1908.
Scheutz, C., Kjeldsen, P., Bogner, J. E., De Visscher, A., Gebert, J., Hilger, H. A., Huber-Humer, M., and Spokas, K. (2009). "Microbial methane oxidation processes and technologies for mitigation of landfill gas emissions." ISSN 0734–242X Waste Management & Research, 27, 409–455.
Schiefner, A., Freier, R., Eichinger, A., & Skerra, A. (2015). Crystal structure of the human odorant binding protein, OBP IIa. Proteins: Structure, Function, and Bioinformatics, 83(6), 1180-1184. https://doi.org/10.1002/prot.24797
Schiffman, S. S., Walker, J. M., Dalton, P., Lorig, T. S., Raymer, J. H., Shusterman, D., & Williams, C. M. (2004). Potential health effects of odor from animal operations, wastewater treatment, and recycling of byproducts. *Journal of agromedicine*, *9*(2), 397-403.
Sela, L., & Sobel, N. (2010). Human olfaction: a constant state of change-blindness. Experimental Brain Research, 205(1), 13-29.
Seok Lim, J., & Missios, P. (2007). Does size really matter? Landfill scale impacts on property values. Applied Economics Letters, 14(10), 719-723.
Sheffield, R., Thompson, M., Dye, B., & Parker, D. (2004). Evaluation of field-based odor assessment methods. Proceedings of the Water Environment Federation, 2004(3), 870-879.
SHIGEOKA, K., NAKATSUJI, Y., OGAWA, K., IWASAKI, Y., & UENO, H. (2009).

The established method of three regulation standards in Japan. Odours and VOCs: Measurement, Regulation and Control Techniques, 31, 179.
Shults, M. D., & Imperiali, B. (2003). Versatile fluorescence probes of protein kinase activity. Journal of the American Chemical Society, 125(47), 14248-14249. https://doi.org/10.1021/ja0380502
Silva, C., Matamá, T., Azoia, N. G., Mansilha, C., Casal, M., & Cavaco-Paulo, A. (2014). Odorant binding proteins: a biotechnological tool for odour control. Applied microbiology and biotechnology, 98(8), 3629-3638.
Sivret, E. C., Le Minh, N., Riese, L., Kenny, S., Parcsi, G., Bustamante, H., & Stuetz, R. M. (2014, May). Preliminary assessment of the impact of thermal drying on volatile sulfur emissions from dewatered biosolids. In Odors and Air Pollutants Conference 2014. Water Environment Federation.
Sneath, R. W. (2001). Olfactometry and the CEN Standard EN13725. Odours in Wastewater Treatment: Measurement, Modelling and Control. Eds Stuetz R. and Frechen BF, IWA Publishing.
Song, H. M., & Lee, C. S. (2008). Simple fabrication of functionalized surface with polyethylene glycol microstructure and glycidyl methacrylate moiety for the selective immobilization of proteins and cells. Korean Journal of Chemical Engineering, 25(6), 1467-1472.
Spinelli, S., Ramoni, R., Grolli, S., Bonicel, J., Cambillau, C., & Tegoni, M. (1998). The structure of the monomeric porcine odorant binding protein sheds light on the domain swapping mechanism. Biochemistry, 37(22), 7913-7918.
Sreejith, R. K., Yadav, V. N., Varshney, N. K., Berwal, S. K., Suresh, C. G., Gaikwad, S. M., & Pal, J. K. (2009). Conformational characterization of human eukaryotic initiation factor 2α: A single tryptophan protein. Biochemical and biophysical research communications, 390(2), 273-279.
St Croix Sensory, I. (2005). A review of the Science and Technology of Odor Measurement.
Straub, T. M., & Chandler, D. P. (2003). Towards a unified system for detecting waterborne pathogens. Journal of Microbiological Methods, 53(2), 185-197
Stuetz, R. M., & Frechen, F. B. (Eds.). (2001). Odours in wastewater treatment. IWA publishing.
Takuwa, Y., Matsumoto, T., Oshita, K., Takaoka, M., Morisawa, S., & Takeda, N. (2009). Characterization of trace constituents in landfill gas and a comparison of sites in Asia. Journal of Material Cycles and Waste Management, 11(4), 305.
Tcatchoff, L., Nespoulous, C., Pernollet, J. C., & Briand, L. (2006). A single lysyl residue defines the binding specificity of a human odorant-binding protein for aldehydes. FEBS letters, 580(8), 2102-2108.
Tegoni, M., Pelosi, P., Vincent, F., Spinelli, S., Campanacci, V., Grolli, S., ... & Cambillau, C. (2000). Mammalian odorant binding proteins. Biochimica et Biophysica Acta (BBA)-Protein Structure and Molecular Enzymology, 1482(1-2), 229-240. https://doi.org/10.1016/S0167-4838(00)00167-9
Trotier, D., Bensimon, J. L., Herman, P., Tran Ba Huy, P., Døving, K. B., & Eloit, C. (2007). Inflammatory obstruction of the olfactory clefts and olfactory loss in humans: a new syndrome?. *Chemical senses*, *32*(3), 285-292.
Turk, A., Haring, R. C., & Okey, R. W. (1972). Odor control technology. Environmental

Science & Technology, 6(7), 602-607.
van den Noort, M., de Boer, M., & Poolman, B. (2021). Stability of ligand-induced protein conformation influences affinity in maltose-binding protein. *Journal of Molecular Biology*, *433*(15), 167036.
van Harreveld, A. P., Shinkre, R., Villatoro, C., Tournier, C., & Naik, S. (2022). Odour Testing Methods and Regulatory Norms. *Odour in Textiles*, 249-277.
Van Riel, D., Verdijk, R., & Kuiken, T. (2015). The olfactory nerve: a shortcut for influenza and other viral diseases into the central nervous system. *The Journal of pathology*, *235*(2), 277-287.
Vidovic, M. (2017). Meteorological Conditions Affecting the Dispersion of Landfill Odor Complaints. Florida Atlantic University.
Wei, Y., Brandazza, A., & Pelosi, P. (2008). Binding of polycyclic aromatic hydrocarbons to mutants of odorant-binding protein: a first step towards biosensors for environmental monitoring. Biochimica et Biophysica Acta (BBA)-Proteins and Proteomics, 1784(4), 666-671. https://doi.org/10.1016/j.bbapap.2008.01.012
Wenjing, L., Zhenhan, D., Dong, L., Jimenez, L. M. C., Yanjun, L., Hanwen, G., & Hongtao, W. (2015). Characterization of odor emission on the working face of landfill and establishing of odorous compounds index. Waste Management, 42, 74-81. https://doi.org/10.1016/j.wasman.2015.04.030
Whitson, K. B., & Whitson, S. R. (2014). Human odorant binding protein 2a has two affinity states and is capable of binding some uremic toxins. Biochemistry and Analytical Biochemistry, 3(2), 1.
Xia, F. F., Zhang, H. T., Wei, X. M., Su, Y., and He, R. (2015). "Characterization of H2S removal and microbial community in landfill cover soils." Environmental Science and Pollution Research, 22(23), 18906–18917.
Xing, B., Khanamiryan, A., & Rao, J. (2005). Cell-permeable near-infrared fluorogenic substrates for imaging β-lactamase activity. Journal of the American Chemical Society, 127(12), 4158-4159.
Xu, P. (2005). A Drosophila OBP required for pheromone signaling. Science, 310(5749), 798-799.
Yazdani, R. (2015). Evaluation of the Landfill Odor Problem at the Sunshine Canyon Landfill.
Ying, D., Chuanyu, C., Bin, H., Yueen, X., Xuejuan, Z., Yingxu, C., & Weixiang, W. (2012). Characterization and control of odorous gases at a landfill site: A case study in Hangzhou, China. Waste management, 32(2), 317-326. https://doi.org /10.1016/j.wasman.2011.07.016
Yoon, H., Lee, S. H., Kwon, O. S., Song, H. S., Oh, E. H., Park, T. H., & Jang, J. (2009). Polypyrrole nanotubes conjugated with human olfactory receptors: high-performance transducers for FET-type bioelectronic noses. Angewandte Chemie International Edition, 48(15), 2755-2758. https://doi.org/10.1002/anie.200805171
Yuwono, A. S., & Lammers, P. S. (2004). Odor pollution in the environment and the detection instrumentation. Agricultural Engineering International: CIGR Journal.
Zarra, T. (2007). Procedures for detection and modelling of odours impact from sanitary environmental engineering plants (Doctoral dissertation, PhD Thesis, University of Salerno, Salerno, Italy).
Zarra, T., Naddeo, V., & Belgiorno, V. (2009). A novel tool for estimating the odour

emissions of composting plants in air pollution management. Global Nest Journal, 11(4), 477-486.
Zarzo, M. (2021). Multivariate Analysis and Classification of 146 Odor Character Descriptors. *Chemosensory Perception*, *14*(2), 79-101.
Zhang, Q. (2001). Odour emissions from confined swine production facilities. In Proc. National Conference "Livestock Options for the Future (pp. 25-27).
Zhuang, Y. D., Chiang, P. Y., Wang, C. W., & Tan, K. T. (2013). Environment-sensitive fluorescent turn-on probes targeting hydrophobic ligand-binding domains for selective protein detection. Angewandte Chemie International Edition, 52(31), 8124-8128